University of Cyprus

University of Cyprus

Department of History and Archaeology

MA Program in Field Archaeology on Land and Under the Sea

Investigating two Late Roman Metallurgical Slag Heaps: An Analytical Approach

Master's Dissertation by

Anna-Maria Sdralia

Thesis Supervisor: Professor Vasiliki Kassianidou

Nicosia, April 2022

Title: Investigating two Late Roman Metallurgical Slag Heaps: An Analytical Approach

Name: Anna-Maria Sdralia

Supervisor: Vasiliki Kassianidou

Committee: Vasiliki Kassianidou, Thilo Rehren and Apostolos Sarris

Master of Arts Program: Field Archaeology on Land and Under the Sea

University of Cyprus, Department of History and Archaeology

Academic year: 2021-2022

Nicosia, 30.04.2022

Final Version

Table of contents

Acknowledgements

This thesis could not have been completed without the help of a number of people. Firstly, I would like to show my gratitude to my supervisor Vasiliki Kassianidou for letting me study the two slag assemblages and trusting me with all the analytical approaches. I am thankful for her guidance, feedback and very fruitful comments throughout this thesis. I would also like to thank Thilo Rehren for showing me the world of microscopy, how intriguing it is, but also kindly explaining everything in detail, no matter how many questions I would ask.

I am grateful to both the Archaeological Research Unit and the Science and Technology in Archaeology and Culture Research Center for providing me the facilities, equipment and colleagues throughout this process. I would like to specifically thank the STARC Lab technician Brunella Santarelli for her huge help by training me in most equipment and walking me through every step tirelessly and Andreas Charalambous for the training and help in the HHpXRF analysis at the ARU. Furthermore, I am grateful to my inspiring professors from the MA program for all their feedback and endless discussions throughout the courses of the program that equipped me with the necessary set of tools to carry out and write this thesis.

Many thanks go to my colleagues at the STARC and my co-students of this Masters Program Elpida Agapitou, Nadia Margrethe Andersen and Filip Hajek for their great support! Finally, I would like to thank my friends and specifically Despina Vandi and Vodka Juniors for keeping me awake during the excel processing.

Chapter 1. Introduction

With Christianity as the newly recognized religion of the Roman Empire in the early 4th century C.E., Cyprus integrates it in its society quite smoothly. The political organization of Cyprus remains the same as in Roman times, with a *vir clarissimus* (consularis) as the state agent of the island responsible for tax collecting, justice and the island's legislature, of course all in accordance with the emperor's will (Lokin 2005: 171-197). From the 4th century onwards more and more religious buildings rise in the cities of Cyprus but also in the rural setting. Religious buildings appear in the main cities of the period, i.e., Hagios Philon, Constantia, Kition, Amathous, Kourion, Paphos, Arsinoe, Soloi, Lapithos, Kerynia, Tamassos, Trimithous, Chytroi and Ledra **(Fig. 1).** What scholars keep on highlighting is the general peace that characterizes the island between the 4th and the mid-7th century C.E. (Lokin 2005, Παναγίδης 2018). This peace refers to Cyprus not being in a war. Natural disasters did make an appearance though, some examples being earthquakes in the first half of the 4th century and tsunamis in the second half of the same century (Κωνσταντίνου and Παναγίδης 2013). The 6th century was also affected by plague epidemic in the Mediterranean; it is, however, uncertain whether Cyprus did suffer from it or not. Although military peace in Cyprus was indeed the case, the Eastern Roman Empire did continue to have problems with its neighbors, which fell on the shoulders of the entire empire to support this warfare, e.g., through food, equipment, hosting captives etc. (Παναγίδης 2018: 183-191).

Figure 1. Map of Cyprus during the 4th to the 7th century C.E. (After Παναγίδης 2018: 181)

In this 'peaceful' setting come the uprising Arab conquests threatening the integrity of the Roman Empire in the end of the first quarter of the 7th century C.E. while their invasion in Cyprus was not until 649 C.E. (Browning 2005). The two invasions happened in the second half of the 7th century. Most of the cities were severely affected with great damages. The Arab conquests

caused the destruction of religious buildings, the movement of people, and even the establishment of New Justinianopolis, located nearby the city of Cyzicus in Turkey, in the very end of the 7th century C.E. The effects of these eventswere not experienced evenly across the island though. Archaeology has brought to light evidence of some cities that were barely or not at all damaged, e.g., Salamis and Kition was not completely destroyed, while the church of Aggeloktisti in Kiti was not destroyed at all (Browning 2005: 254-258). At the same time, the Arabs restricted their presence on the island by bringing a Muslim guard which however did not have an administrative role. It is testified that marriage between Arabs and Cypriots was prohibited (Browning 2005: 261). In 688/9 a treaty between the Roman Empire and the Arabs states that the island will adhere to complete neutrality from then onwards without helping either of the sides, e.g., by providing information. Another part of this treaty declares the division of the taxes of Cyprus equally between the two sides. It is difficult to identify the exact organization of the island at this period, but it is suggested that bishoprics seem to enjoy a leading role in the administration of Cyprus. Other than this, the period spanning from the end of the 7th century to the end of the 8th century in Cyprus seems quite puzzling and the evidence is not enough to reconstruct the major and minor aspects of living on the island.

One key aspect in examining this period concerns the multidimensional role of the church. Religion and state are two very closely associated factors in Late Roman Cyprus. The state – through the face of the *consularis* – has three major responsibilities: tax collection and treasury, administration of justice and legislature. The latter seems the only responsibility in which the church did not play any role at all. On the other hand, tax collection during the 6th century, under Justinian (reign between 527-565 C.E), becomes a responsibility of the church (Lokin 2005: 186). Concerning justice, it is interesting how each bishop acts as a local judge, providing the option of an economic and quick 'court' trial under the holy spectrum (Lokin 2005: 183). Apart from this, the church played a leading role also in education. The economic role of the church is also very evident, since workshop areas are attested in the vicinity of churches. The workshops near churches include the city of Arsinoe, with metal, glass and pottery workshops, Kourion with bread making installations and Ayios Philon, located in the Karspasia peninsula, with evidence of metalworking workshop (du Plat Taylor and Megaw 1981, Papalexandrou and Caraher 2012, Castello 2014). Trying to see where the thin line between state and church begins and ends is not always clear. Nevertheless, it is noticeable that the church is driving most of the aspects that influence one's life.

The church with its bishops represents the main religion, the education, sometimes the law and partly the economy. This one-wheeled vehicle definitely has an immediate influence on its people under the umbrella of a religious-oriented empire.

In this cocktail of factors of this period in the island of Cyprus, comes the question of the exact economic role of Cyprus in the Eastern Mediterranean and the Roman Empire itself. The wine and olive-oil trade are certain during this period, stepping in the footsteps of the Roman state-driven economy across the empire while in Cyprus, amphorae workshops across the island further indicate this trade (Michaelides 1996, Papacostas 2001, Demesticha 2015, Δεμέστιχα 2020, Rautman 2021). Nevertheless, concerning the Cypriot copper industry not much has been discussed concerning this period even though the copper industry may have been a major economic factor on the island as well. The metal deposits on the island have been extensively exploited from prehistoric times until the end of the 20th century C.E. and studies have highlighted the continuation of this exploitation also in Late Antiquity reaching the 8th century C.E (Steinberg and Koucky 1974, Kassianidou 2003, Georgakopoulou and Kassianidou 2013 and Socratous et al 2015). As there are not enough historical sources to shed light to the copper industry of the 4th-8th centuries C.E. archaeological research becomes the major component in investigating this period.

In this context, this thesis is trying to contribute to our understanding of the nature of the copper industry. A part of understanding the bigger picture is the ore procurement and the labor organization, e.g., in terms of being slave-based all the way to a well-paid occupation. Its administration is a third question examined here, the size of the scale and the person/ faculty/ group of people behind it. Another focus of this thesis is whether there is homogeneity of metallurgical practices across the island, for example the smelting conditions, smelting choices and expertise. Studies from around the island will be used as a comparison point. These questions will be addressed through the examination of two slag assemblages coming from two slag heaps to the east of the city of Arsinoe, the current Polis Chrysochous area. Both slag heaps are dated to the 4th-8th centuries C.E. (Socratous et al. 2015). Through the study of their microstructure and chemical nature, it is possible to compare the expertise, choices and technologies of the rest of the island's slags to understand the 'standard' of the period and appreciate the 'exceptions'. Finally, through the application of Geographical Information Systems (GIS) spatial tools, there will be an examination of the landscape around the mines and the two slag heaps, by estimating the distance

and the time needed from the mines to the slag heaps. Maybe an even more important focus in this thesis is to highlight that an interdisciplinary approach is once more used as a key in understanding the past.

Chapter 2. The copper ore deposits of Cyprus

The ophiolite of the Troodos Mountain Range, located in the center of Cyprus and comprising more than 1/3 of the island, has been the focus of a great number of scholars. The reverse stratigraphy of the Troodos Mountains is very informative on the formation of the oceanic crust and the upper mantle of Earth **(Fig. 2).**

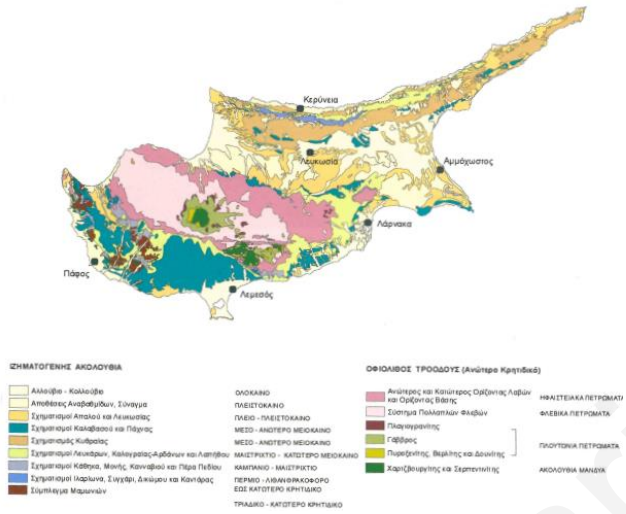

Figure 2. Geological map of Cyprus, after Κωνσταντίνου and Παναγίδης 2013: 36

One of the main aspects of this ophiolite is the very rich metal deposits around the Troodos mountains. The Troodos ophiolite is accompanied by a variety of deposits, amongst which are the copper-rich copper ores. The distribution of the copper ore deposits, of the chalcopyrite ore **(Fig. 3),** is concentrated in the upper pillow lavas, the lower pillow lavas and in the faulted contact of the basal group and the pillow lavas (Bear 1963: 41). The Limni mine and the Kinousa mines, which are the focus of this thesis, are found in the latter, i.e., the faulted contact of the basal group and the pillow lavas (Bear 1963: 41). There are two more nearby opencast mines, namely the Evloimeni/ Evlogimeni (1961-1965) and the Uncle Charles (1956-1960) mines, but neither preserves evidence of ancient exploitation (Bear 1963).There are three zones which are rich in copper ores; Zone A, Zone B and Zone C (Κωνσταντίνου and Παναγίδης 2013: 141-142). Zone A is the richest of ore deposits, with a 40-50% sulfur and 0.5-4.5% copper content and the main ores found here are pyrite (FeS_2), sphalerite (ZnS), chalcopyrite ($CuFeS_2$), marcasite (FeS_2), chalcocite (Cu_2S), covelline (CuS), bornite (Cu_5FeS_4), idaite (Cu_3FeS_4), tenorite (CuO) and cuprite (Cu_2O)

Figure 3. Ochre deposits between copper ore deposits, after Κωνσταντίνου and Παναγίδης 2013: 145.

(Κωνσταντίνου 1997: 60). Zone B has poorer sulfidic ores accompanied by amorphous silicon dioxide, but also crystalline silicon appearances, like opal (SiO_2) and jasper (SiO_2). Zone C has the poorest sulfidic ores of all, namely pyrite (FeS_2) and some chalcopyrite ($CuFeS_2$).

Figure 4. Massive copper sulfide ore from Kokkinoyia orebody (after Constantinou 1992: 338)

Figure 5. Brown umber from Skouriotissa orebody (after Constantinou 1992: 365)

Nearby or through parts of the ore deposits around the island there are appearances of ochre deposits. These deposits have a thickness between 1 and 10 meters and can be accompanied by other calcium-based deposits (Κωνσταντίνου and Παναγίδης 2013: 141**, Fig. 4).** The pillow lavas are partly covered by a basal unit layer, namely umber **(Fig. 5),** which occurs "*as sporadic lenses in depressions on the lava surface*" (Constantinou 1992: 335). Umber is much more abundant than the ochre deposits. Umber, is an iron and manganese-rich amorphous sediment with a thickness between 5 and 20 meters (Fe_2O_3 (· H_2O) + MnO_2·(n H_2O)) (Κωνσταντίνου and Παναγίδης 2013: 157). According to Bear (1963: 74) ''*The Limni ore-deposit consists of a lenticular mass of low-grade, disseminated material formed in the lower pillow lavas along a basal group footwall fault." "The ore is hard and has a siliceous gangue, the richer copper mineralization being associated with later faulting and fracturing of the ore body." "The chalcopyrite forms coarser crystals, which are molded on the pyrite in comb structure or replaces earlier pyrite. Bornite and covellite form thin coatings on the chalcopyrite and sooty secondary chalcocite is fairly widespread in the roman residues. The primary chalcocite is associated with sphalerite in the more silicious ore.*" Chalcopyrite from the Limni mine is closely associated with pyrite and is embedded in a siliceous gangue, while ochre and umber appear in or nearby the copper-ore deposits.

Chapter 3. Late Roman metallurgy in Cyprus

During Antiquity, Cyprus was one of the major copper exporters in the Mediterranean basin. Although it had been suggested in the past that the exploitation of the mines did not continue after the 4th century C.E. (Bruce 1937: 640) it is now proven that not only the production did not stop, but it was even intense reaching an industrial level (Kassianidou 2003, Georgakopoulou and Kassianidou 2013). There is a significant number of studies on Late Roman metallurgy in Cyprus. These studies were done in different decades, with different approaches and methods, some of them with analytical techniques while others were survey-based. Altogether they form a mosaic of different information. There are 11 studies exploring copper metallurgy of Late Antiquity in Cyprus; these are below organized chronologically according to the year they were published. One of the common characteristics of the Late Roman metallurgy is the manganese content evident in the bulk analysis of slags. For this reason, special attention is given to the manganese content throughout this study.

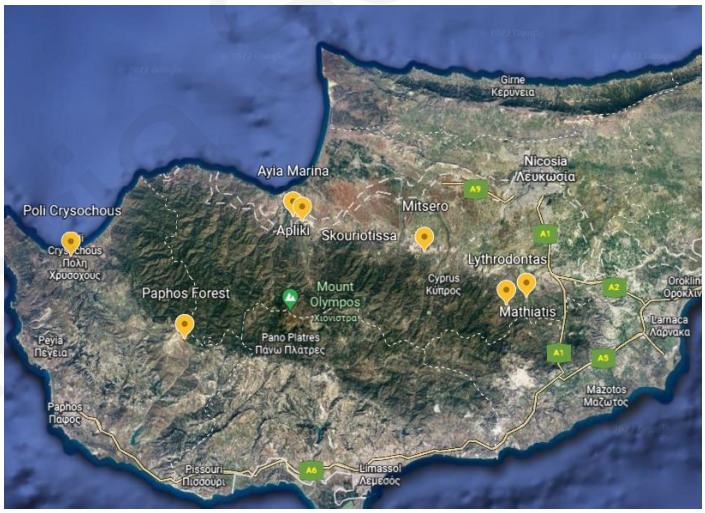

Figure 6. The map of Cyprus, with yellow are the sites mentioned in the text.

1. In 1937 a study was published by Bruce, the Resident Director of the Cyprus Mines Corporation at the time, concerning the antiquities found inside the mines. In this study the mines of a Roman/ Late Roman date included Skouriotissa, Mavrovouni, Mathiati, Mitsero (Bruce 1937) **(Fig. 6).** The only chemical analysis on slags reported came from Skouriotissa and showed a variable manganese content ranging between 0.07% to 49.5% (Bruce 1937: 643). Also, it is mentioned that at Pedoulas Forest there is a large manganiferous slag heap, without further information though (Bruce 1937: 660).

2. Apliki *Karamalos* is a settlement site located at the foothills of the Troodos Mountains, in the Nicosia District, in the vicinity of the Apliki copper ore deposit (du Plat Taylor 1952) **(Fig. 6)**. The site was excavated in 1939 and its connection with mining was evident. Based on the archaeological assemblage the settlement was dated to the Late Bronze Age. The exploitation of the mineral wealth of the ore deposit continued well into Roman and Late Roman times, according to Late Roman or Byzantine pottery found at the foot of the hill of the site near a slag heap but also according to the probable Roman timber construction of the galleries (du Plat Taylor 1952: 150)
3. A survey in the Paphos region was conducted in the early 1980s by the Canadian Palaipaphos Survey Project (CPSP) in search of the metallurgical character of the region (Fox et al 1987) **(Fig. 6)**. Through the chemical analysis carried out it was shown that among the eight sites, four of them included manganese-rich slags. The respective slags are separated into two categories. The first one is described as "*homogeneous, heavy, grey-black chunks with a surface flow structure and little surface weathering; small pores throughout*" with "*deliberate addition of manganese oxide flux, tapped fayalite-type slag with excess silica -copper sulfide ores smelted -produced by same technology as Type II".* The second category is described as '*inhomogeneous, relatively heavy, grey-black chunks; surface weathered green, yellow, rust-colored; some flow structure; tiny inclusions of refractory material and ore (?) large and small pores throughout*' and *'deliberate addition of manganese oxide flux, fayalite-type slag with excess silica; probable furnace slag - produced by same technology as Type I'* (Fox et al. 1987: Table 1).
4. The American Expedition to Idalion in the 1970s brought to light a number of metallurgical remains dating from the Late Bronze Age to the Roman period. Analyses published by Steinberg and Koucky included wet chemistry, XRF and X-Ray Diffraction (XRD) (Steinberg and Koucky 1974). They divided the slag assemblage as "Phoenician" and "Roman" according to their macroscopic characteristics, e.g., color, shininess/glassiness, corrosion. The "Roman" slags "*are black, glassy, fresh and have a flow structure*" while the "Phoenician" slags "*have weathered to a brown or red color*" (Steinberg and Koucky 1974: 153-154). They analyzed 17 slag samples and combined the data from already published studies from around the Troodos Mountain but also unpublished material from the Cyprus Mining Company (CMC) and the Hellenic Mining Company Limited (HMC).

The new analyses presented were on ores and slags from Skouriotissa, Enkomi, Hala Sultan Tekke and Agrokipia but none of them shows a significant manganese concentration, i.e., it is less than 0.2wt% (Steinberg and Koucky 1974: 163) and no further dating was indicated.

5. Zwicker (1986) published a series of ^{14}C dates from both slag heaps and ancient galleries through organic material, like charcoal, wood (sometimes containing copper) and basket remains. The Late Roman sites investigated in this study were Mathiatis (210-330 C.E), Mitsero (320-620 C.E.), Polis (215-510 C.E.), Peravasa (265-365 C.E.) and Skouriotissa (140-360 C.E.) (Zwicker 1986: 101-103).
6. A survey in the Polis region **(Fig. 6)** was conducted during the 1980s to understand the character of mining and metallurgy (Raber 1987) of different periods. Raber within the framework of his PhD thesis presented the results chronologically as follows; Iron Age, Hellenistic/ Early Roman period, Late Roman/ Byzantine and finally Late Medieval. The survey showed that concerning the Late Roman period/ Byzantine, there seem to be more smelting sites on the coastal area of Polis but also in the lower foothills of Troodos mountains of the same area. The amount of slag dating to this period was estimated to be 5700 tons (Raber 1987: 305). According to Raber (1987: 306): *'The appearance of upland sites suggests the widespread and historically-documented insecurity and absence of strong central government typical of this and the succeeding period. The combined data indicate a distinctive mode of production for this period. Smelting sites were located near villages and the town of Arsinoe rather than near the mines, suggesting that relatively small quantities of ore were being mined and transported, a conclusion supported by the production estimates. Production was apparently adapted to local supply and demand rather than to external economic or political forces. A small-scale seasonal or periodic production, using local labor and resources and oriented to a local market is indicated'.*
   The study of Raber was significant to have a first understanding of the retrospective metallurgical heritage of the Polis region and how it transforms throughout the numerous influences.
7. The Sydney Cyprus Survey Project (SCSP) took place in the 1990s and the team examined slag heaps in the north-eastern foothills of the Troodos Mountain, amongst which were two of Late Roman date in Mitsero (Kassianidou 2003) **(Fig. 6).** According to the XRF results,

the smelting technological expertise was quite advanced due to the exceptionally low copper content in the slag (below 1 wt%). It was striking how slags were crushed in generally small pieces and it was suggested that the breaking of the slags served the needs of space-management instead of indicating re-smelting the broken slags to extract the minute copper metal still trapped inside the slag (Kassianidou 2003: 223). Another important addition of this study is the varying manganese content (0.34 wt% - 45.4 wt%) and the presence of zinc, which is probably due to using chalcopyrite ores that were in contact with sphalerite indicating perhaps mining in deeper levels of the deposit (Kassianidou 2003: 226).

8. The Troodos Archaeological and Environmental Survey Project (TAESP), was another important project that focused on the metallurgy of the Troodos Mountain. In this project the team recorded three Late Roman slag heaps one at Skouriotissa and two at Ayia-Marina (Georgakopoulou and Kassianidou 2013: 240) dating between 140 – 650 C.E. 2 sigma (Manning 2013: 49). The slags were firstly studied macroscopically, then with a portable Energy Dispersive X-Ray Fluorescence (P)ED-XRF, with a reflected-light optical microscope and finally with a Scanning Electron Microscope (SEM). Macroscopically the slags are of variable size, shape and color, and analyses came to add that the copper content ranges between 0.4 wt% and 3 wt% and the manganese content between 0.1 wt% and 39.6 wt%, while some of them are suggested to come from a sphalerite ore, due to the high zinc presence (Georgakopoulou and Kassianidou 2013: 252). In the framework of the same project, Graham et al. (2006) focused on the Ayia Marina-*Mavrovouni* area of a Roman/ Late Roman date **(Fig. 6)**. The results of the survey clearly pointed towards a smelting site,

Slag heap	Sample id.	Charcoal identification	Lab. code	Radiocarbon Age BP	Calibrated age	
					1 sigma	2 sigma
MITSERO	DSH2421	*Olea europaea*	KOK24_5	2319 ± 26	BC 401 – BC 386	BC 409 – BC 362
TROULLI	DSH2423	*Olea europaea*	TROU-SI-37-3	2327±31	BC 405 – BC 384	BC 420 – BC 350
TROULLI	DSH2420	*Pinus brutia*	TROU-S2 -38-3	2257 ± 45	BC 293 – BC 230	BC 329 – BC 203
PELATHOUSA	DSH2413	*Pinus brutia*	PEL18-3b	1639 ± 29	AD 381 – AD 434	AD 339 – AD 467
PELATHOUSA	DSH2414	*Pinus brutia*	PEL22- 5	1605 ± 26	AD 484 – AD 532	AD 406 – AD 537
LIMNI	DSH2422	*Alnus orientalis*	LIM1_54_6	1512 ± 34	AD 535 – AD 605	AD 527 – AD 631
LIMNI	DSH2417	*Vitis vinifera*	LIM1-49-1	1388 ± 29	AD 634 – AD 665	AD 606 – AD 672
LIMNI	DSH2419	*Quercus evergreen*	LIM3- 17- 1	1280 ± 32	AD 680 – AD 723	AD 659 – AD 782

Table 1. The Radiocarbon dates of the charcoal coming from the slag heaps of the Woodland project, after Socratous et al. 2015: 379.

as the huge slag heaps indicate, in the vicinity of which there was a settlement. The settlement included storage, transportation, cooking and eating vessels although there were no signs of local agriculture or animal husbandry, maybe due to the poisonous sulfur gases that were produced during the smelting (Graham et al. 2006: 358).

9. "Reconstructing woodland vegetation and its exploitation by past societies, based on anthracological analysis and interpretation" is a project in the framework of which the focus was in understanding the which wood species were chosen as fuel to be used in the smelting operations. This study was done by Socratous et al. (2015) focusing at the identification and ^{14}C dating of charcoal remains in the slag heaps. The slag heaps studied were: Mitsero, Troulloi, Kalavasos, Pelathousa and Limni slag heaps. The first three date to the Classical/ Hellenistic Period while the last two to the Late Roman times **(Table 1).** The latter heaps are the focus of this thesis, to aid the understanding of the Late Roman metallurgy and socio-economic traditions characterizing the period.
10. In the framework of the Project "Camp: The Cyprus Archaeomagnetic project: High resolution dating, magnetic characterizations and archaeointensity correlation of major slag deposits in Cyprus and the Eastern Mediterranean" two slag heaps, Skouriotissa and Mitsero were studied to identify and radiocarbon date the deposits through the charcoal remains, estimate their paleointensities and study the microstructure and chemical composition with SEM-EDS. The results showed that the two slag heaps date in different periods, the Mitsero slag heap between the 7^{th}-5^{th} centuries B.C.E. and the Skouriotissa slag heap between the 4^{th} and the 5^{th} centuries C.E. (Shaar et al. 2015).
11. The most recent investigation of Roman/ Late Roman metallurgy in Cyprus was done in the framework of the "From the metalliferous sources to the citadel complex of Ancient Paphos: archaeo-environmental analysis of the mining and the built environment (MEANING) project, in the Paphos forest and Kouklia archaeological site (Iacovou 2021) **(Fig. 6)**. The results clearly point towards copper production being one of the main economic aspects of the area in this period. During the ICAS-EMME 3 conference held in Nicosia 14-18 of March 2021, Professor Kassianidou presented the analytical results which show a very high but also variable manganese content in the slag samples (Kassianidou et al. 2022).

Figure 7: The map of Cyprus, with blue are the recorded slag heaps of the island and with yellow the ones that analysis showed that are manganese rich.

The total understanding through the above studies is remarkably interesting. It seems that during the Late Roman period there is an intense exploitation of the mineral sources of the island. The past studies have marked an important number of slag heaps of mostly tap slags instead of furnace slags with a noticeable but variable manganese content. This being the case all around the Troodos Mountains, shows that copper metallurgy continued well into the Late Roman times and was not restricted to a specific part of Cyprus **(Fig. 7)**. Meanwhile, the technology seems to be quite the same across the island, i.e., advanced and homogeneous with the only difference being the presence of manganese, which does not seem to change anything in the microstructure of the slags whatsoever.

Chapter 4. The 20th century exploitation in the Limni and Kinousa Mines.

In the 20th century, the Cypriot landscape underwent serious exploitation by several mining companies. The main raw materials that were exploited were copper, pyrite, chromite, asbestos, gold, silver, bentonite, umber and ochre (Constantinou 1992). The Cyprus Mines Corporation, the Hellenic Mining Company Limited, the Berdy Mining Company Limited and the Cyprus Sulphur and Copper Company Limited are the main companies that exploited the copper ore deposits **(Fig. 8) (**Bear 1963, Maliotis 2021: 357-370).

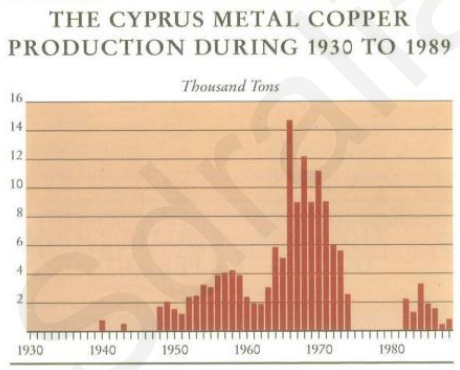

Figure 8. The Cyprus metal copper production during 1930-1989, after Constantinou 1992: 340.

The area of Limni was exploited by several different mining companies since the late 19th century, though it was not until 1937 that the first ore was produced and exported (Cullis and Edge 1927, Bear 1963:72, Maliotis 2021: 357-370). The company that widely exploited the Limni and Kinousa mines and utterly changed the landscape was The Cyprus Sulphur and Copper Company Limited. By the time the severe exploitation started, it should be noted that ancient slag and spoil heaps has already been recorded nearby both mines of Limni and Kinousa (Bear 1963: 72-76). Small and big scale operations took place in the area until 1979 in Limni (Maliotis

TABLE 25 — PRODUCTION FIGURES. CYPRUS SULPHUR & COPPER CO. LTD.

LIMNI MINE

	1937 Tons	1938 Tons	1939 Tons	1940 Tons	1941 Tons	1942 Tons	1943 Tons	1944 Tons	1945 Tons	1946 Tons	1947 Tons	1948 Tons	1949 Tons
Pyrites produced	7,586	10,752	6,302	5,116	1,263	—	45	1,994	7,300	24	—	—	—
Pyrites exported	1,642	12,007	4,649	—	—	—	—	—	4,660	—	—	2,417	—

LIMNI MINE

	1950 Tons	1951 Tons	1952 Tons	1953 Tons	1954 Tons	1955 Tons	1956 Tons	1957 Tons	1958 Tons	1959 Tons	1960 Tons	1961 Tons	1962 Tons
Ore mined	—	2,415	5,186	2,274	2,979	99,432	30,712	—	—	45,161	216,039	277,247	320,316
Ore treated	—	—	—	307	3,673	99,432	30,712	750	42,000	39,013	207,612	286,688	318,716
Cupreous pyrites produced	—	—	—	307	549	1,805	155	—	—	—	—	—	—
Cement Copper produced	—	—	—	—	—	—	—	15	339	457	49	67	59
Copper Concentrates produced	—	—	—	—	—	178	427	57	2,500	1,091	8,419	18,292	20,716
Pyrites produced	—	—	—	—	660	27,241	8,556	—	—	—	—	—	2,300
Cupreous pyrites exported	—	—	2,533	3,400	792	—	155	—	—	—	—	—	n.a.
Cement Copper exported	—	—	—	—	—	—	—	—	256	267	164	—	n.a.
Copper Concentrates exported	—	—	—	—	—	—	568	—	1,970	—	6,232	16,441	n.a.
Pyrites exported	—	—	—	—	—	7,770	11,515	9,660	6,543	—	—	—	n.a.

KINOUSA MINE

	1950 Tons	1951 Tons	1952 Tons	1953 Tons	1954 Tons	1955 Tons	1956 Tons	1957 Tons	1958 Tons	1959 Tons	1960 Tons	1961 Tons	1962 Tons
Ore mined	—	5,765	28,988	44,482	47,257	58,096	46,730	38,376	929	—	—	—	—
Ore treated	—	—	27,348	25,421	55,138	47,373	45,020	32,626	—	—	—	—	—
Cupreous pyrites produced	—	—	27,348	25,421	40,292	42,273	41,709	30,873	—	—	—	—	—
Cupreous pyrites exported	—	—	19,149	28,780	32,838	48,750	34,184	24,517	—	—	—	—	—

KINOUSA OPENCAST

	1950 Tons	1951 Tons	1952 Tons	1953 Tons	1954 Tons	1955 Tons	1956 Tons	1957 Tons	1958 Tons	1959 Tons	1960 Tons	1961 Tons	1962 Tons
Ore mined	—	—	—	—	—	—	—	39,936	90,580	71,214	27,166	—	—
Ore treated	—	—	—	—	—	—	—	39,936	56,548	—	—	—	—
Cupreous pyrites produced	—	—	—	—	—	—	—	37,733	55,085	54,434	—	—	—
Pyrites produced	—	—	—	—	—	—	—	37,733	—	16,143	—	—	—
Pyrites exported	—	—	—	—	—	—	—	29,965	—	15,187	33,175	—	—
Cupreous pyrites exported	—	—	—	—	—	—	—	29,965	61,417	71,326	—	—	—

Table 2. The production of The Cyprus Sulphur and Copper Company Limited, between 1937-1962 (Bear 1963: 73)

2021: 359). Mine exploitation boomed in the 1950s and 1960s. The mined ore in the Limni opencast mine reached a total of 7.857.614 in tons (Maliotis 2021: 359). The Kinousa mine between 1951- 1958 reached 270.623 tons and the Kinousa opencast mine between 1957-1969 reached 222.896 tons of mined ore **(Table 2)**. Since photos from the mines before their exploitation are scarce, it would be challenging to reconstruct the area of either of the mines during the Late Roman period.

The ore that was extracted from the mines was shipped through the Limni Pier which is still preserved in the Polis Chrysochous Bay in the Argaka region **(Fig. 9).** No elaborate port was created and the pier served the needs of the large-scale industry just fine. Today it is renovated but still preserves most of the 20th century characteristics.

Figure. 9: The Limni mine dock by the sea was in use between 1937-1978 (Source: ΠΕΟ Ιστορικό Αρχείο https://www.peo.org.cy/el/ypiresies/mouseio/istoriko-mouseio)

Figure 10: Strike of miners outside the administration offices of the Limni mines (Source: ΠΕΟ Ιστορικό Αρχείο https://www.peo.org.cy/el/ypiresies/mouseio/istoriko-mouseio)

The 20th century working dynamic was based on local labor of both Greek Cypriots and Turkish Cypriots. Not only in Limni and Kinousa, but also at the rest of the active mines, the working conditions were extremely bad for the workers. Although the mining companies sometimes offered some help, the wages were exceptionally low while the mining companies offered houses near the mines without basic amenities. In 1948 these grievances between the workers and the mining companies led to three big strikes by miners, asbestos workers and builders through which they demanded better working conditions (Σακελλαρόπουλος 2017: 271-276, **Fig. 10**).

Chapter 5. The two slag heaps, macroscopic examinations and description

5.1. Introduction

Both slag heaps are located near the foothills of the Troodos Mountains, east of Polis Chrysochous in the Paphos District **(Fig. 11, 12).** The slag heaps are not very close, as they have around five kilometers distance between one another. As presented before, a recent study (Socratous et al. 2015) studied the charcoal remains from the two slag heaps in order to identify both the species of trees selected to be used as fuel and suggested a date for the slag heaps through radiocarbon dating, i.e., 4th-8th centuries C.E.

Looking at the slag heaps through a Late Roman/ Early Byzantine perspective, the nearest city to the slag heaps is Arsinoe, known as Marion during the Hellenistic and Roman times. The Late Roman phase of Arsinoe has been studied, surveyed and excavated extensively by the Princeton University team (Childs 1988, Papalexandrou and Caraher 2012). Written sources of the Late Roman period describe Arsinoe as one of the bishoprics. But the bishopric of Arsinoe was of secondary importance, as indicated by the absence of the respective bishop in the Ecumenical Counsils (Μιτσίδης 2005). Not being a major city religious-wise, does not mean Arsinoe was not a once prosperous and economically important one. It has been suggested that the port of the city may have been at Latchi to the west of Arsinoe, which perhaps silted up, as no other suggested port sites which could serve the needs of the city have yet been identified (Leonard 2005: 269). Concerning the city itself, the Princeton University's excavation of ancient Marion and Arsinoe has brought to light remains of two basilicas, a Roman tetrapylon, a network of

Figure 11. The area of study and the location of Pelathousa and Argaka slag heaps and Limni and Kinousa Mines.

streets, interconnected water-channels, drains, wells, workshops, domestic establishments and overall, a built-up neighborhood (Papalexandrou and Caraher 2012). The workshops are related to metal, glass and pottery, and are all located in the vicinity of the church remains. The survey of Raber (1987) **(Fig. 13)** listed several suggested settlements and metallurgical sites in the region according to surface evidence, which gives a greater picture of the area. According to the archaeological evidence, the peak of the Late Roman city seems to be at the end of the 6th century and the first half of the 7th century. At the turn to the second half of the 7th century the island experienced the Arab conquests. Nevertheless, the surviving evidence testify that Arsinoe did not undergo much destruction by these events. (Papalexandrou and Caraher 2012: 280). To this context are added the two slag heaps which are located close to Arsinoe. One cannot but initially link the slag heaps and

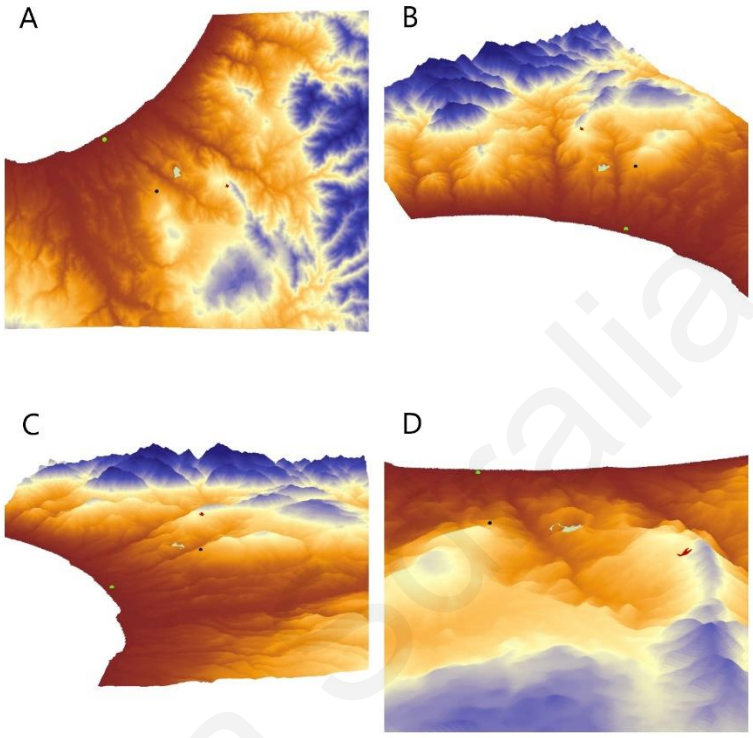

Figure 12. Map of the area from different angle created in ArcScene, Argaka slag heap (green dot), Pelathousa slag heap (black dot) Limni mine (light blue area) and Kinousa mine (red area), A) View from the top. B) view from the north-west, C) view from the east and D) view from the south

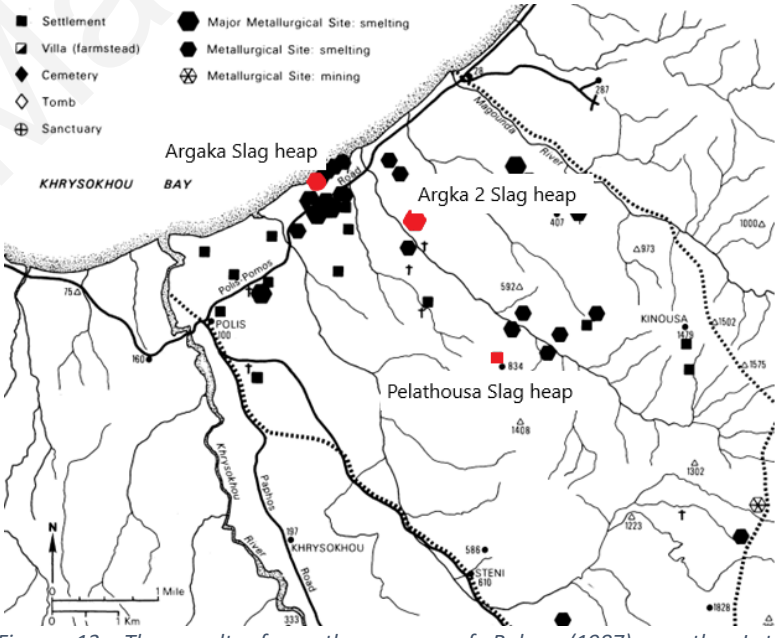

Figure 13. The results from the survey of Raber (1987) on the Late Roman/Byzantine results. Argaka slag heap, Argaka 2 slag heap and Pelathousa slag heap are indicated with red color (edited by the author).

the extensive copper exploitation to Arsinoe.

The location of the Argaka slag heap seems puzzling, being far away from mines and very close to the sea without a nearby port. Instead of suggesting the existence of a port close to the slag heap, it is preferred to highlight the close proximity of the slag heap to the main road network next to it **(Fig. 1).** On the other hand, the Pelathousa slag heap although it is not right by the mine, is much closer. To be noted that in the Limni mine one can find great number of scattered slags, without an undisturbed context though.

5. 2. The Pelathousa slag heap

The Pelathousa slag heap takes its name from the village where it is located, Pelathousa. The village is located around 1 kilometer south-west of the Limni mine. Although there have been no excavations, there has been an archaeological survey with an archaeometallurgical focus in the area. Raber (1987) includes Pelathousa in the map of the 'Late Roman/ Byzantine site distribution' but only as a settlement, without any indication of the presence of metallurgical remains **(Fig. 13)**. The next decade, Gale, Maliotis and Stos-Gale (1998) recorded a great number of slag heaps around the Troodos foothills, but they too did not include the Pelathousa one. The slag heap was first recorded in 2010 within the framework of the "Reconstructing Woodland Vegetation and its Exploitation by Past Societies, Based on Anthracological Analysis and Interpretation or WOODLAND project coordinated by Vasiliki Kassianidou. Samples of charcoal and slag were collected. The anthracological study was carried out by Maria Socratous while the slag samples are the subject of the current project. Some of the samples were used to absolutely date the slag deposit between 339 – 537 C.E (Socratous et al. 2015: 379). The original shape and consequently volume, cannot be estimated due to the lack of spatial distribution information. Satellite images do not give information either as the slag heap is not visible. Finally, during the last few years, what was left of this slag heap was covered by a wall built on the edge of a road. The

Figure 14. The section of the Pelathousa slag heap in 2010.

Figure 15. The Pelathousa slag heap in 2021 covered by a nice rock-façade.

nice façade covers completely the section of the slag heap which was visible in 2010. **(Fig. 14, 15)**.

When it comes to the estimation of the production, it is important to have correct indicators of the size and volume of a slag heap. The estimation of the size of the Pelathousa slag heap is risky. A slag heap which has not been recorded through satellite imagery or previous researchers, makes the research dependent on what is left today.

The section of the slag heap did not permit an observation of all sizes of the slags, e.g., small, medium, large slags. Nevertheless, the samples analyzed here vary between 20 cm and half a centimeter. Most slags did not have any copper mineral incrustations, but were rather black greyish and macroscopically looked alike color-wise and most were generally identified as tap slags, due to the flow texture.

5. 3. The Argaka slag heap

The Argaka slag heap is located in the Argaka region, and it is very close to the Limni pier, the same pier which was used for the exportation of the mineral wealth of Cyprus in the 20th century C.E. The slag heap was recorded by Raber (1987), Koucky and Steinberg (1989: 288) and Stos Gale et al. (1998). Aerial photos dating between 1963 until today show the gradual change of the size and appearance of the slag heap **(Fig. 16).** Nevertheless, a big part of the slag heap still survives, while some of it preserves an undisturbed stratigraphical sequence (**Fig. 17**). Modern road construction, land use and the almost fifteen hundred years that have passed, definitely made an impact

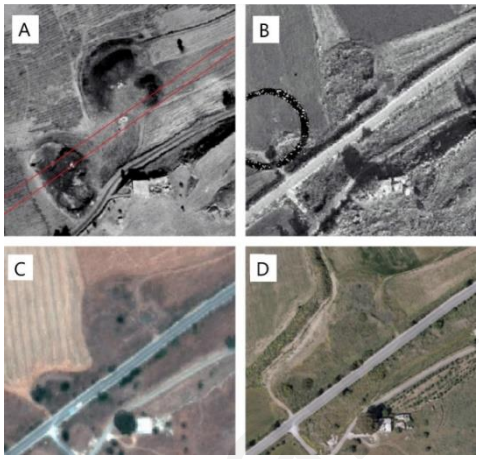

Figure 16. Aerial photos of the Argaka slag heap. A) Aerial photo taken in 1963, B) Aerial photo taken in 1993, C) Aerial photo taken in 2009-2013, D) Aerial photo taken in 2014 (Photos from the Department of Land and Surveys, https://eservices.dls.moi.gov

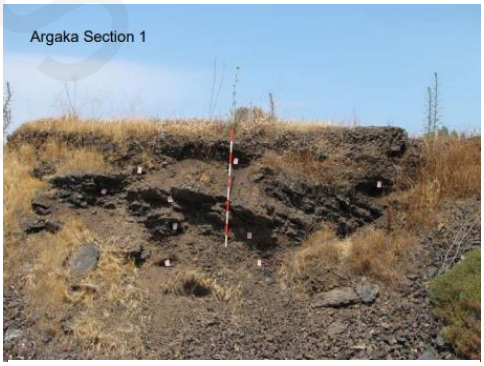

Figure 17. Section of the Argaka 1 slag heap recorded within the framework of the WOODLAND project (Kassianidou unpublished report)

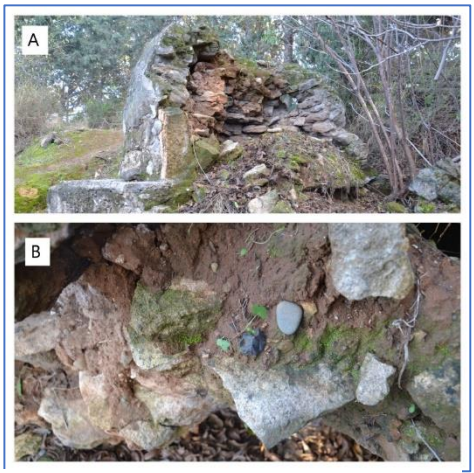

Figure 18. A) A 20th century oven in the vicinity of the Argaka slag heap, B) a detail of the section of the same oven including a piece of slag in the center of the picture.

Figure 19. Note the variety of colors in A) the Argaka slag heap, B) the vicinity of Argaka slag heap, C) the Limni Mine, D) in the Argaka 2 slag heap.

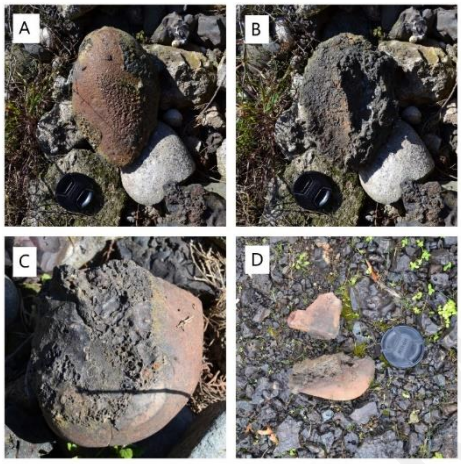

Figure 20. The slagged stones, which were once part of the furnace installations in A) Argaka slag heap, B) same as in A but the other side, C) near the Argaka slag heap and D) in the Argaka 2 slag heap.

Figure 21. The Argaka 2 Slag heap, view from south

in the exposed slag heap. Nearby the slag heap, slags can be found scattered everywhere. Inhabitants of a residency near the slag heap preserved in their plot a half-collapsed 20th century Turkish-Cypriot oven in the section of which there was a slag piece. (**Fig. 18).** This slag heap was also recorded by the Woodland project. Different sections were drawn and samples of slag and charcoal were collected (Kassianidou unpublished report). The charcoal was used to identify the species of plants used as fuel. The ^{14}C dating of three charcoal samples from stratified layers indicated a dating between 527 – 782 C.E. (Socratous et al. 2015: 379, 2 sigma probability). The central part of the slag heap has been quarried away and this has created a hole in the middle. The slag varies in size and color considerably and slagged/ molten stones make their appearance in this slag heap. There are large slag cakes typical of Late Roman slag heaps in the sections and in the debris in front of the sections **(Fig. 19, 20).**

5. 4. A nearby slag heap, Argaka 2

There is one more slag heap located in between the Pelathousa and the Argaka slag heap. It is recorded by Raber (1987) as a metallurgical site and it is also noted by the Department of Land and Surveys in the database of the Geological Survey Department. Since no name has been given, it will be referred here as the "Argaka 2" slag heap. Although no analytical approaches have been carried out in this slag heap, the slags and the igneous slagged rocks are similar macroscopically to the Argaka slag heap. Nevertheless, since there is no dating indication this slag heap is not examined in this study **(Fig. 19, 20, 21).**

5. 5. Comments

Comparing the slag heaps macroscopically one cannot help but notice that they are quite similar. Although their size cannot really be considered here due to the extensive alteration of the landscape, they all show the same variability in shape and size of their slags, all include furnace lining remains-mostly slagged/melted rock fragments- and all show the same color variability, including bluish, black-reddish and dark grey hues **(Fig. 19 and Fig. 20).**

Chapter 6. Analytical applications – Methodology

In order to characterize and interpret the assemblage of metallurgical remains, a series of different approaches were employed **(Table 3).** The first analysis was done with a HHpXRF to see the variability in chemical composition of the slag assemblage. Further on, the slag samples were prepared as polished blocks and studied under an optical microscope to understand the microstructure of the slags. Finally, a smaller group of samples were analysed with SEM-EDS in order to carry out phase characterisation and point analyses. The combination of different analytical techniques not only provides different kinds of information, but also validates the results of each method, as for example both HHpXRF and SEM-EDS are essentially quantitative and qualitative chemical analyses. There will be no discussion on ancient metallurgy studies and analysis as there is a huge amount of literature discussing the subject (For the basic understanding of slags and the past metallurgical technologies the reader is directed to some of the basic literature: Tylecote 1979, Bachmann 1982, Cradock 1995, Hauptmann 2020).

6.1. X-Ray Fluorescence

X-Ray Fluorescence (XRF) has become probably the best and most widely used non-invasive chemical analytical technique used for the investigation of archaeological material. More and more studies based on, or accompanied by, XRF highlight its intensive integration in the research, especially during the last two decades.

This integration of XRF in archaeological research is driven by the technique's four major qualities; it is economic, quick, non-invasive and portable (Shackley 2011, Shugar and Mass 2012, Hauptmann 2020: 221-22). These four qualities provide a solution to the four main problems in the study of archaeological finds. Most of the times there is a limited budget, the researcher will spend a lot of time understanding their material and even more if sample preparation is implemented, permits of invasive approaches are much more difficult to be obtained, and having an analysis done in situ or in the museum gives a whole lot more possibilities. Some examples of XRF integration in archaeological research include analysis on pigments (Mulholland et al. 2017), paintings (McGlinchey 2012), metallurgical ceramics (Davey and Edwards 2007, Ioannides et al 2016, Rademakers and Rehren 2016, Ioannides et al. 2021), slags (Kassianidou 2003, Manasse

and Mellini 2002, Kassianidou and Georgakopoulou 2013), metals (Charalambous and Kassianidou 2012, Charalambous et al. 2014, Charalambous and Webb 2020), glass (Kaiser and Shugar 2012), pottery (Aimers et al. 2012, Bezur and Casadio 2012), plasters (Crupi et al. 2015), sediment samples (Neff et al 2012), and rocks (Francesco et al. 2008, Ferguson 2012, Frahm and Tryon 2019).

On the other hand, each instrument has some limitations, and XRF makes no exception to this. The limitations of XRF are bound with the accuracy of the analysis. There is a series of methodological steps that should be followed to avoid inaccurate results. Apart from analysing a clear-cut straight and dry surface, the analysis should be done in homogeneous samples. When this is not possible, the researcher should carry out a number of analyses which will show the average values for each of the elements (Shugar and Mass 2012: 28). Furthermore, there is a range of XRF instruments, each one appropriate for a different kind of material. Hence, it is important to analyse materials which are in accordance with the XRF software, one has at their disposal. Nevertheless, there is no XRF instrument specifically manufactured to serve the examination of slags, yet. A rather recent study (Scott et al. 2016) highlighted the difficulties of calibrating an instrument to analyse slags with good accuracy.

In this project, XRF was used in order to get a first understanding on the homogeneity of the slag-based assemblage and then continue with more invasive analysis. The analysis took place at the Archaeological Research Unit of the University of Cyprus in Nicosia in November 2021. The assemblage was first cleaned to remove the surface dirt. This was followed by cutting each sample with a diamond saw to expose a clear straight surface where the analysis would take place; the samples were left to dry completely. A handheld portable InnovX Delta ED-XRF analyser (HHpXRF) was applied for the chemical analysis of the samples. The analytical mode (an InnovX term for a material-specific calibration; this is aimed at determining element contents in a silicate matrix) used was Mining Plus. The specific mode uses two beams, the first one at 10kV which excites preferentially the light elements, and the second one at 40kV which excites better the heavier elements. The instrument is equipped with a high-performance Silicon Drift Detector (SDD) with a resolution of 153-155 eV (at the Mn-Kα line), covered by a 20-mm detector window. The X-rays are emitted by a miniaturised X-ray tube, and the use of a collimator restricts the beam diameter from 10 mm to 3 mm; for this project, the selected collimator was 3 mm. Fifty-one

samples were analysed, twenty-seven for the Argaka slag heap and twenty-four for the Pelathousa slag heap. For each sample, three different measurements were taken, avoiding holes and heterogeneous features which were observed macroscopically. From the three measurements, an average was calculated to estimate the bulk composition of each sample (Table 1). The instrument's software reports elements from aluminium (Al) up to lead (Pb); elements lighter than aluminium are not detected because of the limitations of the instrument. The results are reported as weight percent (wt%) as element, based on a manufacturer-provided calibration.

6.2. Optical Microscopy

One of the most informative analytical techniques for the study of ancient metallurgy is optical microscopy. The microstructure of a slag can show the metal produced, as traces of the metal will survive in the slag, the smelting conditions, like the fluxing choices, redox conditions, type of slag and the temperatures reached, the type of the smelting operation, i.e., smelting or refining (Bachmann 1982).

In this study selected samples were further cut and prepared into 30 mm resin blocks. The samples were then ground on silica carbide pads of 180pp, 360pp, 600pp and 1200pp and polished on fabric pads of 9μm, 6μm, 3μm and 1μm. All was done on a spinning wheel at a speed of 120 spins per minute for the grinding and 300 spins per minute for the polishing stage. Between each stage the samples were sonicated to avoid cross-contamination of the abrasive and polishing powders.

The samples were prepared and studied at the Science and Technology in Archaeology and Culture Research Centre (STARC) laboratories at the Cyprus Institute in Nicosia. The optical microscope used was a Zeiss Axio Imager microscope using reflected light.

6.3. SEM-EDS

Scanning Electron Microscopy with Energy Dispersive Spectrometry has been together with optical microscopy the main keys in understanding the past metallurgical operations. The accuracy of the chemical analysis down to 0.1%, its sensitivity in detecting the light elements- compared to the XRF analysis- and the high magnification up to a few thousand times, are some of the reasons why SEM-EDS is justifiably chosen as an analysis method in past copper metallurgy

(Georgakopoulou 2004, Philaniotou et al. 2011, Georgakopoulou and Rehren 2013, Nerantzis et al. 2017, Renzi et al. 2018, Bassiakos et al. 2019).

The SEM-EDS analysis took place in the Laboratories of STARC, in the Cyprus Institute in Nicosia. The instrument used was Zeiss EVO 15 SEM equipped with an Oxford Instrument Ultim Max EDS with a 65 SDD detector. EDS analysis was carried out in high vacuum at 20 kV, 2.5nA, with a 30μm aperture and at 8.5 mm working distance (WD). The images were taken with Zeiss Zen 2 Core software.

Out of the 22 prepared polished blocks, 15 were chosen for further analysis, according to the chemical analysis by HHpXRF. The main questions addressed included phase characterisation, access to higher magnification into the samples' structure and the possible identification of tale-tell spinels or inclusions and melting points, in the case of the rock-furnace installation. Another interesting point was to compare the results from the XRF and the bulk analysis of the SEM-EDS. The polished blocks were cleaned with isopropanol and left to dry completely in a desiccator to make sure there was no humidity still in the samples. The samples were then carbon-coated to make the surface conductive. The analysis was done with a 30-second spectrum acquisition time. Homogeneous areas were chosen to determine the bulk chemical composition, while heterogeneous features and gaps were avoided. The point analyses were carried out in surfaces of more than 20μm width and depth to make sure that the analysis is clear from the surrounding features. Between three and five bulk analyses were taken for each sample and at least five for each different feature/ phase. When a feature showed heterogeneity amongst the analyses further measurements were taken.

Sample	Studied Macroscopically	HHpXRF	Polished block	Optical Microscopy	SEM-EDS
ARG001	✓	✓	✓	✓	✓
ARG002	✓				
ARG003	✓				
ARG004	✓	✓	✓	✓	
ARG005	✓				
ARG006	✓	✓			
ARG301	✓				
ARG302	✓	✓			
ARG303	✓	✓	✓	✓	
ARG304	✓				
ARG305	✓				
ARG306	✓	✓			
ARG307	✓				
ARG308	✓	✓			
ARG309	✓				
ARG310	✓	✓	✓	✓	✓
ARG311	✓	✓	✓	✓	
ARG312	✓	✓			
ARG401	✓				
ARG402	✓	✓			
ARG403	✓	✓	✓	✓	✓
ARG404	✓	✓	✓	✓	✓
ARG405	✓				
ARG406	✓				
ARG407	✓				
ARG408	✓	✓	✓	✓	
ARG601	✓				

Sample	Studied Macroscopically	HHpXRF	Polished block	Optical Microscopy	SEM-EDS
ARG602	✓				
ARG603	✓	✓			
ARG604	✓	✓			
ARG605	✓	✓	✓	✓	✓
ARG606	✓	✓	✓	✓	
ARG607	✓				
ARG608	✓				
ARG609	✓				
ARG610	✓	✓			
ARG611	✓				
ARG612	✓	✓	✓	✓	✓
ARG613	✓				
ARG614	✓	✓			
ARG615	✓	✓			
ARG616	✓	✓	✓	✓	✓
ARG617	✓	✓			
ARG618	✓	✓			
ARG619	✓				
ARG620	✓				
PEL001	✓				
PEL002	✓				
PEL003	✓				
PEL004	✓	✓			
PEL005	✓				
PEL006	✓				
PEL007	✓				
PEL008	✓	✓			

Sample	Studied Macroscopically	HHpXRF	Polished block	Optical Microscopy	SEM-EDS
PEL009	✓				
PEL010	✓	✓	✓	✓	✓
PEL011	✓				
PEL012	✓	✓	✓	✓	
PEL013	✓	✓			
PEL014	✓				
PEL015	✓				
PEL016	✓				
PEL017	✓				
PEL018	✓	✓	✓	✓	✓
PEL019	✓				
PEL020	✓				
PEL021	✓	✓	✓	✓	✓
PEL022	✓	✓	✓	✓	
PEL023	✓				
PEL024	✓				
PEL025	✓				
PEL026	✓	✓			
PEL027	✓				
PEL028	✓	✓	✓	✓	✓
PEL029	✓				
PEL030	✓				
PEL031	✓	✓	✓	✓	

Sample	Studied Macroscopically	HHpXRF	Polished block	Optical Microscopy	SEM-EDS
PEL032	✓				
PEL033	✓	✓			
PEL034	✓				
PEL035	✓				
PEL036	✓				
PEL037	✓				
PEL038	✓	✓	✓	✓	✓
PEL039	✓	✓			
PEL040	✓				
PEL041	✓				
PEL042	✓	✓	✓	✓	
PEL043	✓				
PEL044	✓				
PEL045	✓				
PEL046	✓				
PEL047	✓	✓			
PEL048	✓	✓			
PEL049	✓	✓			
PEL050	✓				
PEL051	✓				
PEL052	✓				

Sample	Studied Macroscopically	HHpXRF	Polished block	Optical Microscopy	SEM-EDS
PEL053	✓				
PEL054	✓				
PEL055	✓				
PEL056	✓				
PEL057	✓	✓	✓	✓	✓
PEL058	✓				
PEL059	✓				
PEL060	✓				
PEL061	✓	✓	✓	✓	✓
PEL062	✓	✓			
PEL063	✓				
PEL064	✓				
PEL065	✓				
PEL066	✓	✓			
PEL067	✓				
PEL068	✓	✓			
PEL069	✓				
PEL070	✓	✓			
PEL071	✓				

Table 3. Sample Catalogue including the analysis and study on each sample.

Chapter 7. Analytical applications – Results

The results are presented in the sequence of the analyses implemented and presented in the previous chapter.

7.1 X-Ray Fluorescence

The results of the HHpXRF included some elements which show a great variability, such as Al, Si, K, Ca, Mn, Fe and Cu, which give a first understanding of the differences throughout the assemblage **(Table 4).** There are two samples which were identified as 'not slag', most likely furnace wall fragments, one clay-based and an iron-rich rock.

Chemical Element	Minimum Value	Maximum Value
Al	3.3	21
Si	17.6	66.9
P	0.1	0.52
S	0.12	4.2
Cl	0.57	5.3
K	1.1	15.8
Ca	0.36	14.8
Ti	0.02	0.46
V	0.01	0.65
Cr	0.01	1.9
Mn	0.08	38.2
Fe	6.3	53
Ni	0.01	0.35
Cu	0.31	5
Zn	0.01	0.22
As	0	0.07
Zr	0	0.06
Mo	0	0.01
Sn	0.01	0.02
Sb	0.01	0.04
Pb	0	0.25

Table 5. Average values of all elements. Presented are the minimum and the maximum values for each chemical element.

The biggest variation composition-wise is the manganese content, which varies from 0.08 wt% to 38.2 wt%. Manganese has been detected in similar studies of slag from Cyprus and was found to be variable and indicative of the metallurgical operations (du Plat Taylor 1952, Bear 1963, Steinberg and Koucky 1974, Kassianidou 2003, Kassianidou and Georgakopoulou 2013). Since the major copper ore of Cyprus is chalcopyrite, manganese cannot have been associated with the ore. Therefore, it is suggested that manganese-based fluxes were used in the smelting processes (Kassianidou 2003: 226). Furthermore, since manganese is only detected in Roman/Late Roman slags it has been argued that this can be used as a trait to relatively date the slag to this period (Kassianidou 2003: 226).

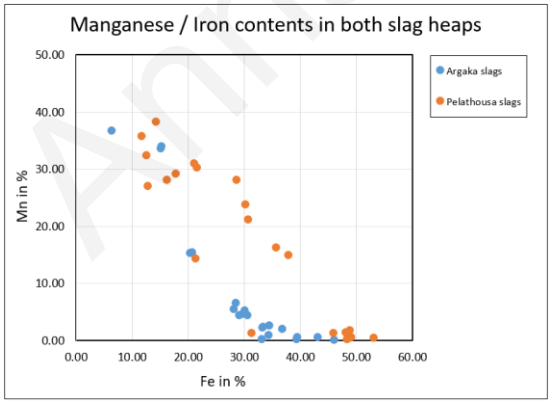

Graph 1. The manganese to iron content in the slag samples, according to the HHpXRF results.

Where manganese is present, it seems to gradually replace iron, with the two elements being

negatively correlated (**Graph 1**). The total of Mn, Fe and Si ranges between 50.9 wt% and 79.8 wt % with an average of 70.0 wt %**.** Apart from the one slag (ARG310) that has a total of 50.9 wt % which is quite corroded, the rest have a total of these three elements of at least 60 wt %.

Another element of importance in the slags is copper. The content of copper in Late Roman slags is expected to be around or below 1 wt% (Kassianidou and Georgakopoulou 2013) due to the advanced expertise of the period. In the assemblage examined here, the copper content varies between 0.31 wt % and 5 wt % with an average of 0.99 wt % which generally agrees with the previous studies. The samples exceeding 1.5 wt % of copper are PEL18 (1.9 wt %), PEL12 (2 wt %), ARG612 (2.7 wt %), ARG310 (4.2 wt %) and ARG617 (5 wt %). It is not possible to determine whether the high-copper slags, which were just mentioned, are tap slags or furnace slags, as they are very small or without any flow texture that would indicate more information.

The aluminum and potassium concentrations are also quite variable, ranging from a small percentage to 21 wt% and 15.8 wt%, respectively, without differentiating between the two slag heaps. The remaining elements seem to not vary considerably; therefore, the grouping of the samples will be based upon the element that showed the greatest variability, i.e., manganese.

The total assemblage was divided in two groups according to the manganese content, excluding the non-slag samples. Group 1, the biggest group, consists of twenty-seven slags, with a manganese content ranging between 0.08 wt% and 6.53 wt%, seventeen from Argaka Slag heap and ten from Pelathousa Slag heap. Group 2 consists of seventeen slags with a manganese content between 14.2 wt% and 38.2 wt%, 5 from Argaka Slag heap and twelve from Pelathousa Slag heap. Therefore, slags from Argaka slag heap are generally low in manganese, while in Pelathousa slag heap the slags are generally manganese-rich. The different compositional groups could show different ‘recipes’ of ore smelting. Microscopic examination and SEM analysis will shed more light on the microstructure and phase characterization of the slag assemblage.

7.2. Optical Microscopy

The study of the assemblage verified that almost all slags are copper smelting ones, while there are two samples related with the furnace construction, a piece of clay furnace lining and a molten stone, once a part of the furnace installations. The microstructure of the slags is quite similar across the assemblage, containing copper matte prills, olivine crystals and sometimes free iron oxides in a glassy matrix. A detailed description of each sample is given in **Appendix 3**.

The copper matte is generally a copper-rich sulfide, and in most slags more than one copper matte phases are present showing the transformation from chalcopyrite to metallic copper **(Fig. 23)**. Copper metal prills are generally absent (**Fig. 24)**. Nevertheless, there is one slag sample which contains mostly metallic copper prills, with some traces of copper matte prills, PEL18 (**Fig. 25**). The microstructure of this slag is also quite different, with a glassy matrix and hardly any crystalline structure of what probably is pyroxene crystals, and no free iron oxides whatsoever. Another copper matte rich slag is similar to PEL18, concerning the absence of crystalline structure, but has hardly any metallic copper prills is ARG616 **(Fig. 26).** Both slags belong to Group 2, i.e., high manganese content. The absence of crystalline structure indicates an extremely quick cooling down of the slags. More questions arise for PEL18 though, since one would expect the copper metal, being heavier than the rest of the gangue of the ore, would not remain in such quantities in the slag matrix. Instead, copper matte would be much more easily trapped since it is lighter that copper metal,

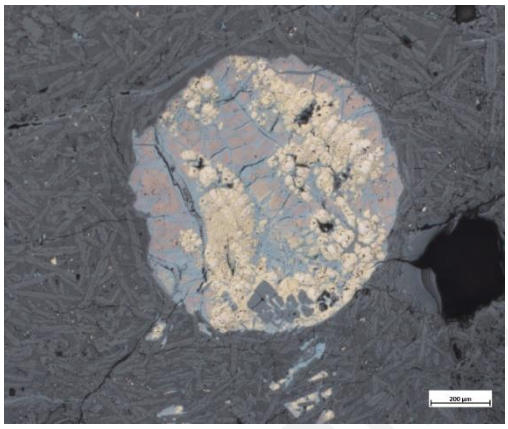

Figure 23. A copper matte prill from sample ARG404 with phases of different copper-sulfur composition. The yellow part is more sulfur rich, while the reddish-blue parts are more copper rich. Olivine crystals (light grey) in the glassy matrix (dark grey).

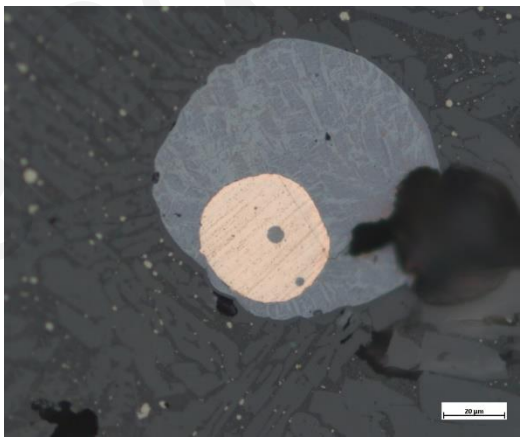

Figure 24. A copper matte prill (blue) with copper metal (orange) in the center in an olivine background (light grey crystals) and a glassy matrix (dark grey) from PEL28.

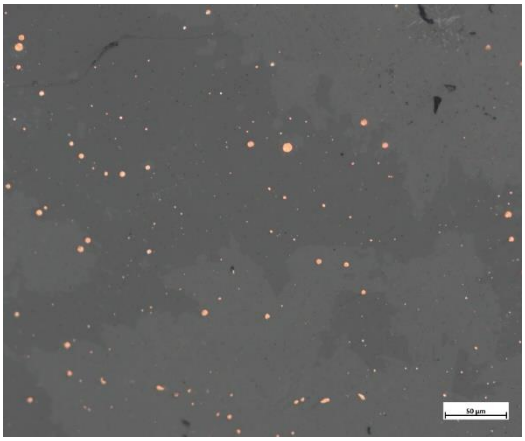

Figure 25. Sample PEL18 with frequent small copper metal prills (orange) in a matrix that is composed of pyroxenes (light grey) in a glassy matrix (dark grey).

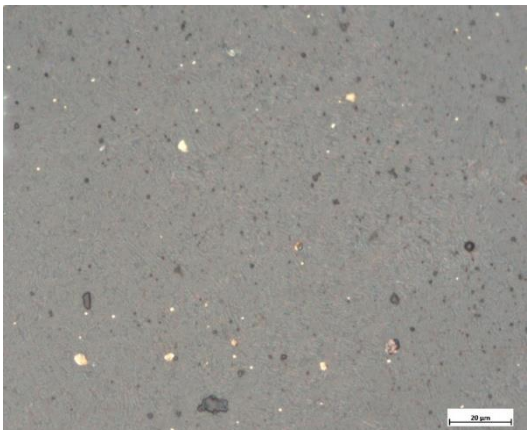

Figure 26. Sample ARG616 with frequent small copper metal prills (orange) in a matrix that is comparted by thin crystals (light grey) in a glassy matrix (dark grey).

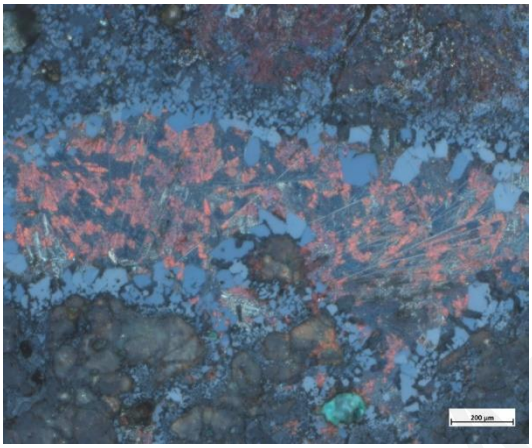

Figure 27. Sample ARG612, free-iron oxides (bluish-grey angular), cuprite (red), delafossite (light grey laths in the cuprite-rich area) (PL).

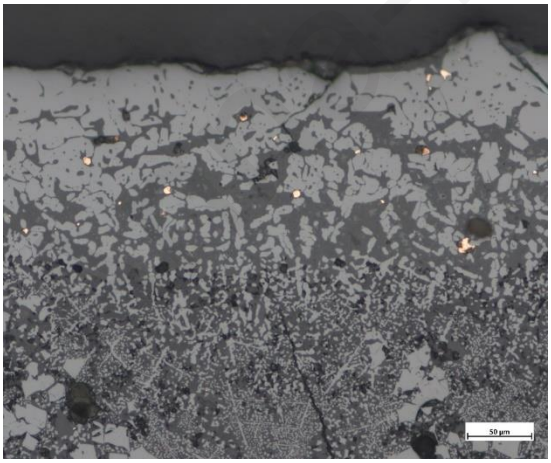

Figure 28. Sample ARG612, small prills of copper metal (orange), free-iron oxides (light grey) in a glassy matrix (dark grey).

nevertheless there is none. The absence of sulfidic phases may indicate a dead roasting stage and not a partial one before the smelting for this slag sample. The rest of the assemblage shows a variety of copper matte phases, phases very close to the actual ore all the way to almost metallic copper. Maybe different ore treatment before the smelting is the key to answering the different sulfidic phases.

The olivine crystals are always elongated and skeletal, testifying for a rapid cooling, i.e., tap slags. Free-iron oxides are generally absent with a few exceptions. Four slag samples (ARG004, PEL10, PEL12, PEL38) have free-iron oxides of globular shape, sometimes in dendritic formations, most probably wüstite (FeO) and only one (ARG612) has more angular free-iron oxides, maybe magnetite. The presence or absence of magnetite shows the redox conditions in the furnace, The samples investigated show that the atmosphere in the smelting furnace was almost exclusively reducing. Sample ARG612 is a one-of-a-kind sample in this assemblage, which preserves clear indications of copper-rich oxides like cuprite (Cu_2O) and delafossite ($CuFeO_2$) **(Fig. 27 and Fig. 28**).

The two pieces of furnace wall, ARG001 and ARG403 were studied under the microscope as well. ARG001 did not preserve any slag remains, but it was possible to see the gradual transformation of the melted rock from one side to the other. The Fe-rich rock in the melted part showed free iron oxides. The

clay piece, once serving as furnace lining, is heavily tempered and preserves a significant number of copper-matte and copper-metal inclusions mostly in the vitrified area.

7.3. SEM-EDS

With the addition of the SEM-EDS analysis, it was possible to both study the samples and acquire photos under a great magnification and carry out accurate analysis for phase characterization. The main phases identified in the assemblage were free-iron oxides, olivine crystals, pyroxene crystals, copper-matte and metallic copper (**Appendix 4**).

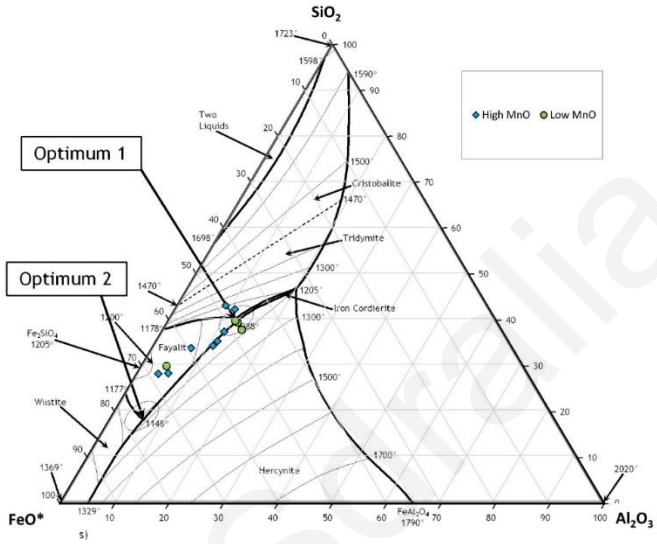

Graph 2. Ternary diagram of FeO, SiO2 and Al2O3 with the slag assemblage, note that most of them are located in the "Optimum 1" area.

1. Six out of thirteen slags preserve free-iron oxides which are always wüstites (FeO) as a result of excessive iron content from the ore and not any surplus of silica to create fayalite/ knebelite crystals. ARG612 has free-iron oxides, but magnetite, $(FeO)(Fe_2O_3)$ or Fe_3O_4, which indicates oxidizing conditions. This sample was the sole example of such a microstructure, characterized by great heterogeneity.
2. The olivine crystals are present in all but one slag samples and are fayalite, knebelite, tephroite and their in-between phases **(Appendix 4, Table 9).** They behave in the same way, creating nice elongated skeletal crystals. The presence of manganese may originate either from the ore or from the flux. Since there is no Mn-Cu ore in Cyprus, it is suggested that the manganese comes from the flux. Two samples (PEL57 and PEL61) preserved MnO or MnO_2 remains that could once more indicate the fluxing origin of manganese in the slags.
3. Pyroxenes are present in only three samples, ARG616, PEL18 and PEL61 **(Appendix 4, Table 10).**
4. Copper-matte, as noted in the optical microscopy section, is evidenced in all samples and shows a great variability in the relation of S-Fe-Cu, changing quite a lot in chemical composition even within the same sample **(Appendix 4: Table 11).**

5. Metallic copper is present in five out of thirteen slags analyzed and is quite pure, with some minor presence of iron, manganese and sulfur **(Appendix 4: Table 12).**

Most slags reached the optimum melting point of temperature at 1088 °C (**Graph 2**). This indicates the standardization of the smelting conditions inside the furnace. It is interesting to note that slags coming from both slag heaps, either of low or high manganese content, are generally under the same pyrotechnological conditions, temperature and atmosphere.

Table 4. The average of the results from the HHpXRF analysis presented in wt %.

Sample	Al	Si	P	S	Cl	K	Ca	Ti	V	Cr	Mn	Fe	Ni	Cu	Zn	As	Zr	Mo	Sn	Sb	Pb
ARG 001	12,4	38,9	ND	0,12	ND	3,7	7,6	0,27	0,05	ND	5,5	12,5	0,01	0,45	0,22	ND	0,00	ND	0,02	0,04	0,02
ARG 004	18,4	30,8	ND	0,73	0,68	2,9	10,3	0,19	0,06	ND	4,3	30,5	0,06	0,78	0,01	ND	0,01	0,00	ND	ND	0,01
ARG 006	20,3	30,2	ND	0,77	ND	2,2	6,1	0,17	0,03	ND	0,18	39,4	ND	0,31	ND	0,01	0,00	ND	ND	ND	ND
ARG 302	19,9	29,9	ND	1,6	ND	2,9	6,9	0,15	0,05	0,33	2,6	34,4	0,02	1,3	0,02	ND	0,01	ND	ND	ND	0,08
ARG 303	7,62	23,3	0,29	1,2	ND	3,1	7,2	0,33	0,21	ND	33,9	15,2	0,14	0,81	ND	ND	0,04	0,01	ND	ND	ND
ARG 306	18,7	26,3	ND	1,1	ND	1,6	4,6	0,12	ND	ND	0,50	43,0	ND	0,46	0,17	0,01	ND	ND	ND	ND	ND
ARG 308	15,4	34,3	ND	0,36	ND	4,6	10,8	0,17	0,05	0,02	5,5	28,2	0,06	0,34	0,03	ND	0,01	ND	ND	0,01	0,03
ARG 310	3,3	16,9	ND	0,27	1,97	4,2	3,9	0,26	0,13	ND	36,7	6,3	0,10	4,2	0,13	ND	0,04	0,00	ND	ND	0,13
ARG 311	7,8	19,9	ND	1,3	ND	3,7	4,0	0,30	0,12	ND	33,5	15,1	0,14	0,66	ND	0,01	0,06	ND	ND	ND	ND
ARG 312	14,9	17,6	ND	4,2	ND	1,1	7,9	ND	0,05	ND	0,17	33,1	0,02	4,9	0,03	ND	ND	ND	ND	ND	ND
ARG 402	15,8	39,8	ND	0,38	ND	2,9	2,9	0,12	0,06	0,02	4,6	29,6	0,05	0,54	ND	ND	0,01	ND	ND	ND	0,01
ARG 403	10,3	30,5	ND	1,2	ND	7,4	0,58	0,46	0,02	0,02	0,59	9,5	0,01	2,8	0,02	ND	0,02	ND	0,01	0,02	0,25
ARG 404	17,2	28,5	ND	2,6	ND	15,8	6,1	0,24	0,03	ND	2,3	33,3	0,04	1,3	0,05	ND	0,01	ND	ND	ND	0,03
ARG 408	15,7	25,3	ND	0,53	ND	2,1	12,8	0,21	0,03	ND	0,89	34,3	0,02	0,49	0,03	ND	0,01	0,01	ND	ND	0,08
ARG 603	19,3	31,0	ND	0,49	ND	3,7	9,3	0,20	0,05	ND	5,2	30,0	0,06	0,34	0,02	0,00	0,01	ND	ND	ND	ND
ARG 604	20,7	27,4	ND	1,0	ND	2,9	7,0	0,19	0,04	ND	0,56	39,4	ND	0,33	ND	ND	0,00	ND	ND	ND	ND
ARG 605	19,1	32,9	ND	0,83	ND	2,8	7,3	0,23	0,05	ND	2,2	33,3	0,35	0,42	ND	ND	0,01	ND	ND	ND	0,01
ARG 606	17,8	27,3	0,52	0,64	ND	2,8	11,1	0,18	0,02	0,02	1,9	36,8	0,19	0,31	ND	0,07	0,01	0,01	ND	ND	ND
ARG 610	18,3	30,8	ND	0,77	0,66	2,9	10,4	0,19	0,06	ND	4,3	30,5	0,06	0,79	0,01	ND	0,01	0,00	ND	ND	0,01
ARG 612	14,8	33,6	0,35	0,27	0,57	1,1	0,36	0,05	0,01	ND	0,08	46,0	ND	2,7	0,02	0,02	ND	0,00	ND	ND	ND
ARG 614	11,4	33,0	ND	0,46	ND	3,3	7,9	0,21	0,08	ND	15,3	20,3	0,09	0,42	ND	ND	0,02	ND	ND	ND	0,01
ARG 615	16,2	33,6	ND	0,35	ND	3,8	10,0	0,23	0,65	0,02	6,5	28,5	0,07	0,34	ND	ND	0,01	ND	ND	0,02	ND
ARG 616	12,4	34,3	ND	0,43	ND	3,2	7,8	0,22	0,07	ND	15,4	20,6	0,09	0,40	0,01	ND	0,02	ND	ND	0,01	0,01
ARG 617	9,8	26,2	ND	1,2	5,3	2,9	1,9	0,14	0,04	1,9	1,9	15,1	0,03	5,0	ND	ND	0,01	0,01	ND	0,02	0,02
ARG 618	14,7	27,8	ND	0,84	1,4	3,5	8,9	0,14	0,04	0,01	4,3	29,1	0,05	4,0	ND	ND	0,01	ND	ND	ND	0,01
ARG stone	ND	66,9	ND	0,26	1,6	2,1	ND	ND	0,05	0,01	0,02	0,63	ND	0,02	ND	0,01	ND	0,01	0,01	0,02	0,00

Sample	Al	Si	P	S	Cl	K	Ca	Ti	V	Cr	Mn	Fe	Ni	Cu	Zn	As	Zr	Mo	Sn	Sb	Pb
PEL 04	20,0	23,0	ND	1,9	ND	3,9	0,54	ND	ND	0,02	0,60	49,0	ND	0,59	0,15	0,01	ND	ND	ND	ND	ND
PEL 08	19,2	21,3	0,34	1,4	4,0	3,5	ND	0,06	ND	0,03	0,70	48,5	ND	0,57	0,21	0,01	ND	ND	ND	ND	ND
PEL 10	14,0	24,4	0,26	3,5	ND	1,2	2,2	0,11	0,12	ND	14,9	37,9	0,25	0,85	0,06	0,01	0,00	0,01	ND	ND	ND
PEL 12	5,3	21,0	0,12	0,98	ND	1,3	4,5	0,16	0,07	ND	32,3	12,6	0,12	2,0	ND	ND	0,02	ND	ND	ND	ND
PEL 13	9,4	26,1	0,41	2,1	ND	2,4	3,8	0,22	0,12	ND	31,0	21,0	0,18	0,81	0,05	ND	0,01	0,01	ND	ND	0,04
PEL 18	12,2	37,3	ND	ND	ND	2,4	8,5	0,08	0,06	ND	14,2	21,3	0,09	1,9	ND	0,01	0,00	ND	ND	ND	ND
PEL 21	8,6	27,3	ND	0,98	ND	4,3	11,2	0,23	0,11	ND	28,1	16,2	0,11	0,63	0,03	ND	0,03	0,00	ND	ND	0,19
PEL 22	3,9	19,5	0,28	1,2	ND	3,9	5,3	0,19	0,09	ND	38,2	14,3	0,15	0,61	0,04	ND	0,03	ND	ND	ND	ND
PEL 26	20,0	21,8	0,27	2,3	ND	3,6	0,36	0,02	ND	0,01	1,7	48,8	0,04	0,64	0,15	0,00	ND	0,01	ND	ND	ND
PEL 28	8,3	27,9	0,27	1,2	ND	5,5	3,3	0,20	0,11	ND	30,2	21,5	0,20	0,81	0,11	0,01	0,04	ND	ND	ND	ND
PEL 31	17,4	34,5	ND	0,79	ND	7,7	6,2	0,10	0,03	0,03	1,2	31,2	0,01	0,42	0,13	0,01	0,00	ND	ND	0,01	ND
PEL 33	9,9	24,2	ND	1,00	ND	5,8	7,9	0,18	0,07	ND	29,1	17,7	0,14	0,49	0,03	0,01	0,04	ND	ND	ND	ND
PEL 38	13,7	24,6	0,41	1,7	ND	4,2	1,3	0,16	0,10	ND	21,1	30,7	0,23	1,3	0,10	0,01	0,03	0,00	ND	ND	ND
PEL 39	20,6	23,6	0,12	2,1	ND	3,2	ND	ND	ND	ND	1,4	48,0	0,08	0,57	0,12	0,01	ND	0,00	ND	ND	ND
PEL 42	20,2	21,5	0,14	2,6	ND	2,8	1,9	0,04	ND	0,03	0,64	48,8	0,02	0,97	0,11	0,01	ND	0,00	ND	ND	ND
PEL 47	19,9	23,4	0,40	1,9	1,27	3,6	1,2	0,06	ND	0,02	1,2	45,8	ND	0,54	0,12	ND	ND	0,01	ND	ND	0,05
PEL 48	21,0	23,8	0,32	1,7	ND	3,6	ND	ND	ND	ND	0,21	48,4	0,03	0,51	0,19	0,01	ND	0,00	ND	ND	ND
PEL 49	16,3	23,6	ND	2,5	ND	3,2	0,95	0,11	0,06	ND	16,2	35,7	0,25	0,67	0,10	0,01	0,02	0,01	ND	ND	ND
PEL 57	19,6	22,6	0,41	2,0	ND	5,0	ND	0,07	ND	0,01	0,47	48,8	ND	0,50	0,17	0,01	ND	0,00	ND	ND	ND
PEL 61	9,9	30,4	ND	ND	ND	2,7	14,8	0,20	0,07	ND	26,9	12,8	0,08	1,4	ND	ND	0,01	ND	ND	ND	ND
PEL 62	10,8	21,1	ND	0,94	ND	3,7	3,4	0,12	0,08	ND	28,1	28,6	0,26	0,53	0,08	0,01	0,02	ND	ND	ND	ND
PEL 66	19,4	20,2	0,10	2,5	ND	3,1	ND	0,02	ND	0,02	0,40	53,0	0,04	0,49	0,16	0,01	ND	ND	ND	ND	ND
PEL 68	10,0	21,6	0,16	1,7	ND	2,9	5,1	0,17	0,07	0,01	23,7	30,1	0,22	0,59	0,10	0,01	0,03	0,00	ND	ND	ND
PEL 70	5,4	19,2	0,44	1,2	ND	5,4	3,0	0,23	0,13	ND	35,81	11,6	0,10	1,0	0,04	ND	0,04	ND	ND	ND	ND

8. Application of Spatial Tools of Geographical Information Systems in estimating the cost of the raw material procurement

8. 1. Geographical Information Systems (GIS) in Archaeology

Geographical Information Systems (GIS) have been increasingly implemented in the archaeological domain showing the potential in terms of their spatial analyses. GIS provide a wide range of analyses that can aid archaeological research in a number of distinct aspects. One of the main spatial analyses used in this field is the Least Cost Path analysis (LCP) (Neubauer 2004). This analysis estimates the `best´ path (in terms of the cost, meaning effort) moving from point A to point B. The parameter which defines the `best´ route depends on the research questions. A good path could try to avoid extreme slopes, lakes and rivers, or even be based upon using water bodies if boats are also offered as a means of transport. For example, studies on LCP considered archaeological evidence verifying that specific paths were chosen not only based on the distance but also at the degree of slope (Güimil-Fariña and Parcero-Oubiña 2015). LCP has earned quite some attention in archaeology to estimate routes, preferences and how the landscape can affect past choices (de Soto 2010, Parcero-Oubiña et al 2013).

The application of GIS can help in investigating the connection between the two slag heaps and the two nearby mines that are the focus of the particular research. The two mines, i.e., Limni and Kinousa, are located on the foothills of the Troodos mountains, but not in the proximity of the respective slag heaps. The Pelathousa slag heap is in close vicinity of the Limni Mine at around a kilometer-long distance, but near the Argaka slag heap the nearest mine is exceeding 5 kilometers. Since the Late Roman organization of the mines is still to be investigated, it is important to explore the reasons behind the location of the Argaka slag heap so far away from the mine, meaning that a lot more labor had to be invested to move the heavy ores.

The questions addressed through GIS are the following:

- What is the distance between the slag heaps and the mines?
- What is the best path to reach the mine and how much time does each path take?
- Why is the Argaka slag heap located far from the mines and near the coast?

8.2. Methodology

Applying an essentially software-based tool in understanding past societies can be tricky and caution is needed. The three factors of importance to implement accurate Least-Cost-Path analyses are first the estimation of the actual beginning and ending of each route, then accessing a rather accurate Digital Elevation Model (DEM) and finally following every step correctly in the software itself.

8.2.1. Estimating the actual areas of the slag heaps and mines

The first step in estimating the least cost paths, is to delineate the areas of interest, i.e., the exact areas the two slag heaps and the two mines cover. Landscapes change constantly, even more anthropogenic landscapes that never rest in time. Slag, although is considered a waste by-product, found its way to be useful in our contemporary society. The hardness and refractoriness of slag made it quite suitable in road making. Thus, slag was systematically quarried and as a result most slag heaps were reduced in size, without preserving their original form (Bear 1963, Kassianidou et al. 2021: 993). One thing to note is that what we see today are the remains of the slag heaps, not their original size. The actual size of a slag heap implies the extent of the production and even pinpoints separate phases, dating, expertise etc. The same holds true for the mines. The current view of a mining landscape does not in any way represent the ancient one in question, even more when there is evidence of the extensive exploitation taking place by CCSC Ltd in the area during the 20th century (Chapter 4).

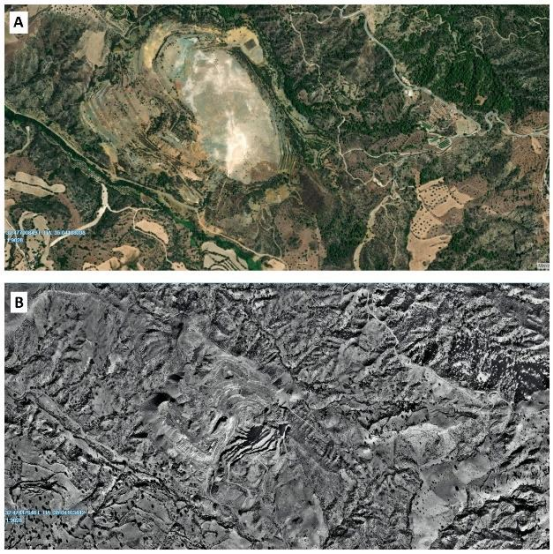

Figure 29. Aerial photos of the Limni mine. A) Aerial photo taken in 2014, B) Aerial photo taken in 1963 (Photos from the Department of Land and Surveys, https://eservices.dls.moi.gov.cy/#/national/geoportalmapviewer)

For these reasons, a comparison among a number of aerial images gave some indications concerning the change of the landscape during the 20th-21st centuries. This methodology was used again in Cyprus by Kassianidou et al. (2021) to estimate the change of the size of the slags. Concerning the slag heaps, the Argaka shows noticeable changes through time. The Argaka slag heap used to be much bigger than what is preserved today, while at the same point between 1963 and

1993 there is a new road cutting the slag heap into two pieces **(Fig. 16).** The Pelathousa one is not discernibleat all in any of the aerial photos.

Concerning the mines, the landscape around the Limni mine shows significant alteration. The changes in the Limni mine are most noticeable if one looks at aerial photographs of the area taken between 1963 and 2022 **(Fig. 28).** Ideally, the comparison should be made between today and right before the first modern exploitation of the site, something that is impossible since the Limni opencast and underground mine exploitation started between 1925-1979 (Maliotis 2021: 38). The Kinousa underground mine was worked for a few years between 1951-1958, but unfortunately the oldest photo available is dated to 1963, so there is no photographic evidence to show how Kinousa used to be before CCSCLtd exploited it. There are two more nearby opencast mines, namely the Evloimeni/ Evlogimeni (1961-1965) and the Uncle Charles (1956-1960) mines, but neither preserves evidence of ancient exploitation (Bear 1963).

8.2.2. Choosing an accurate DEM

Another important parameter is to rely on an accurate enough Digital Elevation Model (DEM). A DEM is a computer-based representation of the elevation of an area. A DEM is usually constructed based on Light Detection and Ranging (LiDAR) measurements, topographic measurements, aerial stereo images or even satellite imagery (https://www.usgs.gov/faqs/what-digital-elevation-model-dem). In our case, the DEM used was based on aerial stereo-photos from the Cyprus Lands & Surveys Department with a 20-meter accuracy.

It is of course plausible to ask at this point whether the recent DEM can correspond to the Late Roman Polis Chrysochous landscape. The answer is quite challenging as one needs to bear in mind all the alterations on the landscape, both environmental and anthropogenic. Earthquakes, flooding episodes, landslides, tsunamis, etc. are just some of the environmental factors influencing the terrain. Anthropogenic alterations include raw material exploitation, cultivation practices such as field terracing and levelling, and other large-scale construction works. Despite the limitations of our knowledge to address all these changes explicitly, we assume that the recent terrain depicts, in a large degree, the landscape of the Late Roman Polis Chrysochous region. The DEM will be primarily used to estimate the minimum effort (cost) in terms of travelling a certain distance on the terrain. Since no other archaeological evidence exists as nodes of reference along particular paths, the analyses will be mostly based on the slope criterion.

8.2.3. Least Cost Path Analysis

Having delineated all four points of interest, it was possible to apply spatial analysis in the respective software, ArcMap (version 10.8.1), to estimate the best paths from each of the slag heaps to each of the mines. The "best path" factor in determining a route in this study, is based on the slope of the surface. The less abrupt slope, the easier the path since slope demands much more effort and time. Assuming that human agents avoided abrupt slopes the most efficient paths were defined.

All the information was added to the ArcMap software. The mines were the starting points, and the slag heaps the destinations. The first step was to estimate the slope of the area of interest according to the Digital Elevation Model (DEM). Slope is measured either in angle degrees or percentage and shows in the inclination of the terrain. The second step was to estimate the Path Distance according to the slope, which estimates what the angle degree is from point A to all other points (pixels) of the area of interest.

One of the most important analyses done was estimating the time needed for each path with walking. This was done by introducing Tobler's hiking function. Tobler's hiking function is a table created by the geocartographer Waldo R. Tobler (Tobler 1997) who calculated the time needed per second to move along all different angles (between –90 and +90 degrees) within the terrain.

The next step was to estimate the Back Link surface based again on the slope. Back Link calculates the direction of a movement from point A to the rest of the surface, e.g., right, left, up, down, up-left, up-right, down-left and down-right. The last step was to calculate the Cost Path according to the Slope, the Path Distance and the Back Link from each destination point (https://pro.arcgis.com/en/pro-app/latest/tool-reference/spatial-analyst/understanding-cost-distance-analysis.htm).

8.3. The results

The results include four different paths, starting from either of the mines to each of the slag heaps. The distance and time of each path are summarized in **Table 6**. The estimated time is based exclusively on Tobler's hiking function. The estimated time in the table is accepted as the minimum value, namely the minimum time someone will need to walk from point A to point B

without encountering any natural obstacles or passing through specific points of interest like nearby villages, rivers or lakes.

Cost Path	Starting Point	Destination	Distance in meters	Estimated walking time in minutes
1	Limni mine	Argaka slag heap	5,034	59
2	Limni mine	Pelathousa slag heap	1,169	23
3	Kinousa mine	Argaka slag heap	8,037	87
4	Kinousa mine	Pelathousa slag heap	3,814	55

Table 6. The results from all the paths summarized, including the starting and destination points, distance in meters and estimated walking time.

8.3.1. Least Cost Path 1

The first path starts from the Limni mine and ends at the Argaka slag heap **(Fig. 30).** The distance was calculated to be 5,034 meters. The slope is between 0 – 6 degrees, making it quite an easy route. The minimum time spent on that is estimated to be 59 minutes.

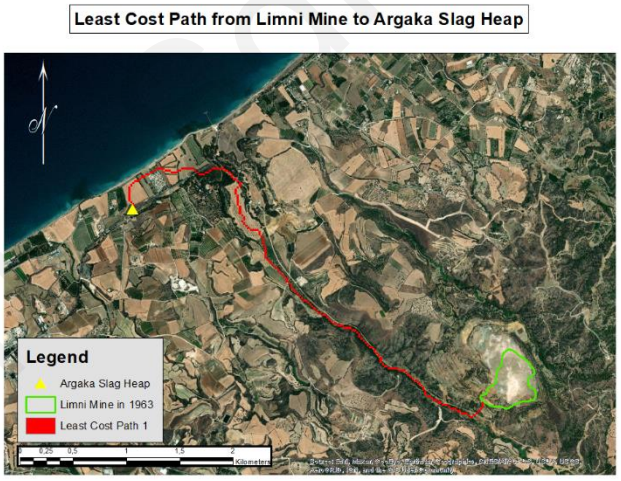

Figure 30. Least Cost Path 1 from the Limni Mine to the Argaka slag heap.

8.3.2. Least Cost Path 2

This path starts from the Limni mine and goes to the nearby –contemporary- village, to the Pelathousa slag heap **(Fig. 31).** It is 1,169 meters long, making it the shortest path examined here. Time wise, this should take abound 23 minutes. In fact, being at the slag heap of Pelathousa, one has a close visual contact with the Limni Mine. Unfortunately, the Pelathousa slag heap is severely affected by modern constructions

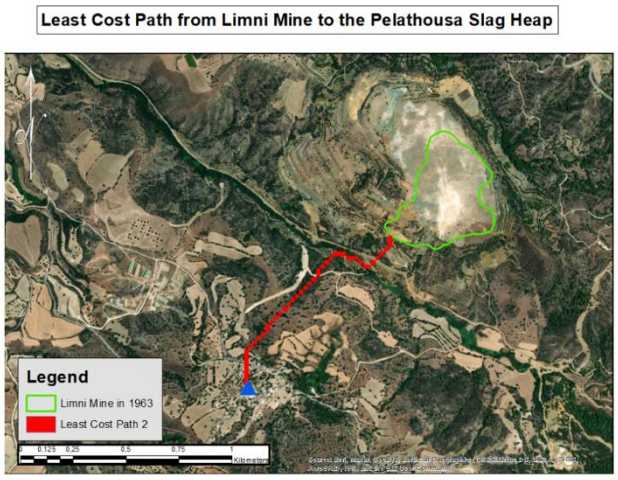

Figure 31. Least Cost Path 2 from the Limni Mine to the Pelathousa slag heap.

and thus it is really hard to investigate the actual size of the slag heap and its relevance with other archaeological evidence.

8.3.3. Least Cost Path 3

The third path from the Kinousa Mine to the Argaka slag heap is the longest one, a total of 8,037 meters **(Fig. 32).** It should be noted that half of it, is identical to Cost Path 1, showing that even further to the mainland it is 'cheaper' to choose this way over following a more northern path. This route would take about 87 minutes.

Figure 32. Least Cost Path 3 from the Kinousa Mine to the Argaka slag heap.

8.3.4. Least Cost Path 4

The last path examines the connection between the Kinousa Mine and the Pelathousa slag heap **(Fig. 33).** The total time of this route is estimated to take about 55 minutes, having a length of 3,814 meters.

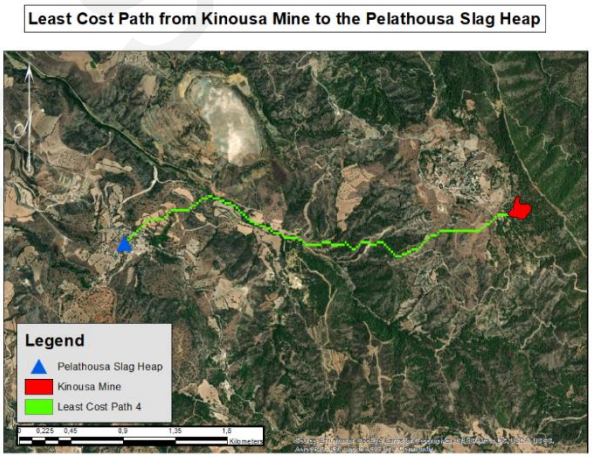

Figure 33. Least Cost Path 4 from the Kinousa Mine to the Pelathousa Slag heap.

8.4. Discussion

The paths calculated are based on the cost-effort human agents are investing. Here, the *easiness* of a path is based on the slope, namely the angle of the surface, and it is understood that more parameters can make a path more difficult apart from the slope. In this thesis, I tried to introduce least cost path analysis to understand the choices of the locations of the slag heaps. As it seems, three out of four routes take less than an hour. It is important to say here that we do not know if all mines were exploited at the same time. Radiocarbon dating (Zwicker 1986: 102, Socratous et al. 2015: 379) showed that the Argaka slag heap is dated between 215 – 510 C.E. and 527 – 782 C.E. The Pelathousa slag heap is dated a bit earlier, 339 –537 C.E., according to the calibrated age of 2 sigma (Socratous et al. 2015: 379).

The ^{14}C was done in specific parts of the slag heaps and of course they might extend more in the past or in the future, but surely during the Late Roman period there is active metallurgy in both slag heaps. We could not go on and estimate the socio-political background of the period since the period discussed extends over four centuries, with each ^{14}C date extending sometimes for more than 100 years. The approach here is more practical, in understanding the effort invested following each path. Two points are also taken for granted, namely that there are no other mines in the area, so the slag heaps should come from these mines, and that the slag heaps are created in the Late Roman period. Lead Isotope Analyses were carried out from both mines throughout the 20th century by Stos-Gale, Gale, Maliotis, Zwicker and Tylecote (available in the OXALID Database). Nevertheless, apart from one analysis of an undated slag from the Kinousa village, no other LIA has been carried out in slags to compare the values between slags and ores. Future Lead Isotope Analysis (LIA) could shed some light on the choices of the mines for each of the slags. It is assumed here that the ore of the slag heaps comes from either Limni or Kinousa mines, which could be validated or rejected by LIA. Although, if the nearby mines are not the source of the ores here, much larger routes had to be chosen, with different socioeconomic balances.

Coming back to the validity of the paths, they were estimated by taking the mines as the starting points and the slag heaps as the destination points. Looking more into the landscape, it is obvious that the mines are at a higher altitude than the slag heaps. The paths starting from the mines to the slag heaps are much easier and faster since they run on a downhill instead of an uphill. The paths from the destinations, i.e., the slag heaps, to the starting points, i.e., the mines, were not estimated, but they would take much longer due to the angle of the uphill, making it much more challenging than walking on a flat terrain, or even a downhill. In LCP1, LCP2 and LCP3 the paths seem to overlap with rivers, according to the data provided by the Department of Land and Surveys. Whether there was water flowing in these rivers or was present as puddles is impossible to know. Different quantities of water would create various levels of accessibility and variation for these paths. If there is a proper river flowing, this could make the transportation of the extremely heavy ore possible through small boats, which would be faster than walking and carrying the ore. Nevertheless, the flow of a river is towards the sea, which means that bringing a cargo from the mines to the seaside would be easy, while returning back to the mine would be much more challenging with a need of elaborate vessels with sail. Additionally, different seasons have different rainfalls and the quantity of rainfall over 400 years is not the same. It has to be noted that

currently there are no flowing rivers in the estimated paths, even in the rainy season. This might be due to the complete alteration of the landscape in the 20th century where the same path was used for the transportation to the Limni Pier. In the area examined there are now four dams, Evretou dam, Argaka dam, Pomos dam and Ayia Marina dam (http://www.moa.gov.cy/moa/wdd/wdd.nsf/page18_gr/page18_gr?opendocument), which serve the needs of the local population. On the other hand, if there is not enough water to navigate with a vessel, then other ways of transporting the ore should be considered. Furthermore, if there is little quantity of water, or not at all, then the same path could be walked, probably with the help of a donkey or other pack animal to carry the heavy weight. The scope of this chapter is not to examine all the factors that could or have changed the landscape, but rather to estimate some possible scenarios of how a minimum time of movement from the mines to the slag heaps could have been achieved. This could be further investigated with coring samples, which would imply whether there was heavy rainfall or rivers in the area, and even a dense archaeological survey in the region to search for the extent of human occupation and use of the area.

The location of the Argaka slag heap far from both mines is remarkably interesting, because it required workers to undergo a long trip carrying heavy quantities of ore. Late Roman ports are not yet testified archaeologically in the area but being close to a port could suggest a need for imported, like wood, flux, workforce or export the final product, i.e., the metal. Wood was found in the region for both slag heaps though, being *Pinus Brutia* for the Pelathousa slag heap and *Alnus Orientalis, Vitis vinifera* and *Quercus evergreen* for Argaka slag heap, as shown by the anthracological studies (Socratous et al: 379). Fluxes, existed next to the ore and maybe the reason why manganese oxide(s) were used in the first place was exactly because it was available right to the source. Another factor can lie in the administration and organization of the production (Kassianidou 2003). While, the export of metal seems to be one of the main reasons of the location of the Argaka slag heap.

The Pelathousa slag heap is located very close to the Limni mine, around 1km, while this path takes just over twenty minutes. Slag heaps are generally found in close vicinity of ore deposits so the Pelathousa Slag heap makes no exception to the rule. Maybe in different time periods different smelting locations were chosen, something that would be very risky to estimate without further evidence.

8.5. Conclusions

Least Cost Path analysis showed that some paths are easier than others, estimating a minimum time for each one. The more interdisciplinary methods are applied in archaeology the closer the research community is in understanding complicated societies properly.

Chapter 9. Discussion

In this chapter the discussion points are separated between analytical and archaeological. The analytical points include the general understanding of the slag heaps, in terms of their microstructure, homogeneity, specific characteristics. With these results an effort is made to reconstruct the past technological choices of the Late Roman period as it was carried out in the mining region of ancient Marion near the modern town of Polis Chrysochous. Furthermore, there is a comparison between the HHpXRF and the SEM-EDS results and a note on the combination of microscopic and macroscopic characteristics. The second part of the discussion, focuses on the archaeological significance of the slag heaps, examining their location and context.

9.1. Homogeneity of the two slag heaps

Through the examination of the slag assemblage, it was possible to underline their great homogeneity, apart from samples PEL18, ARG616 and ARG612 which are discussed below. The microstructure of the slags is olivine-based ranging between fayalite, knebelite and tephroite reflecting the varying manganese content, sometimes with the presence of free-iron oxides which testify for excessive iron and, finally, copper-matte prills. The slag assemblage coming from the Argaka slag heap includes both Groups 1 and 2, i.e., according to the manganese content, and is very homogeneous throughout the three different layers. The Pelathousa slag heap follows the same path, both Groups are present, and the assemblage is very homogeneous. This highlights the established practices that remain the same from the end of the 4th to the end of the 7th / 8th centuries AD. The production reached an almost industrial stage where the smelting procedures, temperatures, fluxes, and the organization of the copper industry followed specific lines. This generalization of copper smelting technology is the same from the Roman times a few centuries before and continue well on. This might indicate that once past metallurgists found the best practices, they continued using them throughout the Late Antiquity. This does indicate stable advancements of a method in a way that is of economic value and is well held upon until the end of the copper production in these two slag heaps.

9.2. Macroscopic comments after the analysis

An important result from the work carried out for this master's thesis was the correlation between macroscopic, microscopic, and chemical analysis. The comments here are based both on the surface of a slag and on a clear-cut section of it. As far as the manganese-poor slags are concerned (Group 1), the ones that have just a few percentages of manganese are easily distinguished. The distinct characteristic in Group 1 is the big red spots and the extreme shininess on the lower part of the slag, that would have been in contact with the surface of the ground**.** These slags reach an iron content of around 50 wt% and show no copper incrustations but yellow and red hues.

The manganese-rich slags (Group 2) can have three different appearances color-wise. The first one is the distinctive blueish color that covers all the slag surface. This blueish hue is met in slags that are very manganese rich (exceeding 25wt%) and very corroded at the same time. The second color is present only in one case (PEL18), still worth to mention though, showing a greenish-black interchanging layering. The third color of the manganese-rich slags is the typical dark grey/black.

Slag heaps in Cyprus are estimated to weigh a few hundred tones or more, with countless slag pieces. Laboratory-based analysis can be extremely time-consuming if one wishes to explore a slag heap in higher detail than analyzing a representative assemblage. Macroscopic examination of the color, texture, incrustations on slags is quite informative and can save time and money from the research. Since the manganese-rich slags are suggested to act as an indicator of a Roman/ Late Roman date, it should be highlighted that the former can have either of the three colors described above, hence not always easy to differentiate macroscopically.

9.3. The origin of the manganese

The manganese, as discussed in Chapter 3, is widely used from the Roman times and further on. Manganese is indeed in association with Late Roman contexts, where the advancements of the smelting technology are remarkably high with minute copper metal loss into the slags.

In the case of the two slag heaps examined here, manganese is evident in all slags from minute concentrations (0.08 wt%) to more than a third of the sample (38.24 wt%). This addresses the question concerning the origin of the manganese. Since the chalcopyrite ore bears no

manganese, the latter was added intentionally as a flux. Fluxes are used to create the ideal conditions for the formation of slags, to lower the melting point inside the furnace and to reduce the amount of charcoal needed. The fluxes added are either metal based (of a $^{2+}$ nature, like iron, zinc, magnesium or manganese) or silicon based to create the typical slag of the following composition (Bachmann 1982: 21):

$$SiO_2 + 2FeO \rightarrow (\text{with } 600\ ^\circ C)\ 2FeO.SiO_2$$

Chalcopyrite ($CuFeS_2$) has already some iron, which would indicate the need of silicon in order to form slags during the smelting. Nevertheless, the slag assemblage shows intentional addition of manganese, and the latter acts like iron, meaning that there was superfluous silicon content and a metal of a $^{2+}$ nature was added in order to form the typical siliceous slags. We know already, that the Limni copper-ore deposit is characterized by a siliceous gangue (Bear 1963: 41).

The manganese can come from two minerals/ rocks in Cyprus, i.e., umber and pyrolusite. Umber is readily available near most of the deposits, e.g., the Pera Pedio/ Parapedi formation (see Chapter 2), and its composition is varying between the main constituents of iron, manganese, and silicon (Παναγίδης and Κωνσταντίνου 2013: 157). Thus, an umber flux would add iron, manganese, and a bit of extra silicon to the slag composition, though a formula for umber cannot be suggested since there are umbers with a wide palette of proportions of these three elements. On the other hand, pyrolusite (MnO_2) exists in the Pachna formation, which can be found also south of Polis **(Fig. 2)**. Pyrolusite, is composed by 63.24 wt% manganese and 36.76 wt% oxygen, which would add only manganese to the slag composition. Fox et al (1987: Table 1) suggested an addition of a manganese-oxide flux.

Coming back to the varying manganese content of the slags, all the slags of Group 1 could chemically have either of the two fluxes, so there will be no suggestion between one or the other manganiferrous material as flux. Group 2, on the other hand is a more complex case. The slags with a manganese presence of 14-25 wt% could come from both fluxing choices as well. Nevertheless, the very manganese-rich slags of more than 25 wt% manganese content, should be further discussed. It is suggested by Koucky and Steinberg (1989: 283) that if an umber is used as a flux, it could not possibly reach the very high manganese percentages met in slags. Therefore, they suggest that the manganese could possibly come from pyrolusite concretions or nodules which are embedded in the black umber deposits (Koucky and Steinberg 1989: 283). In the very

manganese-rich slags, the use of manganese oxides is suggested as a flux, while in the manganese-poor slags an umber is suggested as a fluxing choice. This argument is suggested in one case, i.e., PEL61 where MnO_2 crystal remains were identified. This sample preserves MnO_2 unmolten rock incorporated to the slag matrix after it was tapped out of the furnace. The small manganese dioxide grains could be in the exact proximity due to a number of reasons, but their incorporation in the slag matrix shows that there was some MnO_2 material in the smelting site while the slag was still in a liquid/ semi-liquid state. It has to be noted that this slag has an average manganese content of 23.4 oxides %, and the olivines are knebelite, which highlights the very manganese-rich character of the slag. As mentioned before, Koucky and Steinberg (1989: 283) suggested that such high manganese values could not be expected from an umber flux, but more appropriately from a pyrolusite flux, and the grains found in this sample verify it.

9.4. Samples PEL18, ARG616 and ARG612

Although most of the slags seem quite similar, all olivine-rich with or without the presence of free-iron oxides with copper-matte prills all embedded in a glassy matrix, there are three slags that were pretty different, and special discussion should be devoted to them. The first pair of samples that looks quite similar between one another are PEL18 and ARG616. In these samples there are no olivine crystals, no free-iron oxides, while there is a general absence of crystalline structure with small exceptions in some zones with some pyroxene crystals. PEL18 has very minute presence of copper matte prills while at the same time it has the highest copper content which is present in the form of copper metal prills. The striations characterizing its glassy matrix indicate that the slag did not reach a very liquid state but remained too viscous for the metallic prills to leave the slag. What raises questions here is the general absence of copper-matte prills. If copper metal prills did not manage to get out of the slag, it seems impossible that copper matte prills would manage, being lighter. There are two suggestions for this slag. The first one suggests that this slag was in the lower part of the furnace, close to the copper metal formed in the bottom of the furnace and was tapped out before the copper metal prills joined with the big accumulation of the copper metal. This would justify the absence of sulfur in the slag, since if it was very low in the furnace the sulfur would have turned to sulfur dioxide and evaporated already earlier / higher up in the furnace shaft. The second argument suggests that the absence of copper matte prills is due to a pre roasting stage. With roasting a big proportion of the sulfur would be initially

evaporated and then a cleaner sulfur poor ore would be smelted. Nevertheless, although we know that roasting would have taken place, there is not really evidence concerning whether the roasting would have been a separate step or it would just happen in one procedure together with the smelting, which in this case would be done in the upper part of the furnace. The absence of sulfur and the very high copper content of this slag point towards a different 'recipe' in the smelting procedure. A refining stage is not suggested here due to the very high manganese content in both PEL18 and ARG616. As it is already discussed, manganese is an added flux, and in a refining stage of smelting matte, to remove the iron and sulfur still in the matte, one would need excessive silica instead of an extra Me^{2+} portion (Georgakopoulou and Kassianidou 2013).

ARG616 is similar with PEL18 in the absence of structure and the presence of pyroxene crystals, but copper matte prills are now abundant, while the copper metal prills are almost absent. To note is that this slag also preserves an average of 13.3 Mn oxides% content. The copper-matte prills support even more that in this case it cannot be a refining slag.

ARG612 is a completely different slag being very heterogeneous Fe-rich with copper appearing as tenorite, delafossite and copper metal. The slag fragment is very small not exceeding 3 by 3 by 2 centimeters in all dimensions. Absence of sulfur and presence of tenorite and delafossite point towards a smelting of an iron-copper ore poor in sulfur, or after an extensive roasting stage. The tenorite in particular, being a highly-oxidized copper oxide (CuO), indicates oxidizing conditions more than smelting, and for the latter it could be a crucible slag instead of a smelting one (Bachmann 1982: 16). A refining stage where all sulfur evaporated in the melting stage is therefore a suggestion. As this slag fragment was very small it was not possible to understand the type of slag, e.g., tap slag. Finally, since it is only a single sample, it is difficult to investigate it more. It would be very interesting to have evidence of both smelting and refining slags at the same area. Nevertheless, it should be kept in mind that the Argaka slag heap could be the outcome of moving slags, hence crushed, for space management. So, one refining slag piece would not necessarily suggest that near the Argaka slag heap refining processes were carried out, but it somehow ended up being a sole example and this way making research more interesting. Future research should be done to identify more of this type of slag and to investigate its spatial distribution and technical condition, e.g., smelting after roasting, or refining slag.

9.5. Comparison between HHpXRF and SEM-EDS analysis

It was also interesting to compare HHpXRF and SEM-EDS analysis on the same samples **(Table 7).** The comparison of the two methods shows that the results are very close. HHpXRF although is one of the cheapest, hand-held, non-invasive techniques has been quite often criticized on its accuracy. With the analysis carried out in the framework of this thesis it was possible to compare the results and see how close they are in terms of accuracy. Comparing chemical data coming from different equipment and methods is always risky. The common characteristics of the two methods, do allow an initial correlation. It has to be noted though, that the HHpXRF analysis was carried out in the beginning of this research to get a first understanding of the material, thus, only three measurements were taken for each sample. The SEM-EDS results were carried out on polished blocks, therefore, not necessarily on the same area where the HHpXRF analysis took place. Furthermore, the polished surface of the polished block allowed for an even higher accuracy, compared to the HHpXRF results, which were carried out on freshly-cut surfaces, but not on a polished surface. Furthermore, the HHpXRF results are presented as wt% values, without the light elements included, i.e., O, Na and Mg. The SEM-EDS results are presented by the researcher according to the material analyzed, therefore in the bulk analysis an Oxides% by Stoichiometry was chosen while for the metal parts a wt% by all elements.

In comparing the results between the HHpXRF and the SEM-EDS, the HHpXRF results are presented in weight%, while for the SEM-EDS both weight% and oxides% to compare and contrast the data. The main differences appear in the lighter elements, as they are not detected by the HHpXRF. The elements compared here are between Al and Pb. Starting with Al, Si, P, S, K and Ca, the values are not similar and the HHpXRF data seems to be much higher than in SEM-EDS, sometimes even double as much, e.g., in ARG616 the HHpXRF values for Al, Si and K are 12.4 wt%, 34.3 wt% and 3.2 wt% respectively, while the values for SEM-EDX weight% values for the same elements are 5.9 wt%, 20.1 wt% and 0.41 wt%. On the other hand, values of heavier elements are much closer. For example, in the same sample ARG616 elements Mn, Fe and Cu analysis with HHpXRF showed a composition of 15.4 wt%, 20.6 wt% and 0.4 wt%, while SEM-EDS weight% results showed for the same elements the following values: 14.4 wt%, 17.7 wt% and 0.29 wt%. The variations in the values between the two methods are notable, but still close enough. Apart from the limitations of the HHpXRF already mentioned, it should be noted that in

the SEM-EDS bulk analysis were taken in homogeneous areas, which was possible due to the microscopic properties of the instrument, something that is not possible with the HHpXRF. Overall, the HHpXRF proved to be very useful in getting a concrete first understanding on the assemblage, the most important part of it being the distinction between the manganese-poor and manganese-rich slags.

9.6. The location of the two slag heaps

The two slag heaps although homogeneous enough in their microstructure are not situated in similar landscapes. The Pelathousa slag heap is indeed close to the Limni mine, a bit more than 1 kilometer away as shown in *Chapter 8*, while the Argaka slag heap has no mines located closer than 5km, being situated on the coastal plain of recent sediments and soil washed down from the hinterland. Which suggests that a notable effort was made in order to bring all the copper ores from a mine to the smelting site near the coast, forming this slag heap. Whether the mine quarried was indeed the Limni mine, can be tested in the future by Lead Isotope Analysis. Since the mine was still in use, as the Pelathousa slag heap suggests, it could continue being in use. The radiocarbon dating of the three charcoal samples from the Argaka slag heap indicated a dating between 535 – 782 C.E. which includes a range of different political circumstances in the island, from the stability of the island, to the rise of the church and the nearby churches, to the Arab conquests and even after them. Nevertheless, the slag heap has been quite altered by more recent modern activities, so it is not sure whether the production at this specific locality pre-existed or further continued after the end of the 8th century. Nevertheless, it should be included in the landscape and cultural context to understand it better.

The Argaka slag heap is very close to the coast and very close to the 20th century Limni Pier. The existence of a port would not necessarily have ashlar blocks as foundations, as evidence in the archaeological record. There could have been a construction like the Limni Pier which would not necessarily leave any evidence behind. Furthermore, the Limni Pier managed to serve the need of the large-scale operation of the 20th century so there is no reason to immediately reject the possibility of a similar type of harbor existing nearby the slag heap. The Arsinoe harbor is not yet identified, although the main candidate is in Latchi which has no surviving evidence from the period though that could support the notion that its main port had been there. Nevertheless, we might not need to look for a big harbor, as maybe the maritime activity of the area is restricted to

small-scale trade on small vessels, the evidence of which does not always survive. Nearby ports, e.g., the Soloi port, could be fulfilling Arsinoe's needs. At the same time the slag heap is located near the Roman main road **(Fig. 1)** that could make the location much more approachable with carts or animals, like donkeys or the like, without the need to depend on a sea-borne transportation.

In the study of Socratous et al. (2015) in the Argaka slag heap (LIM-AM) at least 12 different wood species were identified, more specifically Alnus Orientalis, Arbutus Sp., Capparis Spinosa, Cistaceae, Leguminosae, Olea Europea, Pinus Brutia, Pinus Nigra, Pinus Sp., Platanus Orientalis, Quercus (deciduous), Quercus (evergreen), Vitis Vinifera and some indeterminable (Socratous et al. 2015: 381). In Pelathousa slag heap (PEL) there are at least seven different wood species, more specifically Alnus Orientalis, cf Laurus, Moraceae, Pinus Brutia, Pinus Nigra, Pinus Sp., Pistacia Terebinthus/ Pistacia Atlantica and some indeterminable (Socratous et al. 2015: 381). It is highlighted by Socratous et al. (2015: 381-382) that Pinus Nigra is a wood species found in higher altitudes (1200m-1950m) and its presence in the Argaka and Pelathousa slag heap, in such a low altitude, could indicate an intentional search for fuel higher up in the mountains because the local flora is over-exploited or suggest that Pinus Nigra was available in lower altitudes because the climate at the time may have been cooler. Nevertheless, in both slag heaps the main wood species used was Pinus Brutia.

Sample	SEM-EDS wt%	O	Na	Mg	Al	Si	P	S	K	Ca	Ti	V	Mn	Fe	Ni	Cu	Zn	BaO	Pb	Total
ARG 310	HHpXRF	Light Elements			3,3	16,9	ND	0,27	4,2	3,9	0,26	0,13	36,7	6,33	0,10	4,21	0,13	ND	0,13	76,8
ARG 310	SEM-EDS wt%	32,3	0,92	1,1	5,8	15,9	ND	0,90	0,97	2,3	0,43	ND	25,9	12,6	ND	0,78	ND	0,8	ND	100
ARG 310	SEM-EDS oxides%	ND	1,1	1,7	10,3	32,1	0,22	0,82	1,11	3,1	0,36	0,2	31,7	15,4	nd	0,92	0,11	0,96	ND	100
ARG 404	HHpXRF	Light Elements			17,2	28,5	ND	3,7	5,2	4,9	0,15	0,03	1,6	28,98	0,04	1,31	0,05	ND	0,03	92
ARG 404	SEM-EDS wt%	33,4	0,84	1,4	7,0	18,7	ND	0,65	0,79	4,5	0,31	ND	1,8	29,3	ND	1,39	ND	ND	ND	100
ARG 404	SEM-EDS oxides%	ND	1,1	2,1	12,3	37,2	0,17	0,58	0,93	5,9	0,5	ND	2,2	35,4	nd	1,6	ND	ND	ND	100
ARG 605	HHpXRF	Light Elements			19,1	32,9	ND	0,83	2,80	7,3	0,23	0,05	2,27	33,3	0,35	0,42	ND	ND	0,01	99,7
ARG 605	SEM-EDS wt%	34,8	1,0	1,5	7,9	18,0	ND	0,27	0,26	5,2	0,33	ND	1,7	28,7	ND	0,39	ND	ND	ND	100
ARG 605	SEM-EDS oxides%	ND	1,3	2,3	14,1	36,5	0,26	0,3	ND	6,9	0,54	ND	2	35,2	nd	0,47	ND	ND	ND	100
ARG 612	HHpXRF	Light Elements			14,8	33,6	0,26	0,27	1,1	0,36	0,05	0,01	0,08	46,0	ND	2,7	0,02	ND	ND	99,4
ARG 612	SEM-EDS wt%	33,1	ND	0,63	2,0	21,7	ND	ND	0,10	1,2	0,06	ND	0,27	38,9	ND	1,9	ND	ND	ND	100
ARG 612	SEM-EDS oxides%	ND	ND	1	3,4	43,5	0,42	0,1	0,1	1,6	0,1	ND	0,33	47,2	nd	2,2	ND	ND	ND	100
ARG 616	HHpXRF	Light Elements			12,4	34,3	ND	0,43	3,2	7,8	0,22	0,07	15,4	20,6	0,09	0,40	0,01	ND	0,01	95,2
ARG 616	SEM-EDS wt%	36,2	0,50	8,7	5,9	20,1	ND	0,34	0,41	5,3	0,25	ND	14,4	17,7	ND	0,29	ND	0,17	ND	100
ARG 616	SEM-EDS oxides%	ND	0,62	3,5	10,7	40,9	0,14	0,34	0,49	7	0,33	ND	13,3	21,9	nd	0,39	ND	0,26	ND	100
PEL 10	HHpXRF	Light Elements			14,0	24,4	0,26	3,5	1,2	2,2	0,11	0,12	14,9	37,9	0,25	0,85	0,06	ND	ND	99,9
PEL 10	SEM-EDS wt%	34,1	ND	0,37	2,1	13,6	0,10	0,70	ND	0,61	0,13	ND	9,1	38,6	ND	0,83	ND	0,28	ND	100
PEL 10	SEM-EDS oxides%	ND	ND	0,58	3,7	26,7	0,21	1,22	0,15	ND	ND	ND	11,5	53,3	nd	1	ND	0,37	ND	100
PEL 18	HHpXRF	Light Elements			12,2	37,3	ND	ND	2,4	8,5	0,08	0,06	14,2	21,3	0,09	1,93	ND	ND	ND	98,3
PEL 18	SEM-EDS wt%	34,1	0,21	1,5	4,9	20,9	0,10	ND	0,25	4,8	0,15	ND	12,0	19,7	ND	1,5	ND	ND	ND	100
PEL 18	SEM-EDS oxides%	ND	0,29	2,3	8,6	41,6	0,23	ND	0,29	6,2	0,24	ND	14,5	23,8	nd	1,8	ND	ND	ND	100
PEL 21	HHpXRF	Light Elements			8,6	27,3	ND	0,98	4,3	11,2	0,23	0,11	28,1	16,2	0,11	0,63	0,03	ND	0,19	98,1
PEL 21	SEM-EDS wt%	33,7	0,35	1,2	6,1	16,7	ND	0,41	0,54	6,6	0,26	ND	19,0	14,6	ND	0,43	ND	ND	ND	100

PEL 21	SEM-EDS oxides%	ND	0,48	1,9	10,9	34	0,18	0,38	0,64	8,8	0,41	ND	23,4	18	nd	0,52	ND	ND	0,23	100
Sample	SEM-EDS wt%	O	Na	Mg	Al	Si	P	S	K	Ca	Ti	V	Mn	Fe	Ni	Cu	Zn	BaO	Pb	Total
PEL 28	HHpXRF	Light Elements			8,3	27,9	0,27	1,2	5,5	3,3	0,20	0,11	30,2	21,5	0,20	0,81	0,11	ND	ND	99,9
PEL 28	SEM-EDS wt%	29,6	0,66	1,3	3,9	16,3	0,10	0,87	0,84	2,5	0,22	ND	22,7	20,5	ND	0,40	ND	0,42	ND	100
PEL 28	SEM-EDS oxides%	ND	0,8	2	6,8	32,2	0,2	0,79	1	3,2	0,16	ND	27,2	24,5	nd	0,47	0,16	0,59	ND	100
PEL 31	HHpXRF	Light Elements			17,4	34,5	ND	0,79	7,70	6,2	0,10	0,03	1,2	31,2	0,01	0,42	0,13	ND	ND	99,9
PEL 31	SEM-EDS wt%	33,1	1,2	2,1	6,8	19,3	ND	0,47	1,1	4,1	0,14	ND	0,81	30,7	ND	0,18	ND	ND	ND	100
PEL 31	SEM-EDS oxides%	ND	1,5	3,2	11,8	37,9	0,08	0,42	1,2	5,3	0,24	ND	1	36,7	nd	0,24	0,25	ND	ND	100
PEL 38	HHpXRF	Light Elements			13,7	24,6	0,41	1,7	4,2	1,3	0,16	0,10	21,1	30,7	0,23	1,33	0,10	ND	ND	99,9
PEL 38	SEM-EDS wt%	31,6	0,33	0,72	2,9	12,6	ND	1,6	0,65	1,6	0,18	ND	14,9	32,3	ND	0,59	ND	0,43	ND	100
PEL 38	SEM-EDS oxides%	ND	0,42	1,2	5,4	26,8	0,21	1,55	0,79	2,1	ND	ND	18,9	41,1	nd	0,73	0,14	0,56	ND	100
PEL 57	HHpXRF	Light Elements			19,6	22,6	0,41	2,0	5,0	ND	0,07	ND	0,47	48,8	ND	0,50	0,17	ND	ND	99,9
PEL 57	SEM-EDS wt%	30,3	ND	1,4	2,8	13,8	ND	1,1	0,37	0,98	ND	ND	0,43	47,8	ND	0,78	ND	ND	ND	100
PEL 57	SEM-EDS oxides%	ND	ND	2,2	4,4	28,4	0,15	1,07	0,44	1,3	0,11	ND	0,54	59,2	nd	0,94	0,28	ND	ND	100
PEL 61	HHpXRF	Light Elements			9,9	30,4	ND	ND	2,7	14,8	0,20	0,07	26,9	12,88	0,08	1,43	ND	ND	ND	99,5
PEL 61	SEM-EDS wt%	31,3	ND	0,60	6,4	18,5	0,17	ND	0,31	8,6	0,27	ND	19,8	12,2	ND	1,8	ND	ND	ND	100
PEL 61	SEM-EDS oxides%	ND	0,11	0,91	11,1	35,9	0,35	ND	0,36	10,9	0,41	ND	23,4	14,4	nd	2	ND	ND	ND	100

Table 7: Comparison between HHpXRF and SEM-EDS data from Argaka and Pelathousa slag heaps. ND=Not Detected.

9.7. The organization of the production

The ownership of the production is something that would be very interesting to explore, especially during the 4th to 8th centuries C.E. where the economic, state and social factors are changing. The wars of the Roman Empire and the prisoners of war in Cyprus during the wars of the Eastern Roman Empire, the rising church as an important parameter in economy, education and justice after the 6th century C.E. but also partly entangled in stately affairs are the main factors of this period and make this question very interesting. During the Roman Empire the mines of Cyprus belonged and were exploited by the state for the coinage and other needs of the Roman Empire (Χατζηιωάννου 1973: 397). There is no historic information touching upon the ownership of the mines and their organization. Archaeological research tries to shed some light but things are not clear enough to create something more solid than assumptions. Something that is discussed in the literature is the role of the church as an economic factor on the island, indicating its mine-related activities. Parani (2013) highlighted the existence of workshops nearby churches, with the case study of Arsinoe. In Arsinoe the three main workshop activities near the churches include metal, glass and pottery production. The workshop character of churches is testified also in Kourion, most probably on bread-making as one bread seal suggests. A metalworking workshop area in the church remains in Ayios Philon in Ayia Triada Karpasia, exists but the workshop could date after the abandonment of the church (du Plat Taylor and Megaw 1981). Other than that, there are two more studies discussing the church's economic connection, maybe through overseeing the copper-industry, as churches have been identified nearby Late Roman mines (Given 2018, Keane 2021).

Another aspect of the copper-industry is the people that worked there. Working in the mines or working in the smelting precincts was never a favorable occupation or a well-paid one. The people who worked in the ancient galleries or in the opencast mines are not discussed in the literature but would not be of a high status. In the previous periods the mining industry in Cyprus was more or less slave based (Kassianidou 2000) but in the Late Roman period not enough data exist, neither historic nor archaeological, to confirm or deny this.

10.Conclusions

The importance of interdisciplinarity in the archaeological research is demonstrated through this thesis, with historical and archaeological data, chemical analysis, GIS applications all being ingredients of this thesis. Through the combination of the analytical approaches, it was possible to quickly and accurately understand the assemblage. The implementation of HHpXRF allowed a quick and quite accurate qualitative and quantitative analysis on the slag assemblage, identifying two compositional groups by their manganese content. This was very helpful in managing to choose representative samples for more detailed analysis that would come from both compositional groups. Further, with the application of the SEM-EDS more detailed analyses were carried out in the selected samples. The most interesting part is coming back to the macroscopic analysis and trying to see how the analyses can be identified macroscopically. Matching macro and micro-observations open up a new understanding of the material, as there is not always enough time to analyze everything. This is not to suggest though that the microscopic observations are not important, but rather the opposite. Without the microscopic examination and analysis, research would be doomed to neglect the details that are only visible in the microscope.

As far as the metallurgy of the Late Antiquity in Cyprus is concerned, it has become apparent that the same set of tools and processes were employed across the island. The tools referred, include the knowledge, smelting practices and procedures, and fluxing agents. Whether there was one central authority, or small-scale productions that would work for someone else or themselves is yet not sure. By urging the archaeologists of Late Antique Cyprus to work on more and more excavations in rural areas, would very much help in the understanding of the people that formed the past societies. The tendency in focusing on the powerful elite has been long-lasting in archaeology, but the elite was -and continue to be- just a tiny fragment of the society. However, societies are what they are not only due to the authorities but mostly due to the rest of the people. Hence, farmsteads and rural settlements might not be as fascinating as churches would probably are expected to be, but they sure are equally important.

11.References

Aimers, J.J., Farthing, D.J. and Shugar, A.N. 2012. Handheld XRF analysis of Maya ceramics: a pilot study presenting issues related to quantification and calibration. In Shugar A., N. & Mass, J. L. (Eds.) *Studies in Archaeological Sciences: Handheld XRF for Art and Archaeology*, Leuven University Press, 423-448.

Bachmann, H.G., 1982. *The identification of slags from archaeological sites* (No. 6). Routledge.

Bassiakos, Y., Nerantzis, N. and Papadopoulos, S., 2019. Late Neolithic/Early Bronze Age metallurgical practices at Limenaria, Thasos: Evidence for silver and copper production. *Archaeological and Anthropological Sciences*, *11*(6), 2743-2757.

Bear, L., M. 1963. The mineral resources and mining industry of Cyprus: Bulletin No1.

Bezur, A. and Casadio, F., 2012. The analysis of porcelain using handheld and portable X-ray fluorescence spectrometers. In Shugar A., N. & Mass, J. L. (Eds.) *Studies in Archaeological Sciences: Handheld XRF for Art and Archaeology*, Leuven University Press, 249-312.

Bruce, J.L. 1937. Appendix V: Antiquities in the mines of Cyprus. In E. Gjerstad, J. Lindros,E. Sjoqvist and A. Westholm (eds.) *The Swedish Cyprus expedition: finds and results of the excavations in Cyprus 1927 – 1931*, volume III, 639–71.

Charalambous, A. and Kassianidou, V., 2012. Chemical analyses of metal artefacts from Late Cypriote tombs excavated in the Limassol area, with the employment of pXRF. In Karageorghis, V. and Violaris, Y. (Eds.), T*ombs of the Late Bronze Age in the Limassol Area, Cyprus (17th–13th CBC)*. Municipality of Limassol, Nicosia, 300-308.

Charalambous A., Kassianidou, V. and G. Papasavvas. 2014. A Compositional Study of Cypriot Bronzes Dating to the Early Iron Age Using Portable X-ray Fluorescence Spectrometry (pXRF). *Journal of Archaeological Science*, 46, 2014, 205 – 216.

Charalambous, A. and Webb, J.M., 2020. Metal procurement, artefact manufacture and the use of imported tin bronze in Middle Bronze Age Cyprus. *Journal of Archaeological Science*, *113*, 105047, 1-13.

Childs, W. A. P., 1988. First Preliminary report on the excavations at Polis Chrysochous by Princeton University. *Report of the Department of Antiquities*, Cyprus 1988. 121-130.

Constantinou, G., 1992. The mining industry of Cyprus in modern times. In: A. Marangou and K. Psillides, (eds.). *Cyprus Copper and the Sea*. Nicosia, 328-367.

Costello, B., 2014. Architecture and Material Culture from the Earthquake House at Kourion, Cyprus: a Late Roman Non-Elite House Destroyed in the 4th century AD, *BAR international series*, *Archaeopress*, Oxford.

Craddock, P.T., 1995. *Early metal mining and production*, Edinburgh: Edinburgh University Press.

Crupi, V., Galli, G., La Russa, M.F., Longo, F., Maisano, G., Majolino, D., Malagodi, M., Pezzino, A., Ricca, M., Rossi, B. and Ruffolo, S.A., 2015. Multi-technique investigation of Roman decorated plasters from Villa dei Quintili (Rome, Italy). *Applied Surface Science*, 349. 924-930.

Davey, C.J. and Edwards, W.I., 2007. Crucibles from the Bronze Age of Egypt and Mesopotamia. *Proceedings of the Royal Society of Victoria, 120(1),* 148-156.

De Francesco, A.M., Crisci, G.M. and Bocci, M., 2008. Non-destructive analytic method using XRF for determination of provenance of archaeological obsidians from the Mediterranean area: A comparison with traditional XRF methods. *Archaeometry*, *50*(2), 337-350.

Demesticha, S., 2015. (ed.) *Per terram, per mare: Seaborne Trade and the Distribution of Roman Amphorae in the Mediterranean*. Studies in Mediterranean archaeology and literature, Pocket-book 180. Uppsala, Åströms förlag, 2015. Cahiers du Centre d'Études Chypriotes, 45(1).

de Soto, P. (2010) Transportation costs in NW Hispania. In C. Carreras and R. Morais (ed.), *The Western Roman Atlantic Façade. A study of the economy and trade in the Mar Exterior from the Republic to the Principate*, Oxford, Archaeopress, 31-43.

du Plat Taylor, J., 1952. A Late Bronze Age settlement at Apliki, Cyprus. *The Antiquaries Journal*, *32*(3-4), 133-167.

Ferguson, J.R., 2012. X-ray fluorescence of obsidian: approaches to calibration and the analysis of small samples. *Handheld XRF for Art and Archaeology*, 401-422.

Fox, W. A., Zacharias, S., and Franklin U.M. 1987. Investigation of ancient metallurgical sites in the Paphos district, Cyprus. In *Western Cyprus: Connections: an Archaeological Symposium Held at Brock University, St. Catharines, Ontario, Canada, March 21-22,* Göteborg: P. Åströms Förlag.169-184.

Frahm, E. and Tryon, C.A., 2019. Origin of an Early Upper Palaeolithic obsidian burin at Ksar Akil (Lebanon): Evidence of increased connectivity ahead of the Levantine Aurignacian?. *Journal of Archaeological Science: Reports*, *28*, 102060.

Georgakopoulou, M., 2004. Examination of copper slags from the Early Bronze Age site of Daskaleio-Kavos on the island of Keros (Cyclades, Greece). *Institute for Archaeo-Metallurgical Studies Newsletter*, *24*,.3-12.

Georgakopoulou, M. and Rehren, Th., 2013. Report on the analyses of metallurgical samples from Ambelikou Aletri. *Ambelikou Aletri Metallurgy and Pottery Production in Middle Bronze Age Cyprus, Studies in Mediterranean Archaeology.* Aaströms förlag, Uppsala. 197-200.

Georgakopoulou, M. and Kassianidou, V., 2013. Archaeometallurgical finds and analytical results. In Given, M., Knapp, A.B., Noller, J.S., Sollars, L. and Kassianidou, V. (eds), *Landscape and Interaction: The Troodos Archaeological and Environmental Survey Project, Cyprus. Volume 1*, London, Council for British Research in the Levant. 237-253.

Given, Michael. 2018. The Materiality, Monumentality, and Biography of Copper Slag on Cyprus. In: *An Age of Experiment: Classical Archaeology Transformed* (1976–2014). Edited by Lisa Nevett and James Whitley. Cambridge: McDonald Institute for Archaeological Research, 161–176.

Graham, A., Jacobsen, K.W. and Kassianidou, V. 2006. Agia Marina-Mavrovouni: preliminary report on the Roman settlement and smelting workshop in the central northern foothills of the Troodos mountains, Cyprus. *Report of the Department of Antiquities, Cyprus*, *2006*, 345-367.

Güimil-Fariña, A. and Parcero-Oubiña, C. (2015) "Dotting the joins": a non-reconstructive use of Least Cost Paths to approach ancient roads. The case of the Roman roads in the NW Iberian Peninsula. *Journal of Archaeological Science*, Vol. 54, 31-44.

Hauptmann, A., 2020. Archaeometallurgical Slags and Other Debris. In *Archaeometallurgy–Materials Science Aspects*. Springer. 99-293.

Iacovou, M. 2021. From the metalliferous sources to the citadel complec of ancient Paphos: Archaeo-environmental analysis of the mining and the build environment.

Ioannides, D., Kassianidou, V., Bonnerot, O. and Charalambous, A., 2016. A preliminary study of the metallurgical ceramics from Kition, Cyprus with the application of pXRF. *Journal of Archaeological Science: Reports*, *7*, 554-565.

Ioannides, D., Kassianidou, V. and Papasavvas, G., 2021. A new approach to an old material: an examination of the metallurgical ceramic assemblage of Enkomi, Cyprus, with the use of handheld portable X-ray fluorescence spectrometry. *Archaeological and Anthropological Sciences*, 13(1), 1-17.

Kassianidou, Vasiliki. 2000. Hellenistic and Roman Mining in Cyprus. In *G.*, Ioannides and S., A., Hadjistyllis (eds.*) Acts of the Third International Congress of Cypriot Studies (Πρακτικὰ τοῦ Τρίτου Διεθνοῦς Κυπρολογικοῦ Συνεδρίου (Λευκωσία, 16-20 Ἀπριλίου 1996)*. Nicosia: Society of Cypriot Studies, 745–756.

Kassianidou, V., 2003. Archaeometallurgy: data, analyses and discussion. *The Sydney Cyprus Survey Project: Social Approaches to Regional Archaeological Survey, Monumenta Archaeologica*, *21*, 214-227.

Kassianidou, V. Unpublished Report in the framework of the WOODLAND project.

Kassianidou, V., Charalambous, A., Ioannides, D., Iacovou, M., Agapiou, A. and Zomeni, Z. 2022. Recording the copper slag heaps in the hinterland of the kingdom of Palaepaphos, In *Third International Congress on Archaeological Sciences in the Eastern Mediterranean and the Middle East (Nicosia 14-18 March 2022),* 45. (Last visited in (https://icasemme.cyi.ac.cy/images/Registration/ICAS-EMME_3_Book_of_Abstracts.pdf)

Keane, C.T., 2021. Ecclesiastical Economies: The Integration of Sacred and Maritime Topographies of Late Antique Cyprus. *Religions*, 12(11), 989. 1-27

Leonard, J.R., 2005. Roman Cyprus: Harbors, hinterlands, and "hidden powers". State University of New York at Buffalo.

Manasse, A. and Mellini, M., 2002. Chemical and textural characterisation of medieval slags from the Massa Marittima smelting sites (Tuscany, Italy). *Journal of Cultural Heritage*, *3*(3), 187-198.

Manning, S. 2013. Absolute dating of charcoal samples from the slag heaps. In Given, M., Knapp, A.B., Noller, J.S., Sollars, L. and Kassianidou, V. (eds), *Landscape and Interaction: The Troodos Archaeological and Environmental Survey Project, Cyprus. Volume 1*, London, Council for British Research in the Levant. 48-54.

McGlinchey, C., 2012. Handheld XRF for the examination of paintings: proper use and limitations. In Shugar A., N. & Mass, J. L. (Eds.) *Studies in Archaeological Sciences: Handheld XRF for Art and Archaeology*, Leuven University Press, 131-158.

McManamon, P. (2019*) LiDAR Technologies and Systems*, SPIE Press: Bellingham, WA, USA.

Michaelides, D., 1996. The economy of Cyprus during the Hellenistic and Roman periods. In Michaelides, D. and Karageorghis, V. (eds) *The Development of the Cypriot Economy from the Prehistoric Period to the Present Day*, 139-152.

Mulholland, R., Howell, D., Beeby, A., Nicholson, C.E. and Domoney, K., 2017. Identifying eighteenth century pigments at the Bodleian library using in situ Raman spectroscopy, XRF and hyperspectral imaging. *Heritage Science*, 5(1), 1-19.

Neff, H., Voorhies, B. and Paredas Umana, F., 2012. Handheld XRF elemental analysis of archaeological sediments: some examples from Mesoamerica. In Shugar A., N. & Mass, J. L. (Eds.) *Studies in Archaeological Sciences: Handheld XRF for Art and Archaeology*, Leuven University Press, 379-400.

Nerantzis, N., Bassiakos, Y. and Papadopoulos, S., 2016. Copper metallurgy of the Early Bronze Age in Thassos, north Aegean. *Journal of Archaeological Science: Reports*, *7*, 574-580.

Nerantzis, N., Bassiakos, Y., Georgakopoulou, M., Filippaki, E. and Mastrotheodoros, G., 2017. Copper production in Early Bronze Age Thassos: New finds and experimental simulation in the context of contemporaneous Aegean metallurgical practices. In *Archaeometallurgy in Europe IV* . Consejo Superior de Investigaciones Científicas, CSIC. 115-126.

Neubauer, W. 2004. GISin Archaeology - the Interface between Prospection and Excavation. Archaeological Prospection 11. 159-166.

Papacostas, T., 2001. The economy of late antique Cyprus. In Kingskey, S. and Decker, M. (eds) *Economy and exchange in the East Mediterranean during Late Antiquity*, Oxbow, 107-128.

Papalexandrou, A. and Caraher, 2012. W. Arsinoe in Late Antiquity and the Middle Ages, In W.A.P. Childs, J. S. Smith and J. M. Padgett, *City of Gold: The Archaeology of Polis Chrysochous, Cyprus*. Princeton University Art Museum, 267-282.

Parani, M., 2013. Artisanal production in Late Antique Cyprus, In: *The Insular System of the Early Byzantine Mediterranean: Archaeology and History*, D., Michaelides, P., Pergola and E., Zanini (Eds), BAR International Series 2523, Oxford.

Parcero-Oubiña, C., Fábrega-Álvarez, P., Güimil-Fariña, A., Fonte, J. and Valdez-Tulett, J., 2013. Castros, caminos, rutas y ocupación del espacio. Modelización y análisis de las formas de movilidad asociadas a los asentamientos de la Edad del Hierro a través de herramientas SIG. In Petroglifos, paleoambiente y paisaje. Estudios interdisciplinares del arte rupestre de Campo Lameiro (Pontevedra), F. Criado-Boado, A. Martínez-Cortizas and M. V. García Quintela (ed.), Madrid, CSIC, 171-185.

Philaniotou, O., Bassiakos, Y. and Georgakopoulou, M., 2011. Early Bronze Age Copper Smelting on Seriphos (Cyclades, Greece). *Metallurgy: Understanding How, Learning Why; Studies in Honor of James D. Muhly*, 157-164.

Pollard, A.M. and Bray, P., 2014. Chemical and isotopic studies of ancient metals. In *Archaeometallurgy in Global Perspective* (pp. 217-238). Springer, New York, NY.

Raber, P. 1987. Copper production in the Polis region, western Cyprus. *Journal of Field Archaeology*. Vol 14. No 3, 297-312.

Rademakers, F.W.and Rehren, Th., 2016. Seeing the forest for the trees: assessing technological variability in ancient metallurgical crucible assemblages. *Journal of Archaeological Science: Reports, 7*, 588-596.

Renzi, M., Georgakopoulou, M., Peege, C., Fasnacht, W. and Rehren, Th., 2018. 6. Technology of Copper Smelting at Agia Varvara-Almyras. *Agia Varvara-Almyras: An Iron Age Copper Smelting Site in Cyprus*, 269-294.

Shaar, R., Tauxe, L., Ben-Yosef, E., Kassianidou, V., Lorentzen, B., Feinberg, J.M. and Levy, T.E. 2015. Decadal-scale variations in geomagnetic field intensity from ancient Cypriot slag mounds. *Geochemistry, Geophysics, Geosystems*, 16(1), 195-214.

Scott, R.B., Eekelers, K. and Degryse, P., 2016. Quantitative chemical analysis of archaeological slag material using handheld X-ray fluorescence spectrometry. *Applied Spectroscopy*, *70*(1), 94-109.

Shackley, M.S., 2011. An introduction to X-ray fluorescence (XRF) analysis in archaeology. *X-ray fluorescence spectrometry (XRF) in geoarchaeology*. Springer, New York, NY. 7-44.

Shugar, A.N. and Mass, J.L., 2012. Introduction. In Shugar A.N. and Mass J.L (eds) *Studies in Archaeological Sciences: Handheld XRF for Art and Archaeology*, Leuven University. 17-36.

Shugar, A.N., 2013. Portable X-ray fluorescence and archaeology: limitations of the instrument and suggested methods to achieve desired results. In *Archaeological Chemistry* VIII. American Chemical Society. 173-193.

Socratous, M.A., Kassianidou, V. and Di Pasquale, G. 2015. Ancient slag heaps in Cyprus: the contribution of charcoal analysis tothe study of the ancient copper industry. In A. Hauptmann & D. Modarressi-Tehrani (ed.) Archaeometallurgy in Europe III: proceedings of the third International Conference, Deutsches Bergbau-Museum Bochum, June 29 – July 1, 2011. *Der Anschnitt Beiheft* 26, Bochum:Deutches Bergbau Museum. 377-384.

Steinberg, A. and Koucky, F. 1974. Preliminary metallurgical research on the ancient Cypriot copper industry. *Bulletin of the American Schools of Oriental Research. Supplementary Studies*, (18). 148-178.

Tobler, W. 1993. *Three presentations on geographical analysis and modelling*. Santa Barbara, National Center for Geographic Information and Analysis.

Tylecote, R.F., 1987. *The early history of metallurgy in Europe*. Longman.

Greek Literature

Browining, R. 2005. Η Κύπρος και οι Άραβες (Ζ'-Η' αι.). . In Παπαδόπουλος, Θ., (ed*) Ιστορία της Κύπρου, τόμ. 3, Βυζαντινή Κύπρος*, Λευκωσία, Ίδρυμα Αρχιεπισκόπου Μακαρίου Γ', Γραφείον Κυπριακής Ιστορίας. 235-292.

Κωνσταντίνου Γ. and Παναγίδης, Ι. 2013. *Κύπρος και Γεωλογία. Επιστήμη - Περιβάλλον - Πολιτισμός.* Bank of Cyprus Cultural Foundation, Nicosia.

Μαλιώτης, Γ. 2021. *Τα Μεταλλεία της Κύπρου: Συμβολή στην Καταγραφή και Μελέτη της Κυπριακής Μεταλλευτικής Βιομηχανίας.* Λευκωσία.

Μιτσίδης, Α., 2005. Η Εκκλησία της Κύπρου από τον 2ο μέχρι τον 5ο αιώνα. In Παπαδόπουλος, Θ., (ed*) Ιστορία της Κύπρου, τόμ. 3, Βυζαντινή Κύπρος*, Λευκωσία, Ίδρυμα Αρχιεπισκόπου Μακαρίου Γ', Γραφείον Κυπριακής Ιστορίας. 107-128.

Σακελλαρόπουλος, Σ. 2017. Ο *Κυπριακός Κοινωνικός Σχηματισμός (1191-2004): Από τη συγκρότηση στη διχοτόμηση*. Εκδόσεις Τόπος & Σπύρος Σακελλαρόπουλος, Αθήνα.

Χατζηιωάννου, Κ., 1973. *Η Αρχαία Κύπρος εις τας Ελληνικάς Πηγάς*, Τόμος Β: Μυθολογία και Θρησκεία - Γεωγραφία και Γεωλογία. Λευκωσία.

Online

https://www.peo.org.cy/el/ypiresies/mouseio/istoriko-mouseio (Last viewed 30.03.2022 01:55)

https://www.facebook.com/aerikostavounatoutroodous/photos/1071576013579801(Last viewed 30.03.2022 01:55)

https://eservices.dls.moi.gov.cy/#/national/geoportalmapviewer (Last viewed 30.03.2022 01:55)

https://www.usgs.gov/faqs/what-digital-elevation-model-de (Last viewed 30.03.2022 01:55)

https://pro.arcgis.com/en/pro-app/latest/tool-reference/spatial-analyst/understanding-cost-distance-analysis.htm (Last viewed 30.03.2022 01:55)

https://oxalid.arch.ox.ac.uk/Cyprus/Cyprus.html (Last viewed 30.03.2022 01:55)

http://www.moa.gov.cy/moa/wdd/wdd.nsf/page18_gr/page18_gr?opendocument (Last viewed 30.03.2022 01:55)

Appendix 1: Sample Catalog

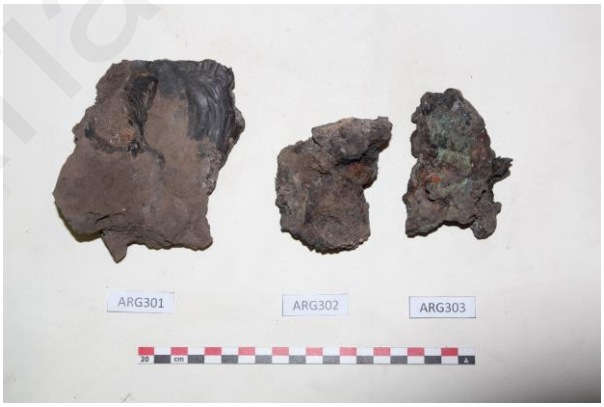

Appendix 2: Sample catalog of polished blocks

ARG001

ARG004

ARG310

ARG311

ARG403

ARG404

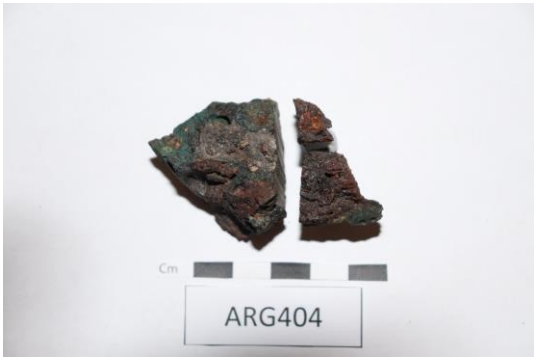

ARG408

ARG605

ARG606

ARG612

ARG616

PEL10

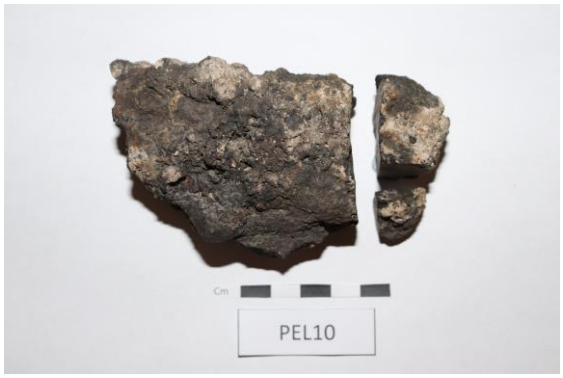

PEL12

PEL18

PEL21

PEL22

PEL28

PEL31

PEL38

PEL42

PEL57

PEL61

Appendix 3: Optical microscopy observations

A.1. Introduction

The assemblage studied is divided into two groups according to the manganese content in each sample, based on the HHpXRF results. The first group includes samples of a low manganese content (0.08 wt% - 6.53 wt%) and the second group of a medium to high manganese content (14.28 wt% - 38.24 wt%).

A.2. Group 1 (Mn = 0.08 - 6.53 wt%)

The first group is also the biggest one, reaching 60% of the samples analysed with hhXRF and 50% of the assemblage was prepared into polished blocks. The prepared samples from this group include nine slags, one rock and one ceramic.

A.2.1. The Argaka slag heap

ARG001

Description

Iron rich rock. On one edge the sample preserves its original structure, while on the other side it is altered due to exposure to high temperatures. At this side it is molten and the structure changes in mostly a glassy matrix and free iron oxides, namely magnetites (to insert photo with the molten part).

Interpretation

A piece of rock used for the furnace construction. One side was very close to the inside of the furnace and hence it is molten.

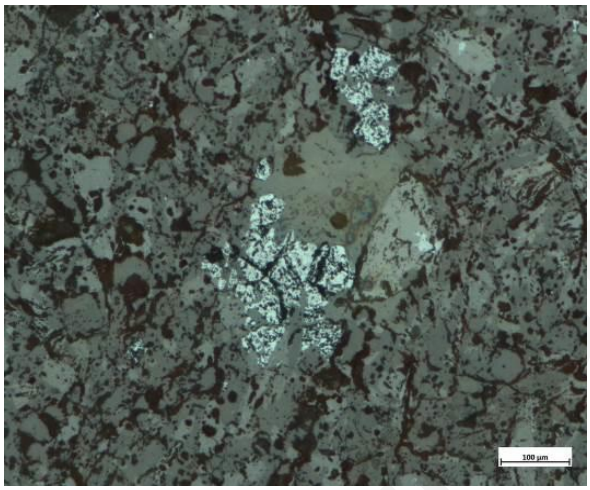

Figure 34: The normal microstructure of the rock (RL).

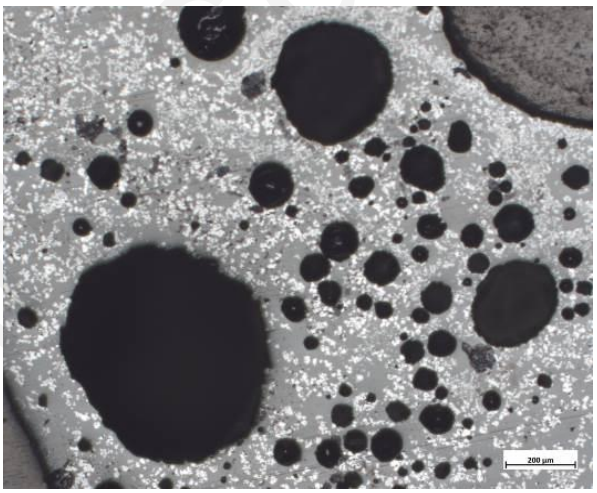

Figure 35: The part of the rock after exposure to high temperatures, there are free iron oxides (light grey) in a glassy matrix (dark grey) while there is high porosity (black) (RL).

ARG004

Description

Heavily corroded copper slag, free iron oxides partly turning from wüstite to magnetite (light grey), probably due to late-stage oxidation in the cooling slag, or subsequent corrosion. Some copper matte fragments (yellow) are not that common and the glassy matrix (dark grey).

Interpretation

Copper tap slag from matting process in a strongly reducing atmosphere, as indicated by the occurrence of primary wüstite.

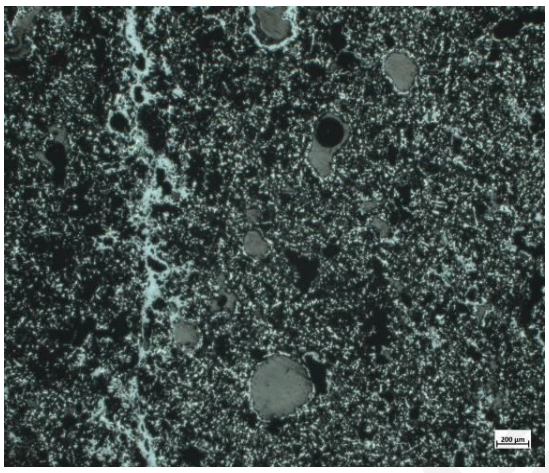

Figure 36. The corroded part of the slag (RL).

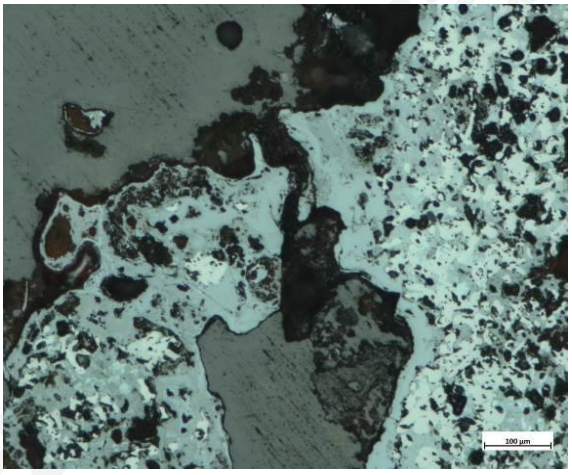

Figure 37. Copper matte (yellow) surviving (RL).

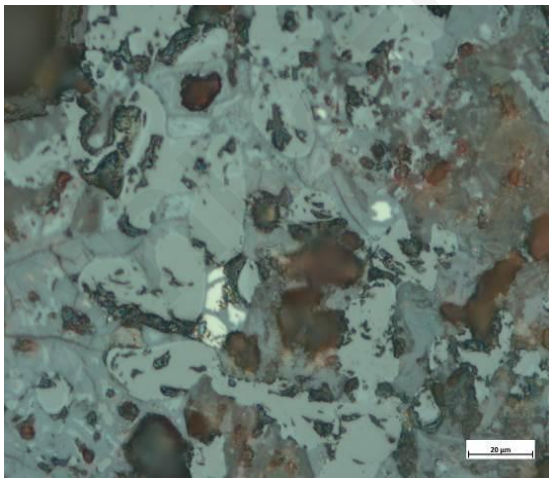

Figure 38. Wüstite (light grey) turning to magnetite (brownish-grey) (RL).

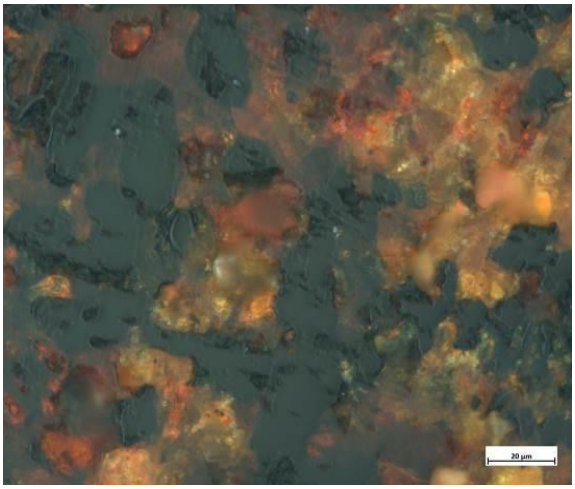

Figure 39. Same as Fig. 5 (PL).

ARG403

Description

Technical Ceramic fragment, heavily tempered, probably furnace wall fragment. There is some metallic copper surviving (orange) at the vitrified part of the ceramic and some copper matte inclusions (yellow) mostly entering through cracks.

Interpretation

Fragment from furnace lining of copper smelting.

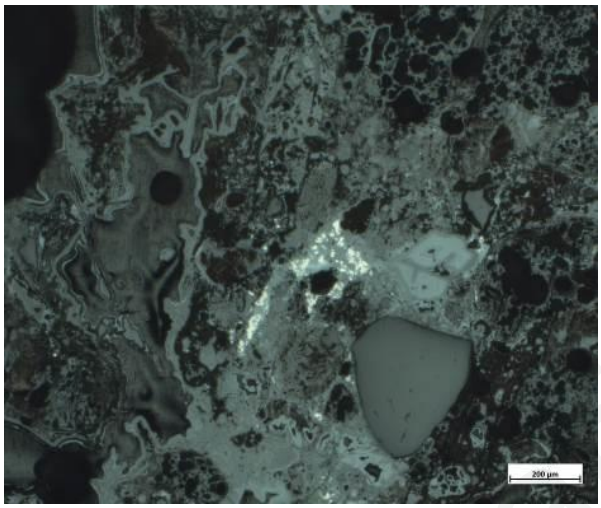

Figure 40. Copper matte (yellow) (RL).

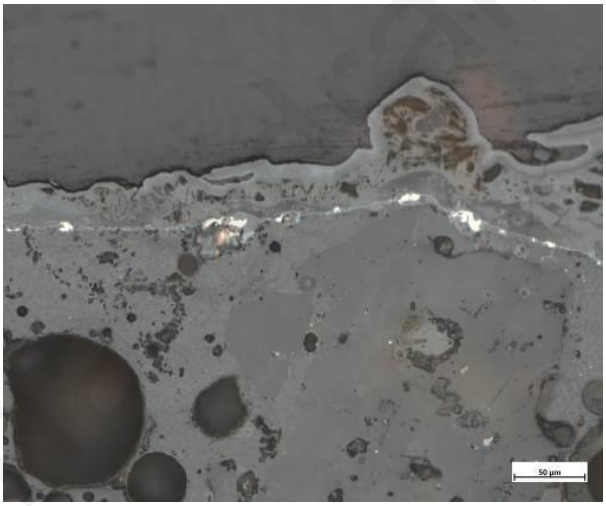

Figure 41. Copper matte (yellow) (RL).

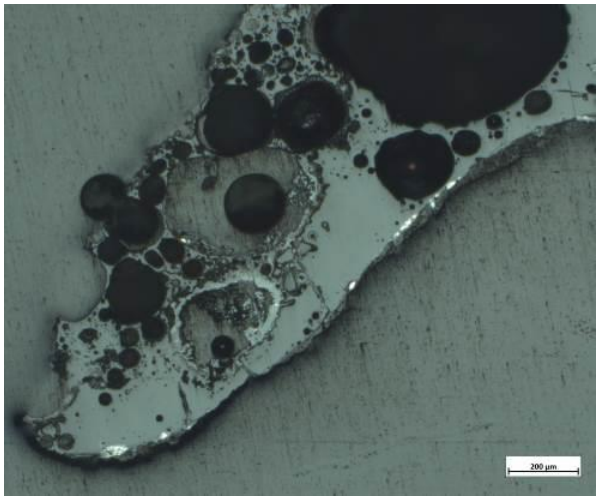

Figure 42: Metallic copper (bright orange prills) at the vitrified part of the ceramic (RL).

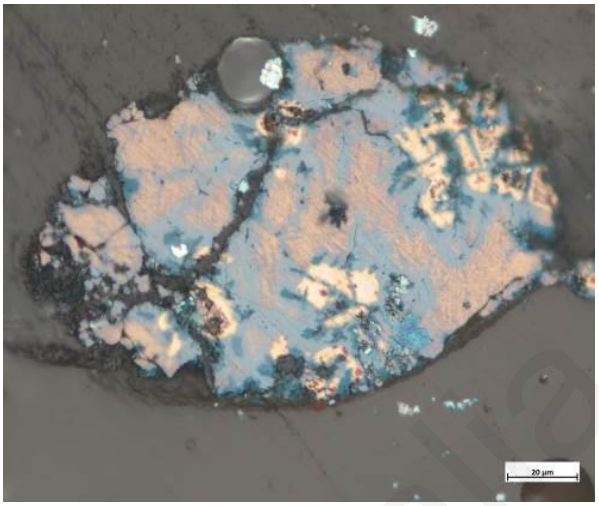

Figure 43. Copper matte of different matte phases (RL).

ARG404

Description

Copper slag, homogeneous. There are olivine crystals, small and fractured. Two big copper matte prills are close to the upper surfaces, while smaller particles are scattered in the rest of the slag matrix. Minute free iron oxide particles, most likely magnetite, are visible in the prills as eutectic formation, where they move iron from the matte to the rest of the slag as part of the oxidation and desulfurization of the primary ore. Hardly any free iron oxide / magnetite in the slag itself.

Interpretation

Copper tap slag, matting process, reducing atmosphere.

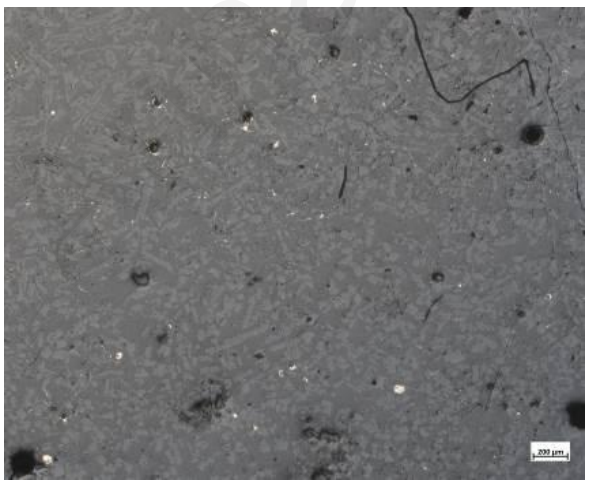

Figure 44. Olivine crystals (light grey), copper matte (yellow), glassy matrix (dark grey) (RL).

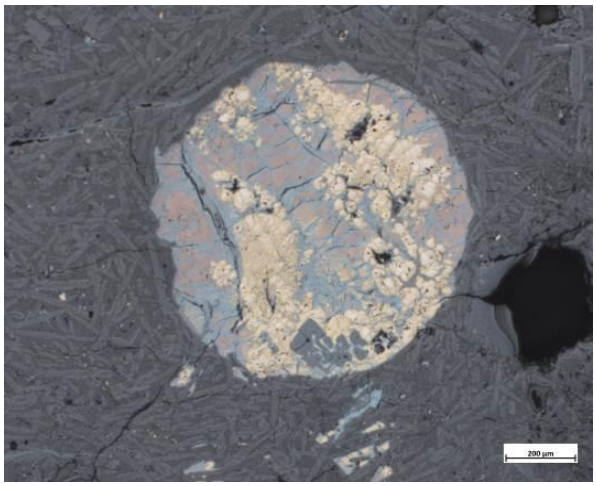

Figure 45. Copper matte prill showing different matte phases indicated by different colors (RL).

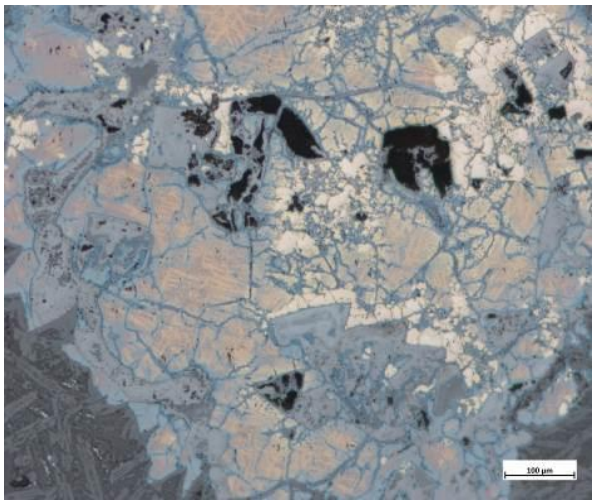

Figure 46: Copper matte prill, showing different copper matte phases (yellow orange, reddish, grey blue, purple), notice the grey crystal in the center and lower part of the picture which preserves the original ore crystalisation (RL).

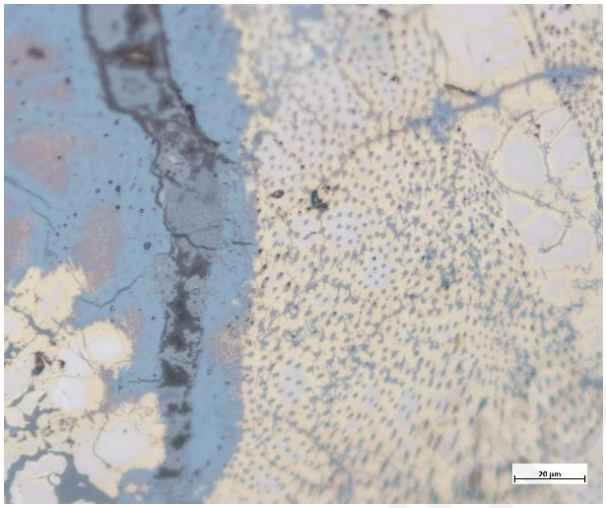

Figure 47. Detail of the prill of Fig. 13. Where the magnetite (light grey dots) move away from the copper matte (yellow) (RL).

ARG408

Description

Copper slag, quite homogeneous. Elongated skeletal olivine crystals (light grey), which tend to be smaller towards the edges and bigger in the centre. There is copper matte (yellow, light blue) but no free iron oxides. There are big gas holes (black) and the glassy matrix (dark grey).

Interpretation

Copper tap slag of matting process in a reducing atmosphere.

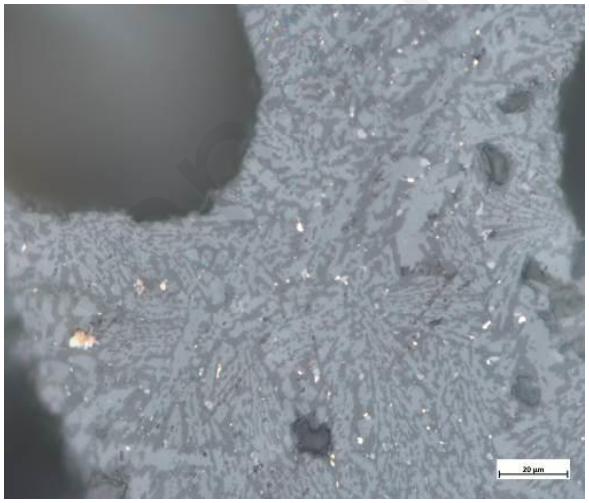

Figure 48: Olivine crystals (light grey) and copper matte (yellow) in the glassy matrix (dark grey) (RL).

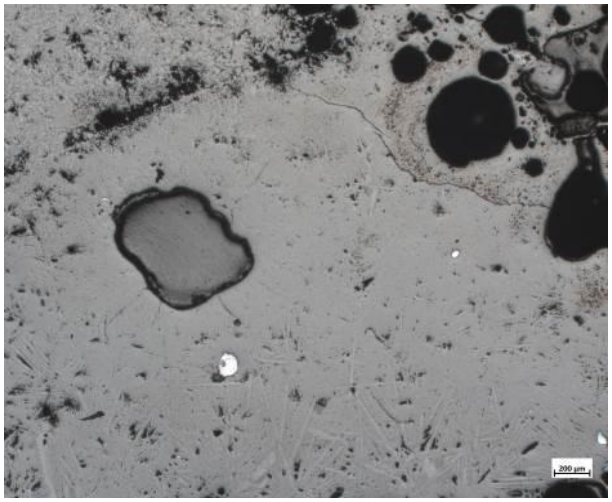

Figure 49: Same as in Fig. 48. But with blue copper matte prills (RL)

ARG605

Description

Copper slag which is homogeneous but partially corroded. There are elongated skeletal olivine crystals (light grey). Copper sulphides (Cu – Fe sulfides ranging between covellite and chalcopyrite, yellow, orange, reddish and blue colours) showing there was a matting process, in a glassy matrix (dark grey). There is a sole crystal (spinel) of a rounded triangular shape (medium grey). There are no free iron oxides.

Interpretation

Copper tap slag, matting process, reducing atmosphere. Olivine crystal shape indicating rapid cooling, as is typical for tap slag.

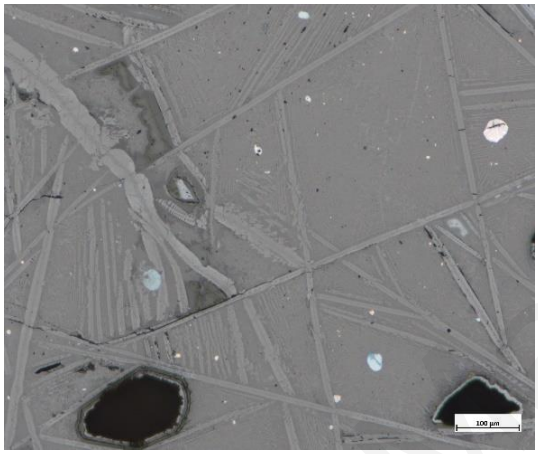

Figure 50. Olivine crystals (light grey), copper matte prills (light blue) in a glassy matrix (dark grey) (RL).

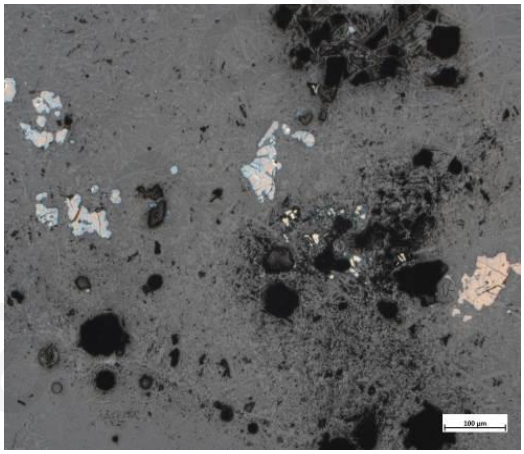

Figure 51. Same as in Fig. 50. But with more copper matte phases (yellow, blue, light blue) (RL).

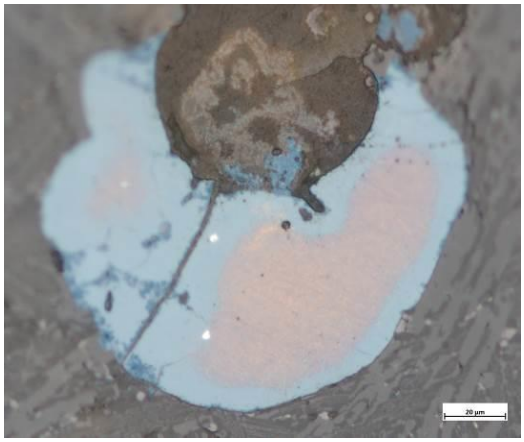

Figure 52. Copper matte prill (blue, red-orange) (RL).

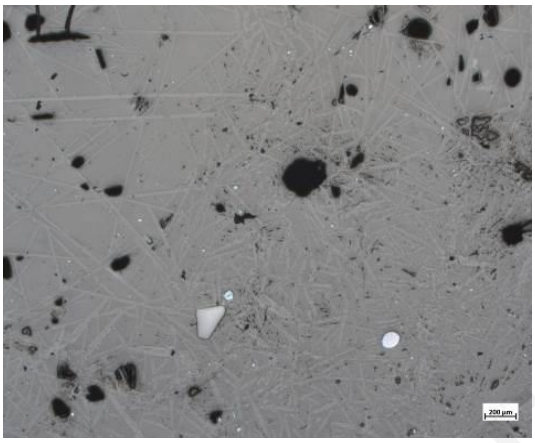

Figure 53. Same as in Fig. 50 and 51 with a rounded triangular crystal (light grey) (RL).

ARG606

Description

Copper slag, quite homogeneous. Elongated skeletal olivine crystals (light grey) and copper matte (yellow, orange, blue) in a glassy matrix (dark grey). There are no free iron oxides.

Interpretation

Copper tap slag of matting process in reducing atmosphere. Olivine crystal shape indicating rapid cooling, as is typical for tap slag.

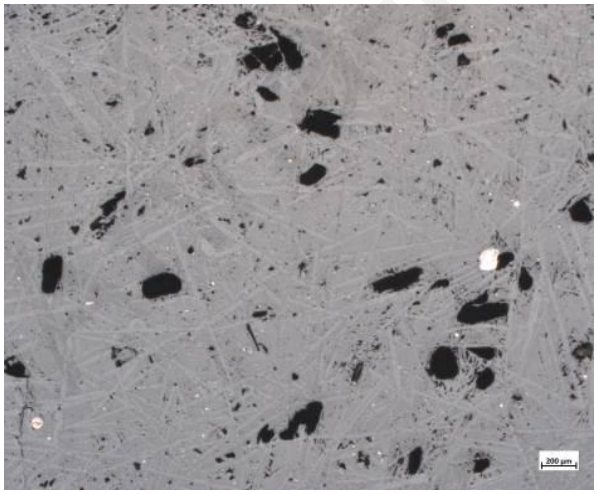

Figure 54: Olivine crystals (light grey), copper matte (yellow, orange, blue) in a glassy matrix (dark grey) (RL).

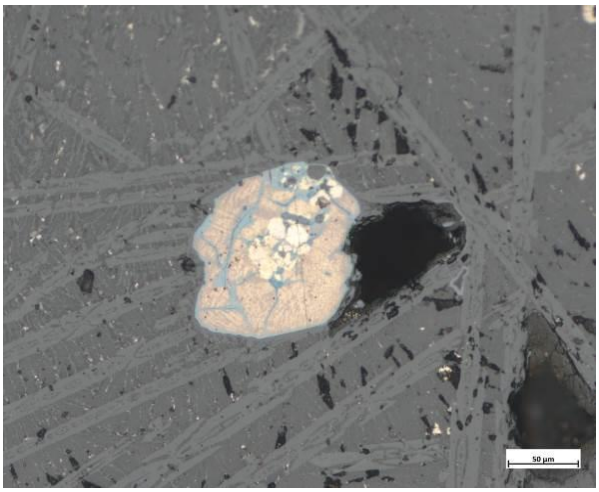

Figure 55: Copper matte of different phases (yellow, blue, orange) (RL).

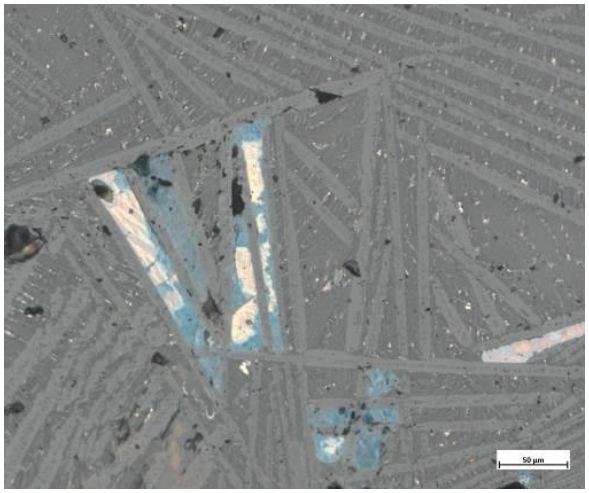

Figure 56: Copper matte (yellow, blue) filling the space between olivine crystals (light grey) (RL).

ARG612

Description

Copper slag, very heterogeneous. There are a lot of free iron oxides, namely magnetite (light grey), of various sizes. There are a few different copper phases, e.g., delafossite (light grey laths-needles), cuprite (grey under RL, red under PL) and metallic copper (orange). Everything in a glassy matrix (dark grey).

Interpretation

Copper melting tap slag under oxidising atmosphere with a iron-corroded area taking approximately a third of the sample analysed.

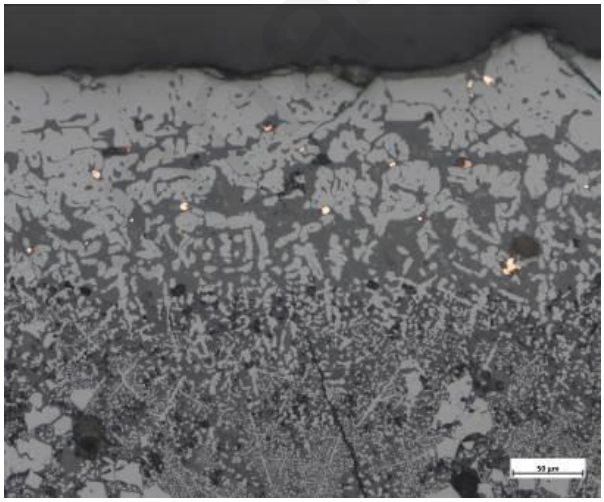

Figure 57: Free iron oxides (light grey) in a glassy matrix (dark grey) with metallic copper prills (orange) (RL).

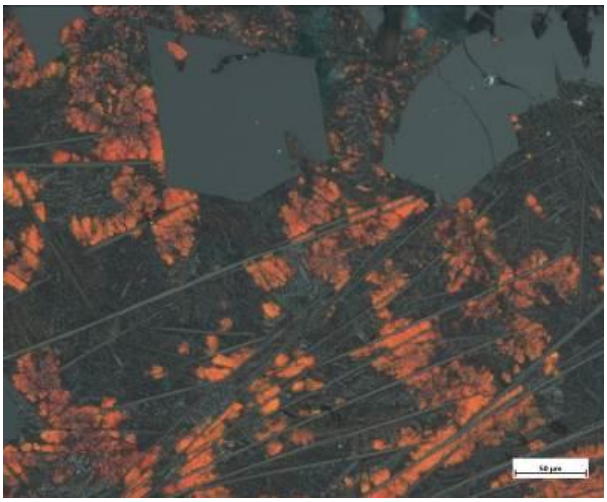

Figure 58: Free iron oxides of angular shape, magnetite, (light grey), delafossite crystals needle-shaped (light grey) and cuprite dendrites (red) (PL).

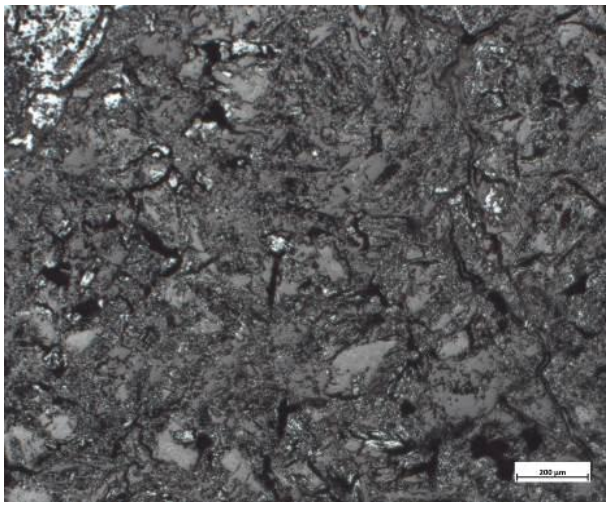

Figure 59: The corroded iron area (RL).

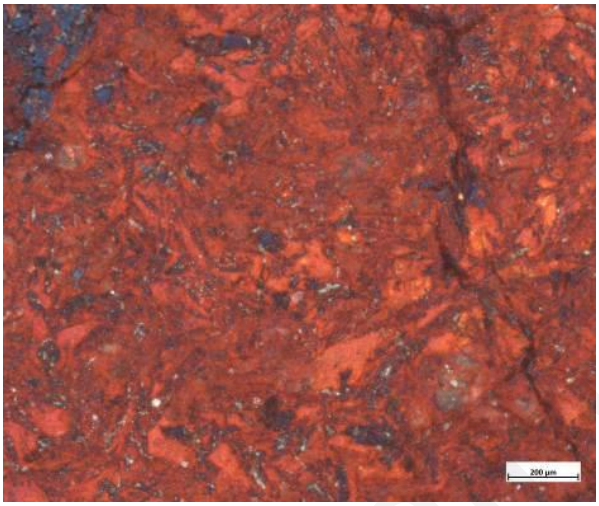

Figure 60: Same as in Fig. 58 (PL).

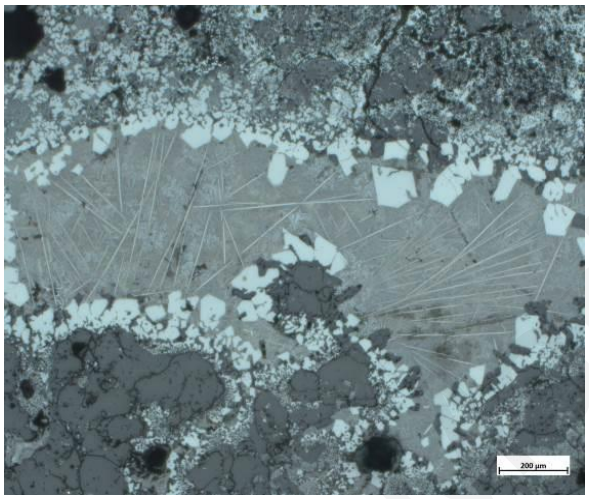

Figure 61. Same as in Fig. 58, spinels surrounding delafossite and cuprite formations (RL).

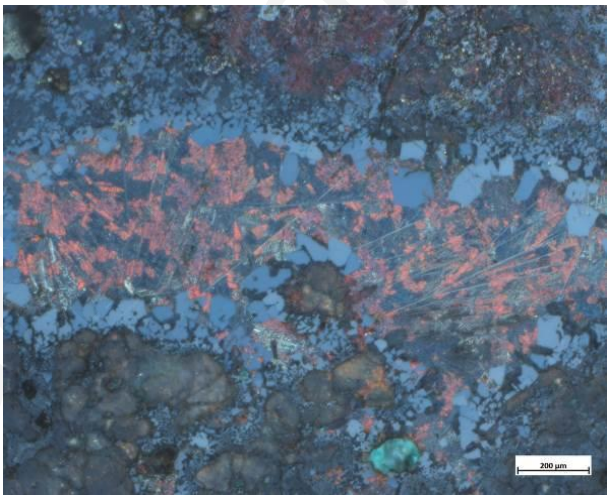

Figure 62. Same as in Fig. 61 (PL).

A.2.2. The Pelathousa slag heap

PEL31

Description

Copper slag, quite homogeneous. Skeletal elongated olivine crystals (light grey), copper matte (yellow, orange, blue), metallic copper (orange) in a glassy matric (dark grey). There are no free iron oxides.

Interpretation

Copper tap slag of matting process in a reducing atmosphere. Olivine crystal shape indicating rapid cooling, as is typical for tap slag.

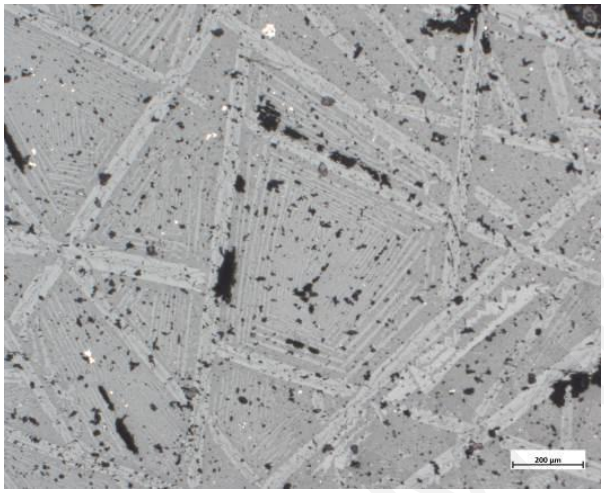

Figure 63. Olivine crystals (light grey) in a glassy matrix (dark grey) (RL).

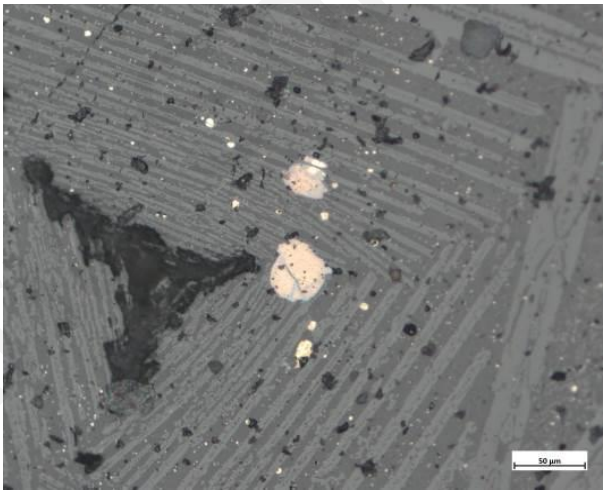

Figure 64. Copper matte prills (yellow, orange) (RL).

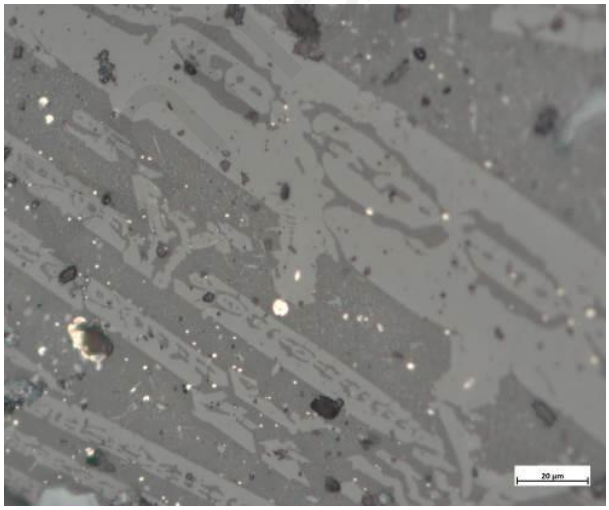

Figure 65. Metallic copper prills (orange) (RL).

PEL21

Description

A copper slag, quite homogeneous. Elongated skeletal olivine crystals (light grey), copper matte (yellow, blue) and small bits of metallic copper (orange) in the copper matte prills, in a glassy matrix (dark grey). There are no free iron oxides.

Interpretation

Copper tap slag of matting process under reducing atmosphere. Olivine crystal shape indicating rapid cooling, as is typical for tap slag.

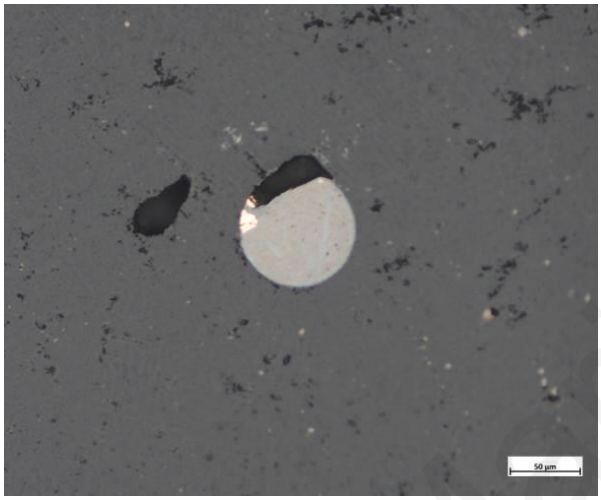

Figure 66. Copper matte prill (yellow) with metallic copper (orange) (RL).

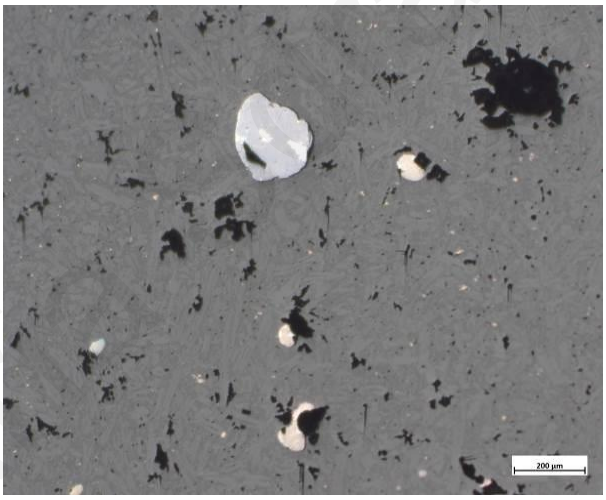

Figure 67. Olivine crystals (light grey), copper matte (yellow and light blue) in a glassy matrix (dark grey) (RL).

PEL42

Description

Copper slag, homogeneous. There are skeletal olivine crystals (medium grey), free iron oxides (light grey) partly turning from wüstite to magnetite, probably due to late-stage oxidation in the cooling slag, or subsequent corrosion, spinels (light-medium grey) and copper matte (yellow and blue) in a glassy matrix (dark grey). Iron oxides, magnetite, indicate the flow lines of the tap slag.

Interpretation

Copper tap slag of matting process in a reducing atmosphere. Olivine crystal shape indicating rapid cooling, as is typical for tap slag.

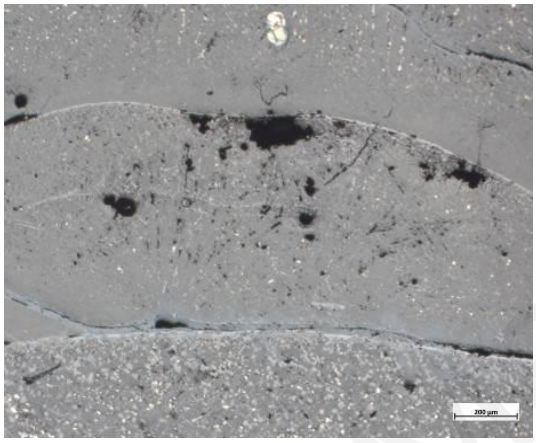

Figure 68. : Iron oxides (light grey) define the flow lines of the tap slag, copper matte (yellow) and glassy matrix (dark grey) (RL).

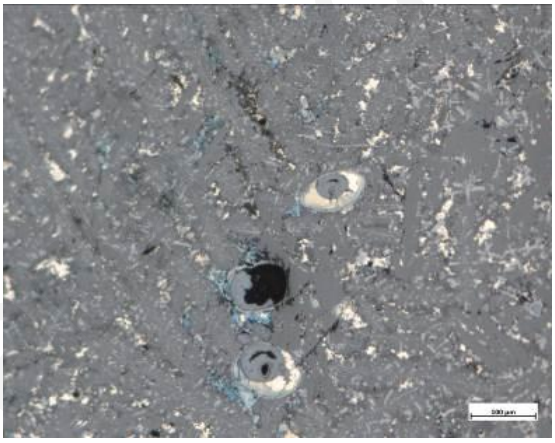

Figure 69. Olivine crystals (medium grey), spinels (light-medium grey), free iron oxides (light grey), copper matte (yellow and blue) and glassy matrix (dark grey) (RL).

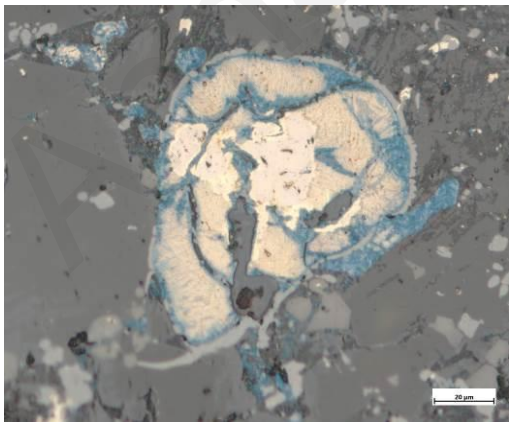

Figure 70. 69: Copper matte prill (yellow and blue) (RL).

PEL57

Description

A homogeneous copper tap slag with olivine crystals (light medium grey), copper matte (yellow and light grey), some corrosion (light grey) all in a glassy matrix (dark grey)

Interpretation

Copper tap slag of primary smelting procedures.

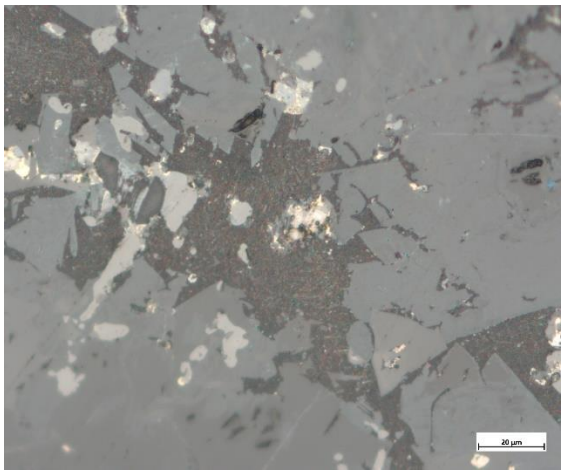

Figure 71. Fayallite crystals (medium grey), and copper matte (light grey, yellowish) in a glassy matrix (dark grey).

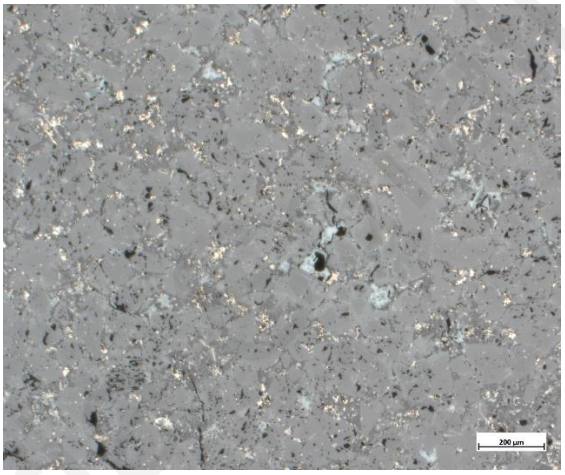

Figure 72. Same as in Fig. 71.

A.3. Group 2 (Mn = 14.28 – 38.24 wt%)

This group encompasses the rest of the sample. It was a challenge on how to divide the rest of the samples, namely whether they should form two more groups or just one. Though, since there was not really manganese gap that would indicate clear lines in the two groups it was decided to form one. Afterall most of the samples behave in the exact same way.

A.3.1. The Argaka slag heap

ARG616

Description

Copper slag, homogeneous. The matrix is very glassy (dark grey), there are some pyroxene crystals (light grey), copper matte prills (yellow, blue) and some minute metallic copper prills (orange).

Interpretation

Copper tap slag of melting/refining process under reducing atmosphere.

Figure 73. Copper matte prill (yellow) with small bits of metallic copper (orange) (RL).

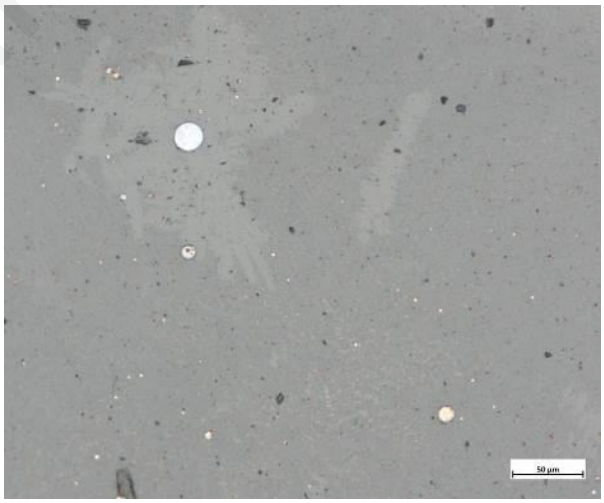

Figure 74. Pyroxene crystals (light grey), copper matte prills (light blue, yellow), metallic copper prills (orange) in a glassy matrix (dark grey) (RL).

ARG310

Description

Copper slag, quite corroded. Olivine crystals are elongated and skeletal (medium grey) in a glassy matrix (dark grey). Copper matte (yellow, blue, light blue) is evenly distributed in the sample.

Interpretation

Copper tap slag of matting process under reducing atmosphere. Olivine crystal shape indicating rapid cooling, as is typical for tap slag.

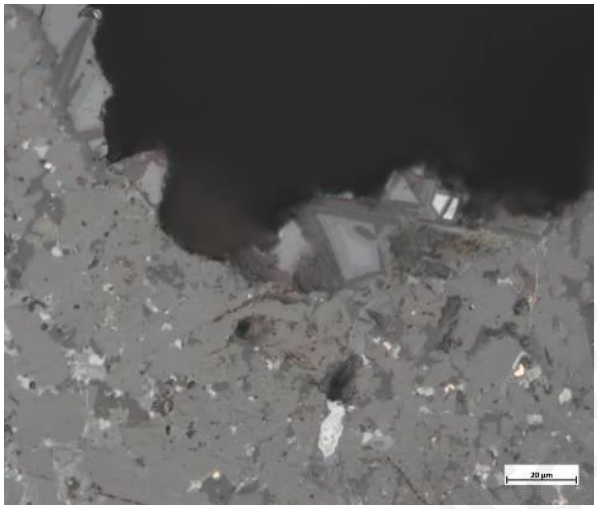

Figure 75. Olivine crystals (medium grey), copper matter (yellow), spinels (?) (light grey) in a glassy matrix (dark grey) (RL).

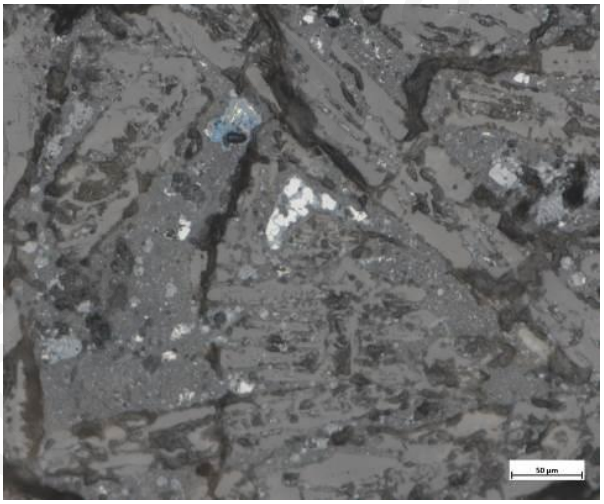

Figure 76. Same as in Fig. 74 with a clearer view on the glassy matrix (RL).

ARG311

Description

Homogeneous copper slag. Olivine crystals are skeletal and fractured (light grey) in a glassy matrix (dark grey). Copper matte (yellow, red, purple, blue) of different sizes and shapes. Some metallic copper is rare (orange) and surrounded by copper matte.

Interpretation

Copper tap slag of matting process under reducing atmosphere. Olivine crystal shape indicating rapid cooling, as is typical for tap slag.

Figure 77. Olivine crystals (light grey), copper matte (purple, yellow) in a glassy matrix (dark grey) (RL).

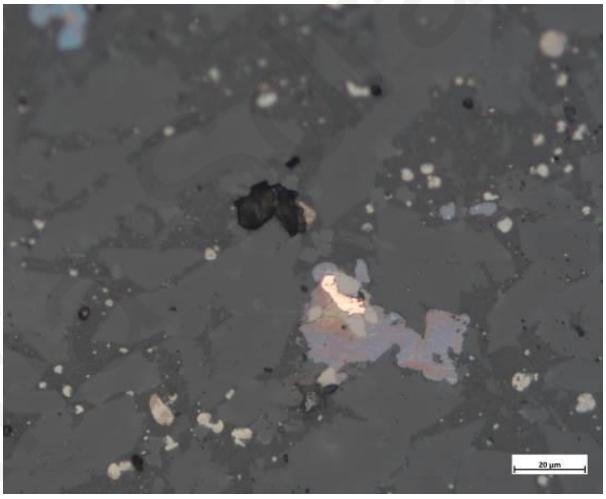

Figure 78. : Detail of Fig. 77, notice the metallic copper (orange) emerging from the copper matte (RL).

A.3.2. The Pelathousa slag heap

PEL10

Description

Copper slag, quite corroded. Olivine crystals (medium grey but also a hue a bit darker). Free iron oxides partly turning from wüstite to magnetite (light grey), probably due to late-stage oxidation in the cooling slag, or subsequent corrosion, into a glassy matrix (dark grey). Copper sulphides, matte (yellow, light blue, blue). Lines of iron oxides, most likely magnetite, outline the different flows of tap slag. Close to the flow lines there are different sizes of fayalite crystals showing that the lower slag was already cool when the upper flow touched it, this way leaving little time for the crystals to grow.

Interpretation

Copper tap slag, matting process, reducing atmosphere.

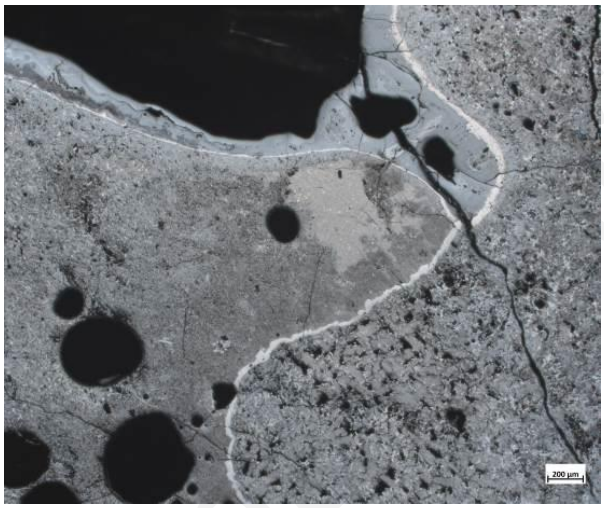

Figure 79. Iron oxides (light grey) delineating the flow lines of the tap slag (RL).

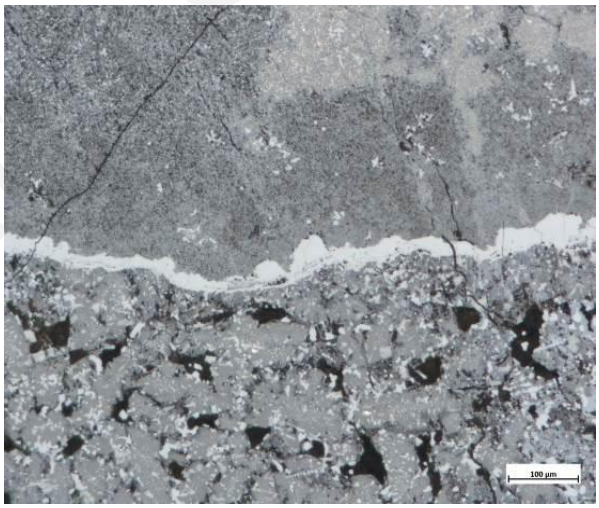

Figure 80. Detail of Fig. 79 with iron oxides (light grey), olivine crystals (medium grey). Notice the different size of the olivine crystals in the upper part of the picture and the lower, indicating that the lower flow was already cold when the upper one touched it (RL).

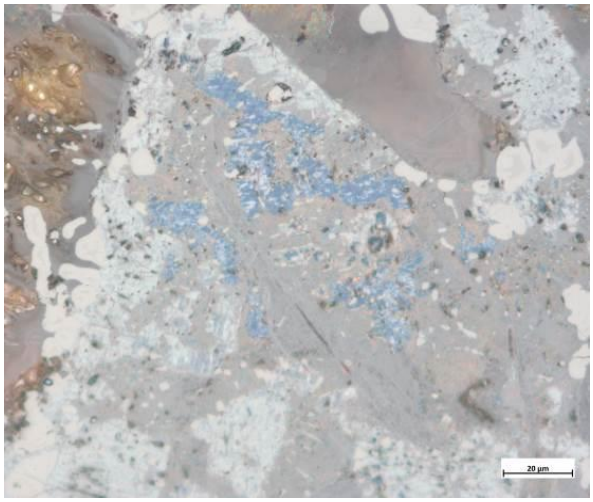

Figure 81. Copper matte (yellow and blue) (RL).

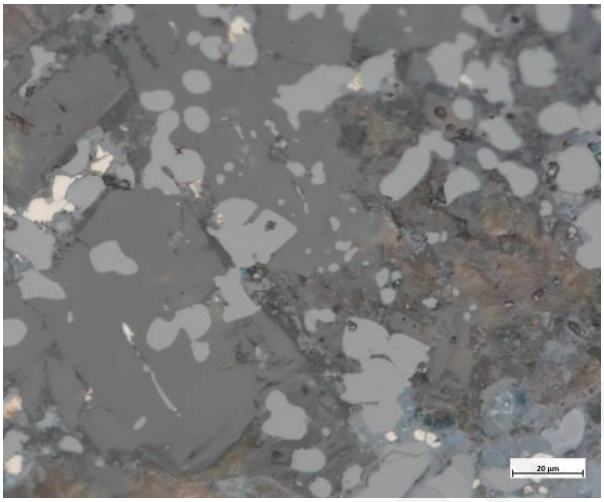

Figure 82. Free iron oxides (light grey), blocky olivine crystals (medium grey) and copper matte (yellow) (RL).

PEL18

Description

Copper tap slag, quite homogeneous. There are some very small olivine crystals close to the outer surface of the slag (light grey- insert picture), pyroxenes (medium grey), copper matte (light blue) but mostly metallic copper prills (orange) in the glassy matrix (dark grey). The matrix is extremely glassy with some striations showing the flow of the slag. There are no free iron oxides.

Interpretation

Copper tap slag of copper smelting operations under reducing and very high atmosphere.

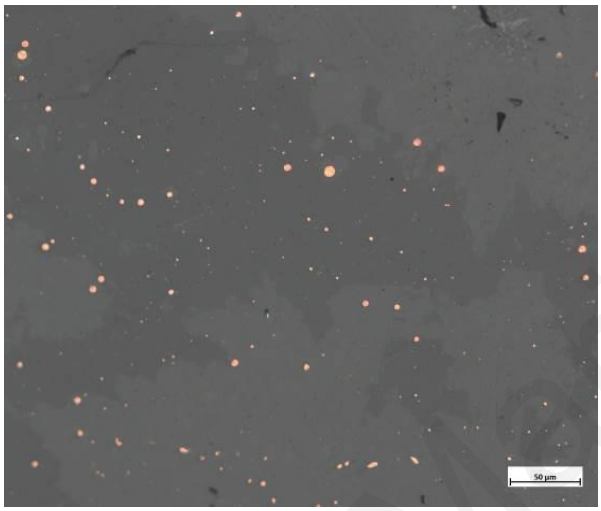

Figure 83. Pyroxenes (light grey), metallic copper (orange) in the glassy matrix (dark grey) (RL).

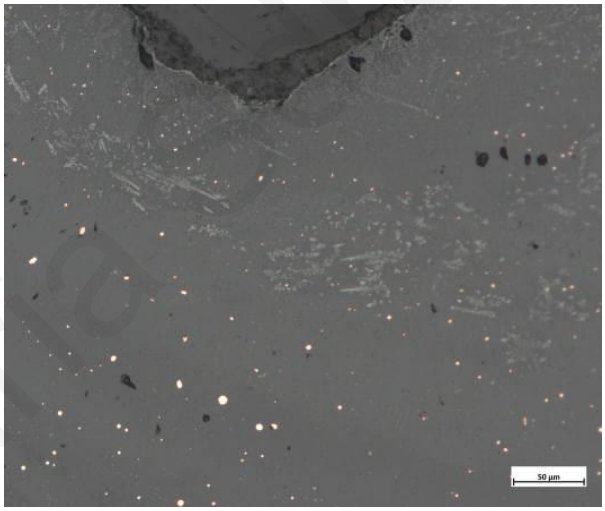

Figure 84. Same as in Fig. 82 but with some smaller crystals close to the surface (pyroxenes).

PEL12

Description

Copper slag, quite homogeneous but heavily corroded. There are free iron oxides partly turning from wüstite to magnetite (light grey), probably due to late-stage oxidation in the cooling slag, or subsequent corrosion, and some small remains of copper matte (white-yellow), everything in the glassy matrix (dark grey). Iron oxide creating lines, magnetite, signify the different flows (light grey).

Interpretation

Copper tap slag of multiple flows of matting process under reducing atmosphere.

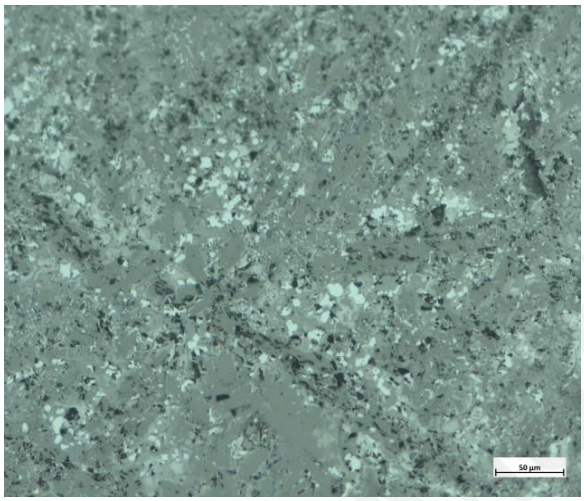

Figure 85. Corroded slag, iron oxides (light grey), copper matte (yellow) (RL).

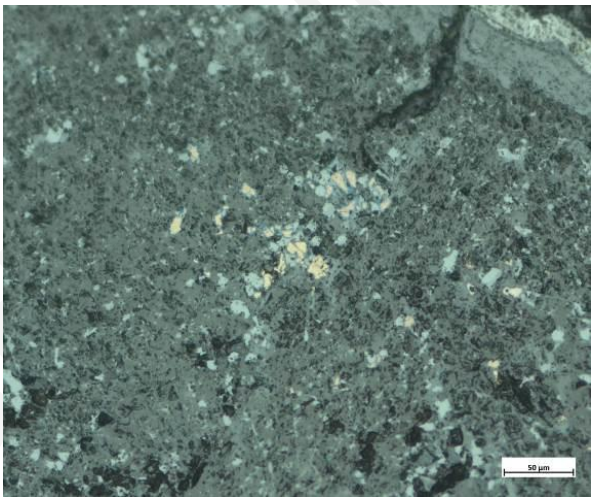

Figure 86. Same as in Fig. 85 with better detail (RL).

PEL21

Description

Copper slag, homogeneous. Elongated skeletal olivine crystals (light grey) in a glassy matrix (dark grey). Copper matte of different sizes (yellow, blue).

Interpretation

Copper tap slag of matting process under reducing atmosphere. Olivine crystal shape indicating rapid cooling, as is typical for tap slag.

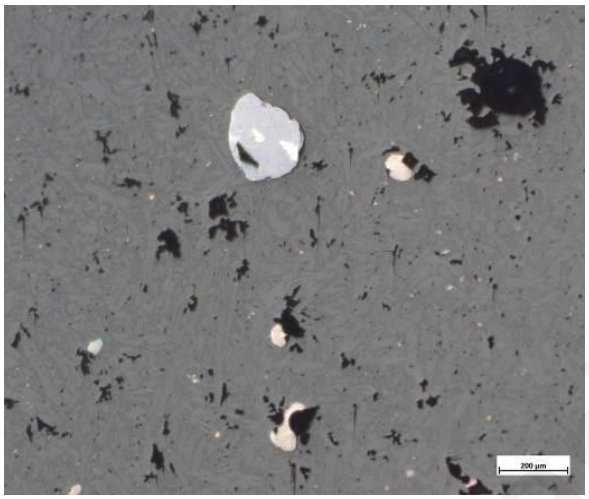

Figure 87. Olivine crystals (light grey), copper matte (yellow, blue) and glassy matrix (dark grey) (RL).

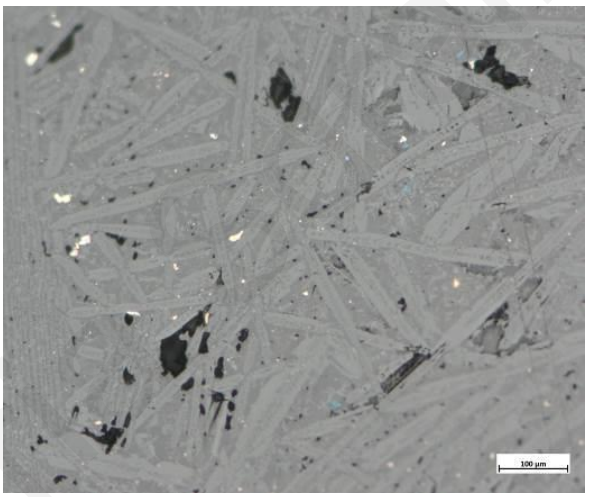

Figure 88. Same as in Fig. 87 (RL).

PEL22

Description

Copper slag, homogeneous. Skeletal olivine crystals (medium grey) in a glassy matrix (dark grey). Copper matte of various shapes and colours (yellow, blue, white-yellow) are scattered evenly. Different flows are outlined by iron oxides, magnetite (light grey).

Interpretation

Copper tap slag of multiple flows of matting process under reducing atmosphere. Olivine crystal shape indicating rapid cooling, as is typical for tap slag.

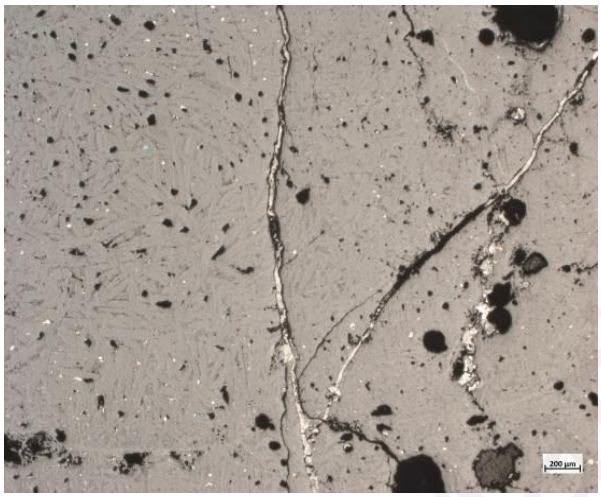

Figure 89. Olivine crystals (light grey), copper matte (yellow, blue) and glassy matrix (dark grey) (RL).

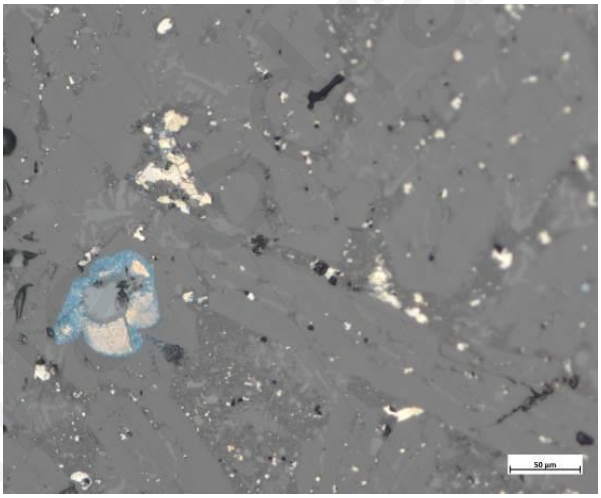

Figure 90. Same as in Fig. 89 (RL).

PEL28

Description

Homogeneous copper slag. Skeletal olivine crystals, copper matte (blue, yellow, red, purple) in a glassy matrix (dark grey). Some rare copper metal prills (orange) are generally surrounded by copper matte.

Interpretation

Copper tap slag of matting process under reducing atmosphere. Olivine crystal shape indicating rapid cooling, as is typical for tap slag.

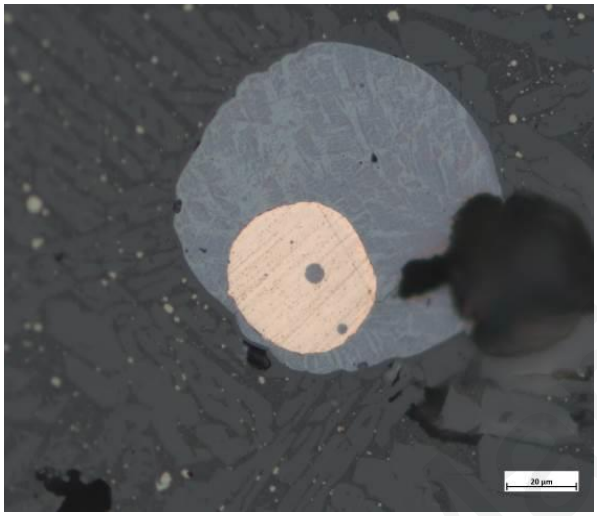

Figure 91. Olivine crystals (light grey), copper matte (light and dark blue), metallic copper (orange) in the copper matte and glassy matrix (dark grey) (RL).

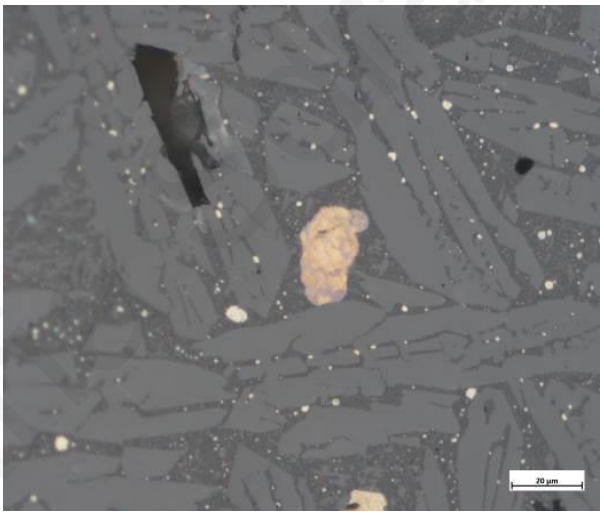

Figure 92. Same as in Fig. 91 (RL).

PEL38

Description

A quite homogeneous copper slag. There are skeletal olivines (medium grey), free iron oxides sometimes forming dendrites (light grey) and a glassy matrix (dark grey). There is copper matte (light yellow) scattered more or less evenly in the slag. Lines of magnetite (light grey) show the different flows of the slag.

Interpretation

Copper tap slag of matting process under oxidising atmosphere.

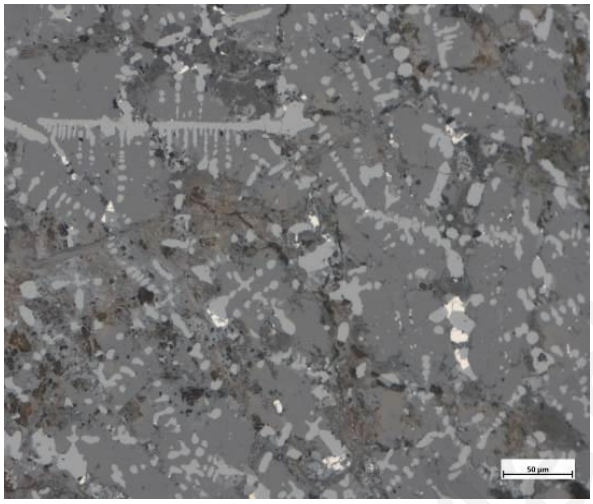

Figure 93. Olivine crystals (medium grey), iron oxides (light grey) copper matte (yellow) and glassy matrix (dark grey) (RL).

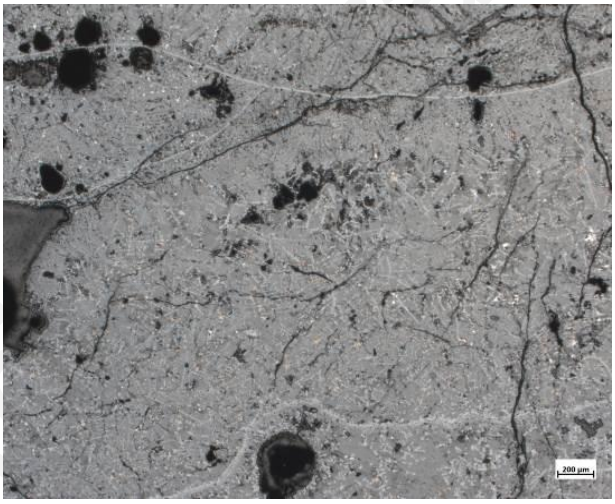

Figure 94. Same as in Fig. 93, notice the iron oxides (light grey) creating lines that indicate the flow lines of the tap slag (RL).

PEL61

Description

A homogeneous copper slag. Skeletal olivine crystals of various sizes, depending on how quickly they were cooled down (medium grey). A small amount of free iron oxides, magnetite, are also present (light grey), in a glassy matrix (dark grey). Metallic copper (orange) prills of mostly minute size are sometimes surrounded by copper sulphides, covellite (blue).

Interpretation

Copper tap slag of matting process under reducing conditions. Although there is some magnetite, it is not enough to support the atmosphere was very oxidising. Olivine crystal shape indicating rapid cooling, as is typical for tap slag.

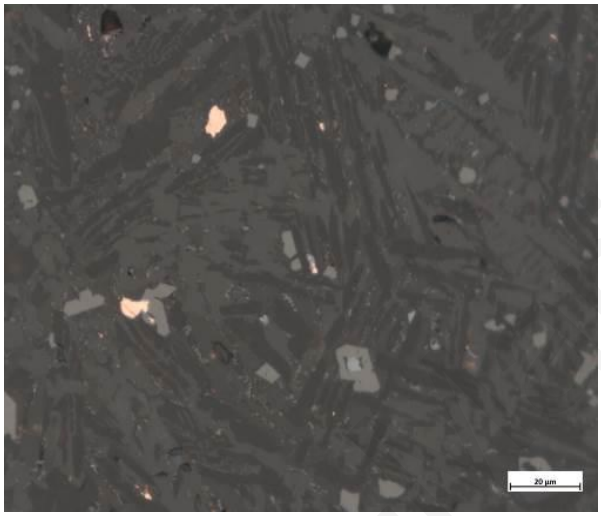

Figure 95. Olivine crystals (medium grey), spinels (light grey), metallic copper (orange) and glassy matrix (dark grey) (RL).

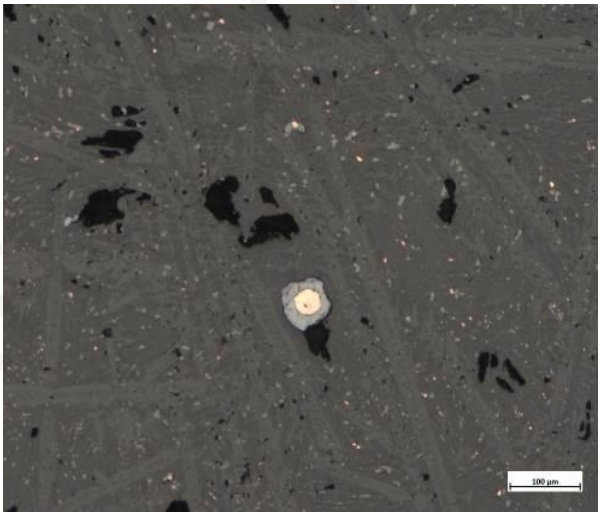

Figure 96. Same as in Fig. 93, with metallic copper (orange) surrounded by copper matte (blue) (RL).

Appendix 4. SEM-EDS tables and photos

Average values of bulk analysis in Oxides% by Stoichiometry																	
Sample	Na_2O	MgO	Al_2O_3	SiO_2	P_2O_5	SO_3	K_2O	CaO	TiO_2	V_2O_5	MnO	FeO	CuO	ZnO	BaO	PbO	Total
ARG310	1,1	1,7	10,3	32,1	0,22	0,82	1,11	3,1	0,36	0,2	31,7	15,4	0,92	0,11	0,96	ND	100
PEL28	0,80	2,0	6,8	32,2	0,20	0,79	1,0	3,2	0,16	ND	27,2	24,5	0,47	0,16	0,59	ND	100
PEL61	0,11	0,91	11,1	35,9	0,35	ND	0,36	10,9	0,41	ND	23,4	14,4	2,0	ND	ND	ND	100
PEL21	0,48	1,9	10,9	34,0	0,18	0,38	0,64	8,8	0,41	ND	23,4	18,0	0,52	ND	ND	0,23	100
PEL38	0,42	1,2	5,4	26,8	0,21	1,55	0,79	2,1	ND	ND	18,9	41,1	0,73	0,14	0,56	ND	100
PEL18	0,29	2,3	8,6	41,6	0,23	ND	0,29	6,2	0,24	ND	14,5	23,8	1,8	ND	ND	ND	100
ARG616	0,62	3,5	10,7	40,9	0,14	0,34	0,49	7,0	0,33	ND	13,3	21,9	0,39	ND	0,26	ND	100
PEL10	ND	0,58	3,7	26,7	0,21	1,22	0,15	ND	ND	ND	11,5	53,3	1,0	ND	0,37	ND	100
ARG404	1,1	2,1	12,3	37,2	0,17	0,58	0,93	5,9	0,50	ND	2,2	35,4	1,6	ND	ND	ND	100
ARG605	1,3	2,3	14,1	36,5	0,26	0,30	ND	6,9	0,54	ND	2,0	35,2	0,47	ND	ND	ND	100
PEL31	1,5	3,2	11,8	37,9	0,08	0,42	1,2	5,3	0,24	ND	1,0	36,7	0,24	0,25	ND	ND	100
PEL57	ND	2,2	4,4	28,4	0,15	1,07	0,44	1,3	0,11	ND	0,54	59,2	0,94	0,28	ND	ND	100
ARG612	ND	1,0	3,4	43,5	0,42	0.1	0.1	1,6	0,10	ND	0,33	47,2	2,2	ND	ND	ND	100
ARG403	0,30	1,0	20,8	57,2	0,16	0,19	1,4	1,1	1,3	ND	0,15	12,5	0,86	ND	ND	ND	100
ARG001	4,4	3,6	16,8	61,6	ND	ND	0,24	6,0	0,41	ND	ND	6,8	ND	ND	ND	ND	100

Table 8. Average bulk analysis.

Average values of olivine crystals in Oxides% by Stoichiometry														
Sample	Na_2O	MgO	Al_2O_3	SiO_2	P_2O_5	SO_3	K_2O	CaO	TiO_2	MnO	FeO	CuO	ZnO	Total
ARG001	NONE													
ARG310	ND	3,8	0,59	29,7	ND	ND	ND	5,2	0,10	51,6	8,8	ND	ND	100
ARG403	NONE													
ARG404	ND	8,1	0,60	32,2	ND	ND	ND	0,62	ND	3,2	54,6	0,49	ND	100
ARG605	ND	8,7	0,55	30,8	ND	ND	ND	0,87	ND	3,4	55,6	ND	ND	100
ARG612	NONE													
ARG616	ND	12,9	0,4	33,7	ND	ND	ND	0,84	ND	19,6	32,25	ND	ND	100,00
PEL10	ND	4,3	0,50	29,6	0,12	ND	ND	3,2	ND	33,7	28,3	ND	ND	100
PEL18	0,2	3,8	5,6	36,6	0,23	4,2	ND	ND	0,13	19,3	29,1	0,74	ND	100
PEL21	ND	5,3	0,35	30,8	ND	ND	ND	3,1	ND	37,7	22,4	ND	ND	100
PEL28	ND	4,1	0,24	29,9	ND	ND	ND	0,93	ND	37,0	27,8	ND	ND	100
PEL31	ND	12,8	0,29	31,9	0,09	ND	ND	0,44	ND	1,4	52,7	ND	0,21	100
PEL38	ND	3,4	0,40	29,6	ND	ND	ND	3,3	ND	35,5	27,7	ND	ND	100
PEL57	ND	3,2	1,1	31,5	0,13	ND	ND	0,93	ND	1,1	59,6	ND	0,28	100
PEL61	ND	2,0	4,7	32,1	0,27	ND	ND	7,8	0,21	33,9	18,7	0,24	ND	100

Table 9. Average olivine analysis.

Average values of pyroxene crystals in Oxides% by Stoichiometry													
Sample	Na_2O	MgO	Al_2O_3	SiO_2	P_2O_5	SO_3	K_2O	CaO	TiO_2	MnO	FeO	CuO	Total
ARG001	NONE												
ARG310	NONE												
ARG403	NONE												
ARG404	NONE												
ARG605	NONE												
ARG612	NONE												
ARG616	0,4	4,8	10,5	41,9	ND	0,15	0,32	6,7	0,34	13,6	20,8	0,17	100
PEL10	NONE												
PEL18	ND	2,8	8,1	40,7	0,19	ND	0,25	6,0	0,23	16,1	24,9	0,68	100
PEL21	NONE												
PEL28	NONE												
PEL31	NONE												
PEL38	NONE												
PEL57	NONE												
PEL61	ND	1,2	1,4	46,3	0,21	ND	ND	17,0	0,30	23,5	10,0	0,11	100

Table 10. Average pyroxene analysis.

Average of copper matte in weight% by All Elements															
Sample	Cu variation	O	Al	Si	P	S	Cl	Ca	Mn	Fe	Cu	Zn	Ba	Pb	Total
ARG001	NONE														
ARG310	0.38 - 50 Cu%	3,3	0,37	0,80	ND	30,3	ND	ND	21,4	21,0	20,6	ND	1,8	ND	100
ARG403	0.69 - 59.6 Cu%	18,2	1,3	0,85	ND	20,5	ND	0,16	0,10	35,5	16,0	ND	ND	6,7	100
ARG404	0.4 - 75.6 Cu%	9,8	0,11	0,22	ND	18,9	ND	ND	0,45	44,0	26,4	ND	ND	ND	100
ARG605	50 - 70 Cu%	1,2	0,17	0,17	ND	25,5	ND	ND	ND	10,5	62,3	ND	ND	ND	100
ARG612	54 - 76 Cu%	13,5	0,11	0,09	ND	17,7	ND	ND	ND	6,2	62,1	ND	ND	ND	100
ARG616	37 -73 Cu %	3,0	0,46	1,1	ND	25,0	ND	0,32	1,5	16,0	52,2	ND	ND	ND	100
PEL10	29.8 & 44.4Cu %	12,0	0.58	0.4	ND	22,5	ND	ND	1,0	26,1	37,1	ND	ND	ND	100
PEL18	72.7 - 77.2 Cu%	2,1	0,28	0,61	ND	18,6	ND	ND	0,91	2,4	74,7	ND	ND	ND	100
PEL21	51,9 - 69.7 Cu%	1,9	0,28	0,33	ND	25,0	ND	0,14	1,2	9,1	61,9	ND	ND	ND	100
PEL28	27.3 - 67.2 Cu%	3,0	0,16	0,22	ND	27,0	ND	ND	1,6	20,4	47,3	0,2	ND	ND	100
PEL31	4.3 - 55.1 Cu%	3,0	0,37	0,57	ND	29,1	ND	0,10	0,10	35,0	31,1	0,4	ND	ND	100
PEL38	0.33 - 1.24 Cu%	6,6	0,15	0,15	ND	29,6	ND	0,06	4,5	58,1	0,68	ND	ND	ND	100
PEL57	0.47 - 61.9 Cu%	6,5	0,33	0,65	ND	27,8	ND	ND	ND	40,7	23,6	ND	ND	ND	100
PEL61	62 - 84.7 Cu%	12,9	0,62	1,4	ND	4,8	5,9	0,52	2,5	1,8	69,5	ND	ND	ND	100

Table 11. Average copper matte.

Average values of copper metal in weight% by All Elements											
Sample	O	Mg	Al	Si	S	Ca	Ti	Mn	Fe	Cu	Total
ARG001	NONE										
ARG310	NONE										
ARG403	NONE										
ARG404	NONE										
ARG605	1,56	ND	0,46	1,5	ND	ND	ND	ND	3,2	93,3	100
ARG612	9,71	0,45	0,68	3,0	ND	0,62	ND	ND	4,1	81,2	100
ARG616	0,55	ND	ND	ND	0,27	ND	0,81	3,5	2,4	92,4	100
PEL10	NONE										
PEL18	0,79	ND	0,24	0,18	ND	ND	ND	ND	2,7	95,7	100
PEL21	NONE										
PEL28	NONE										
PEL31	NONE										
PEL38	NONE										
PEL57	NONE										
PEL61	3,67	ND	0,22	0,28	0,14	0,16	ND	1,42	1,4	92,7	100

Table 12. Average copper metal.

Bulk analyses in Oxides% by Stoichiometry															
Spectrum Label	Na_2O	MgO	Al_2O_3	SiO_2	P_2O_5	SO_3	Cl	K_2O	CaO	TiO_2	MnO	FeO	CuO	ZnO	BaO	Total
Spectrum 39	0,11	0,96	11,1	35,9	0,43	ND	ND	0,36	10,9	0,44	23,4	14,5	1,8	ND	ND	100
Spectrum 40	ND	0,98	10,9	35,9	0,31	ND	ND	0,33	10,7	0,41	23,4	14,6	2,2	ND	ND	100
Spectrum 48	0,15	0,87	11,2	35,8	0,31	ND	ND	0,36	10,9	0,43	23,7	14,4	2,0	ND	ND	100
Spectrum 49	0,18	0,87	11,2	36,2	0,37	ND	ND	0,37	11,2	0,38	23,7	14,2	1,3	ND	ND	100
Spectrum 50	0,13	0,86	11,0	35,6	0,35	ND	ND	0,36	11,0	0,41	23,1	14,3	2,8	ND	ND	100

Table 13. All bulk analysis on sample 61.

Photographs acquired by the SEM-EDS:

ARG001

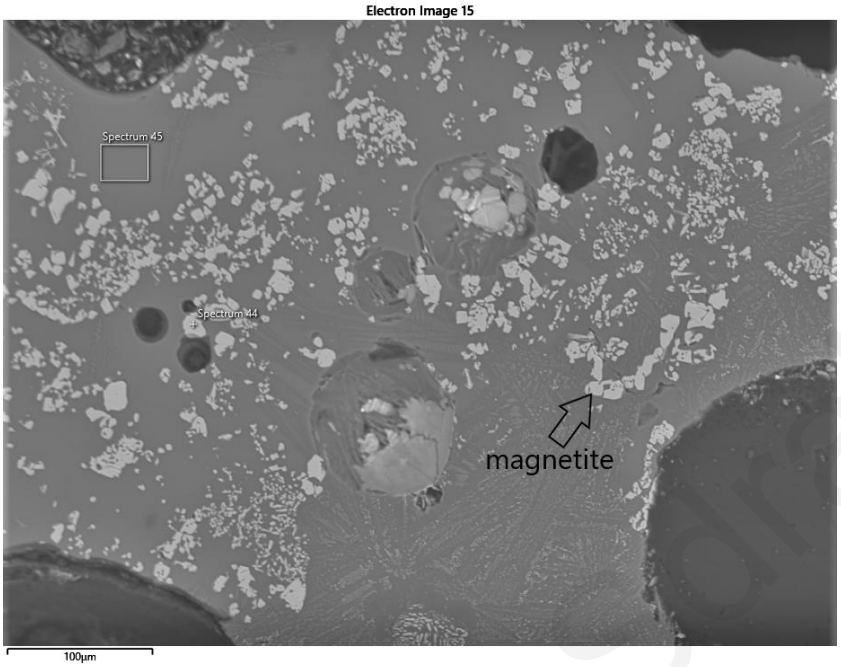

Figure 97. Sample ARG001. The vitrified area of the rock fragment. The free iron oxides are magnetite and are much more frequent in this area.

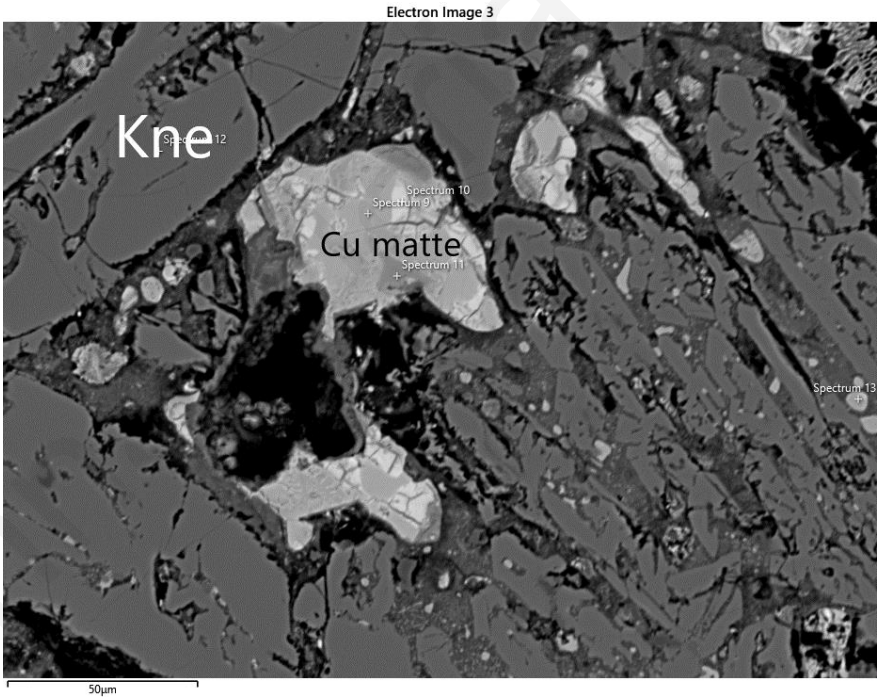

Figure 98. Sample ARG310. Elongated olive crystals (of a knebelite composition) and copper matte in the center of the photo

ARG403

ARG404

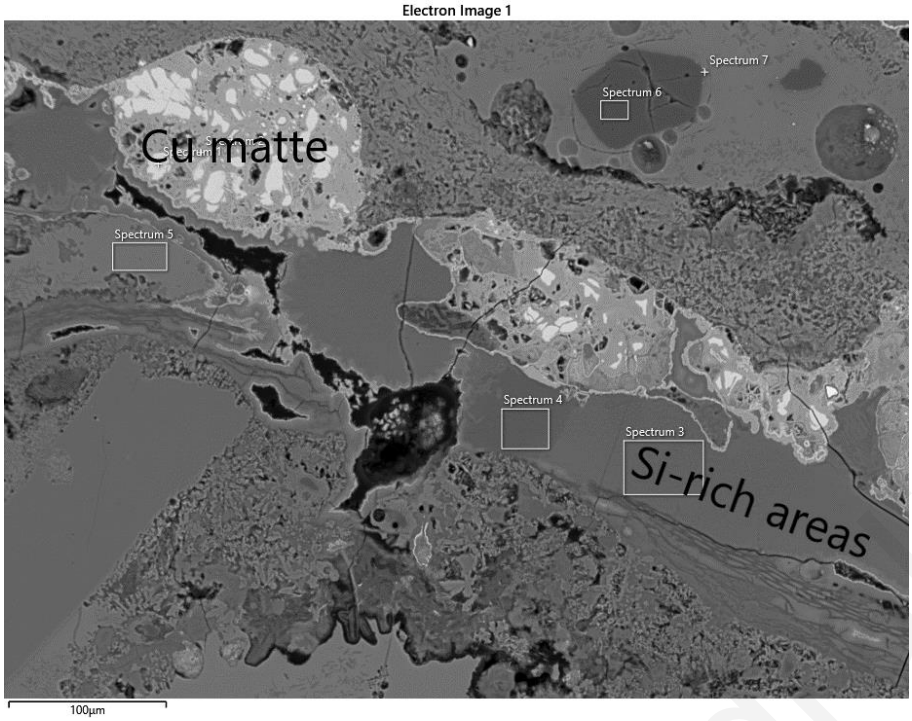

Figure 99. Sample ARG403. Heterogeneous clay frabric, not he copper matte which is very iron rich and the silica rich areas.

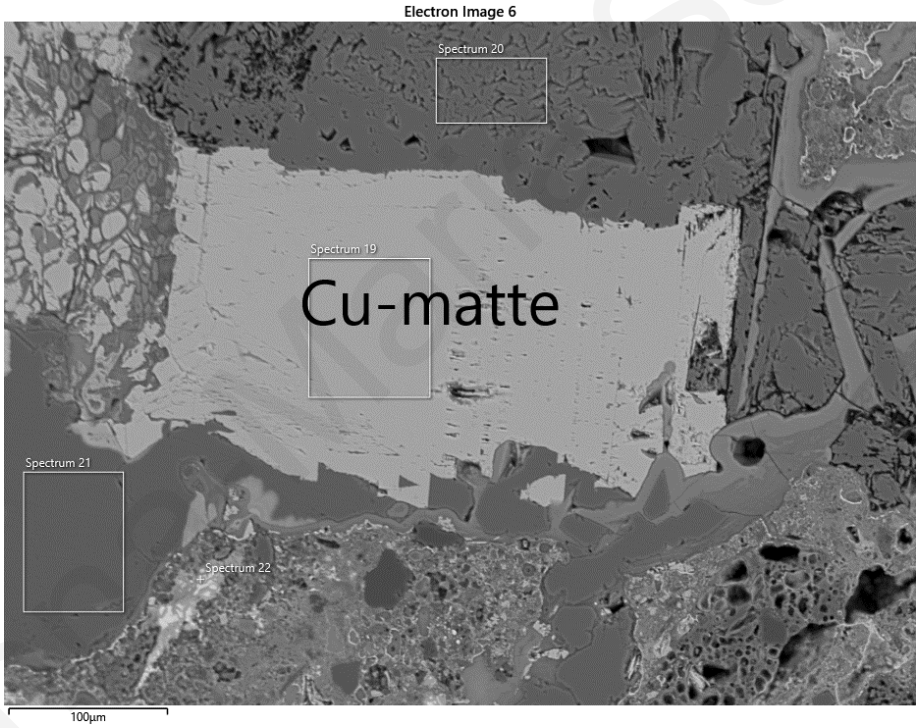

Figure 100. Sample ARG403. Note the the very rich copper matte surrounded above it and below it by almost pure Calcium (98.4% and 94.1% by Elements by Stoichiometry in oxides% respectively).

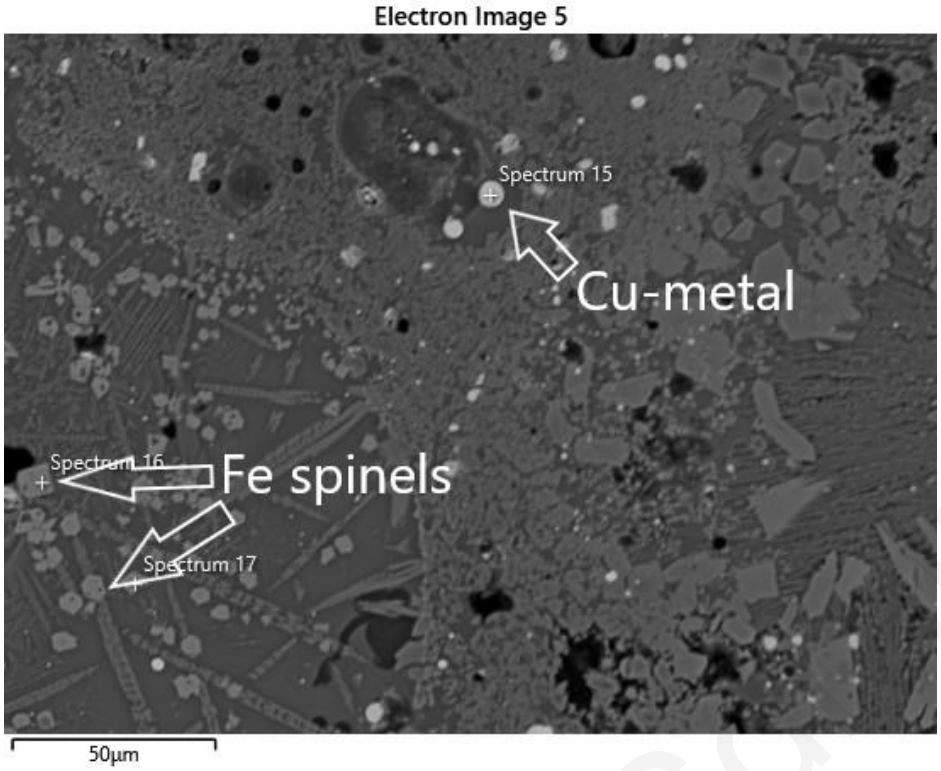

Figure 101. Sample ARG605. Copper metal and Fe-rich spinels (76.8% Fe, 13.1% Al, 3.6% Si, 1.5% Ti, 1.3% Mn by Elements by Stoichiometry in Oxides%).

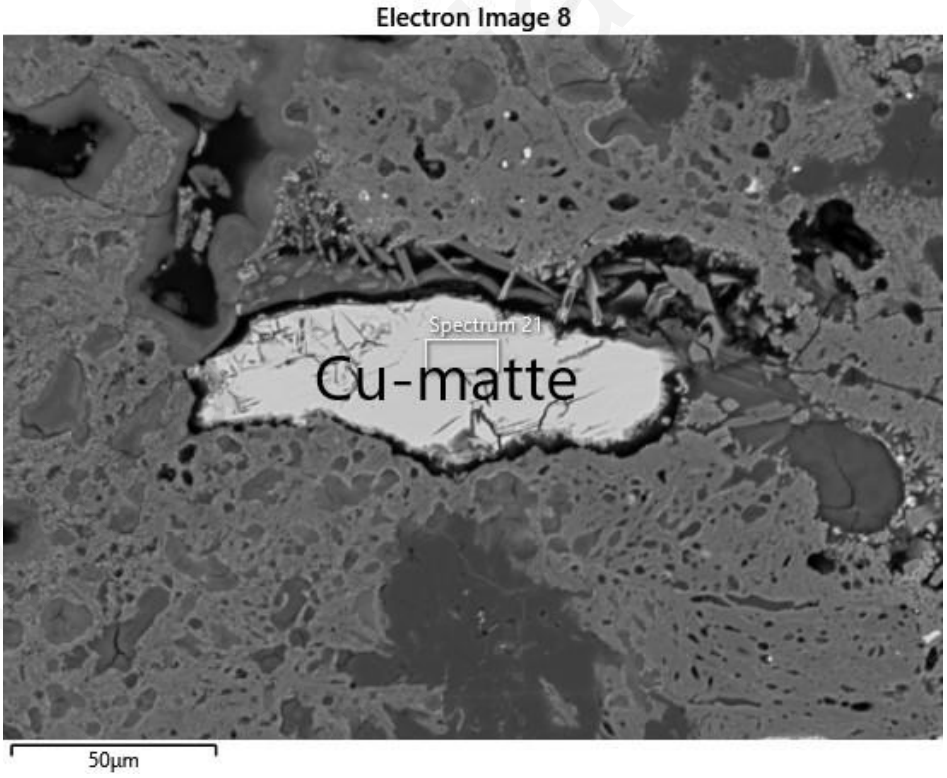

Figure 102. Sample ARG605. Copper rich matte (67.3 wt% Cu, 30.1 wt% S, 1.5wt% Fe by All Elements).

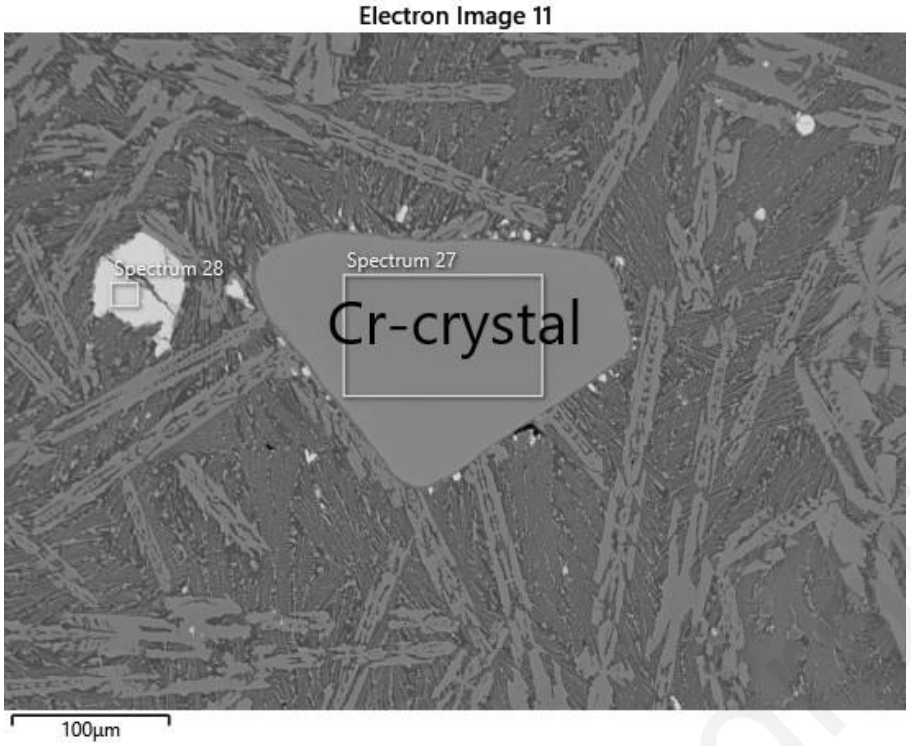

Figure 103. Sample ARG605. Chromite crystal (60.6% Cr, 24.2% Fe, 7.8% Al, 7% Mg by Elements by Stoichiometry in Oxides%).

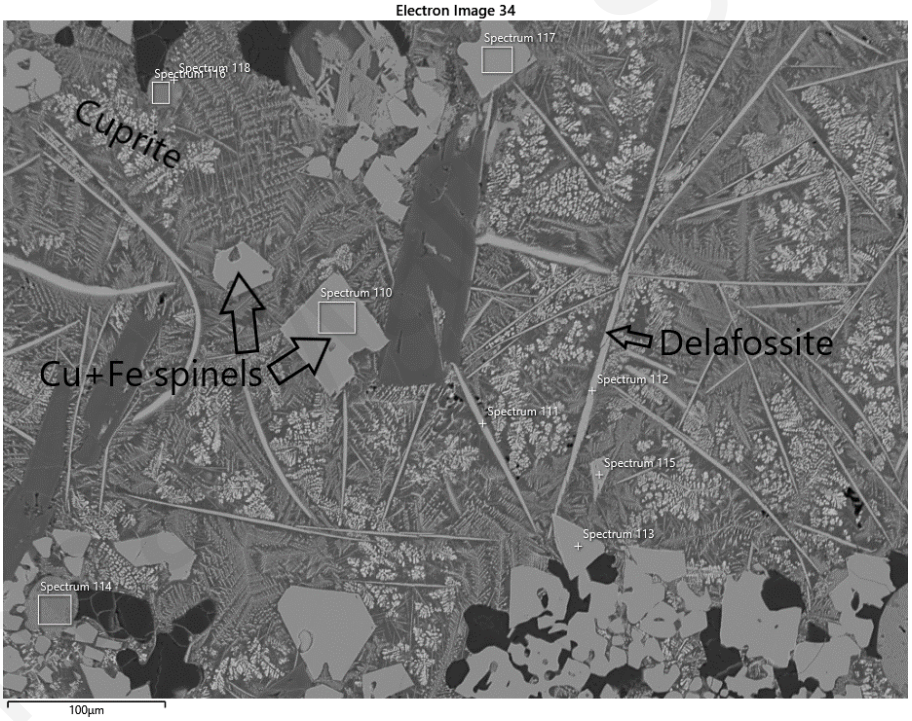

Figure 104. Sample ARG612. Copper rich phases, like cuprite and delafossite. Cu-Fe spinels surround the area (63.7% Fe, 30.1% Cu, 3.1% Al, 2.5% Mg, 0.4% Si By Elements by Stoichiometry in Oxides %).

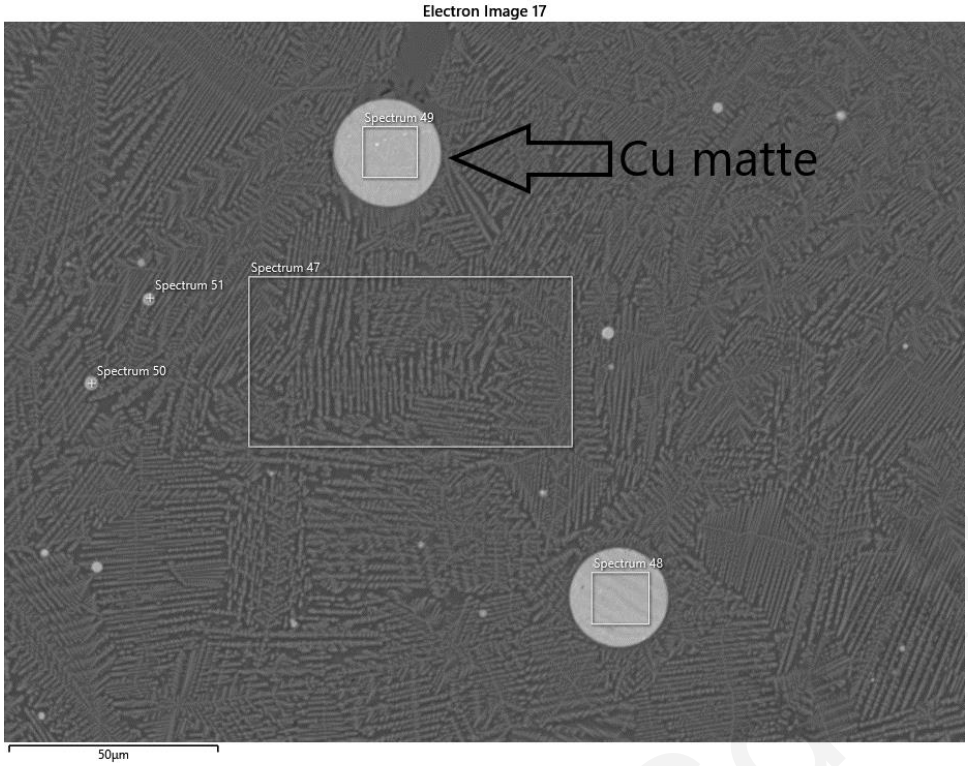

Figure 105. Sample ARG616. Copper rich matte in the microcrystalline background (of a composition 41.2% Si, 21.7% Fe, 13.3% Mn, 10.8% Al, 7.1% Ca by Elements by Stoichiometry in oxides%).

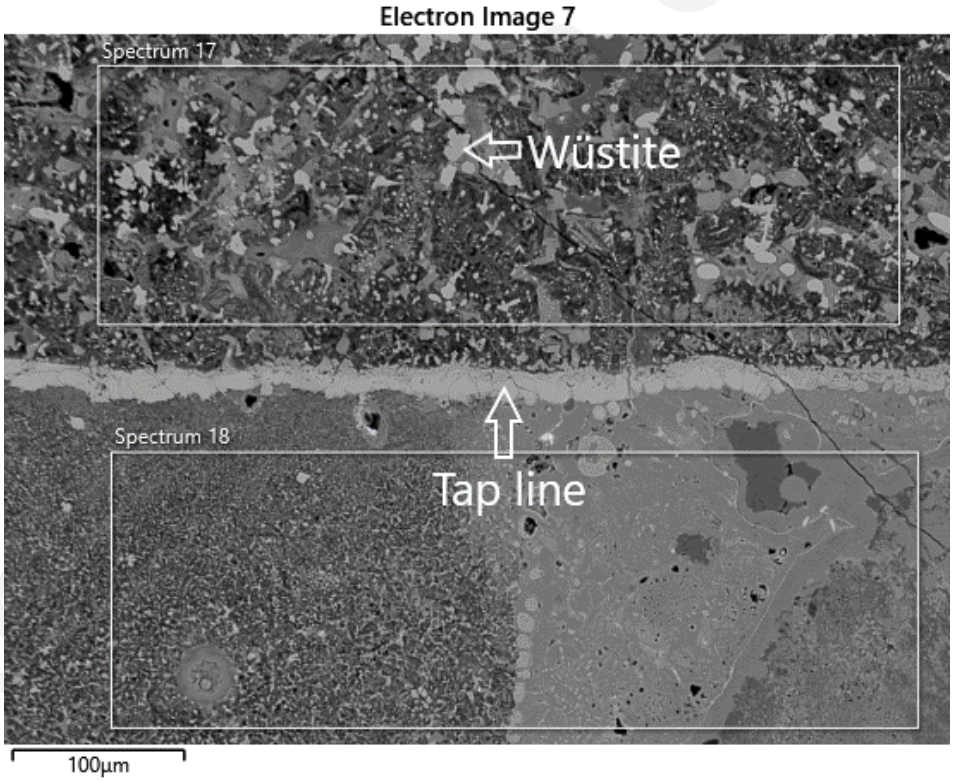

Figure 106. Sample PEL10. Free iron oxides of a wuestite composition, note the tap line indicating multiple slag flows.

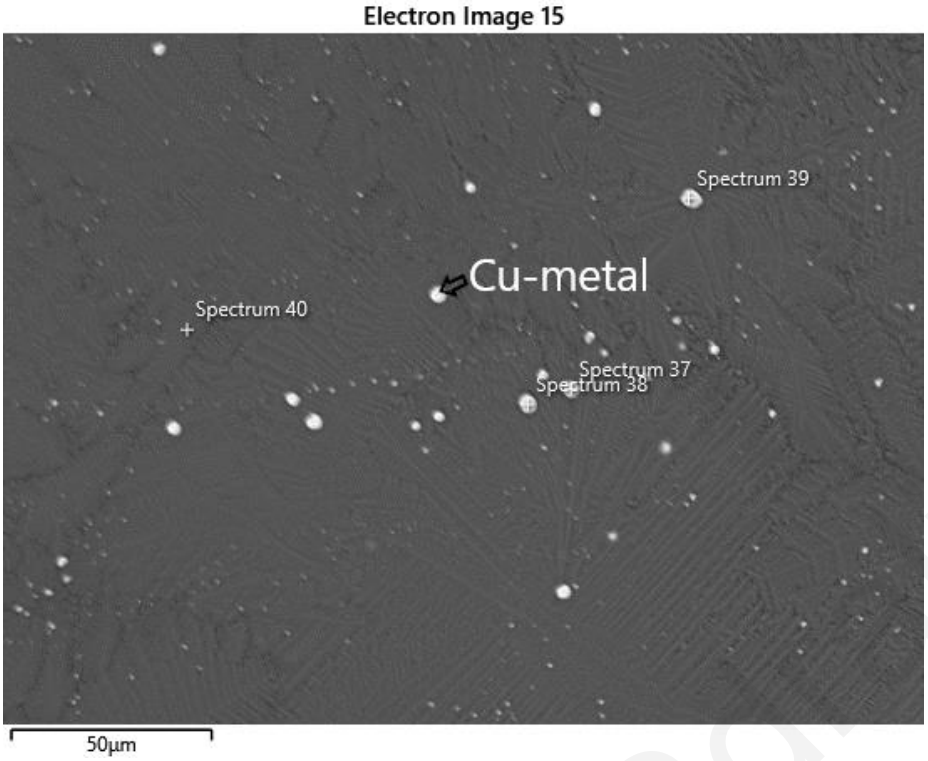

Figure 107. Sample PEL18. Copper metal prills in a microcrystalline background.

Figure 108. Sample PEL21. Note the barium rich formation (38% Ba, 35.7% S, 18% Sr, 5.3% Pb, 1.1% Ca, 0.9% Fe by Elements by Stoichiometry in oxides%) in the middle of the picture embedded in a microcrystalline matrix.

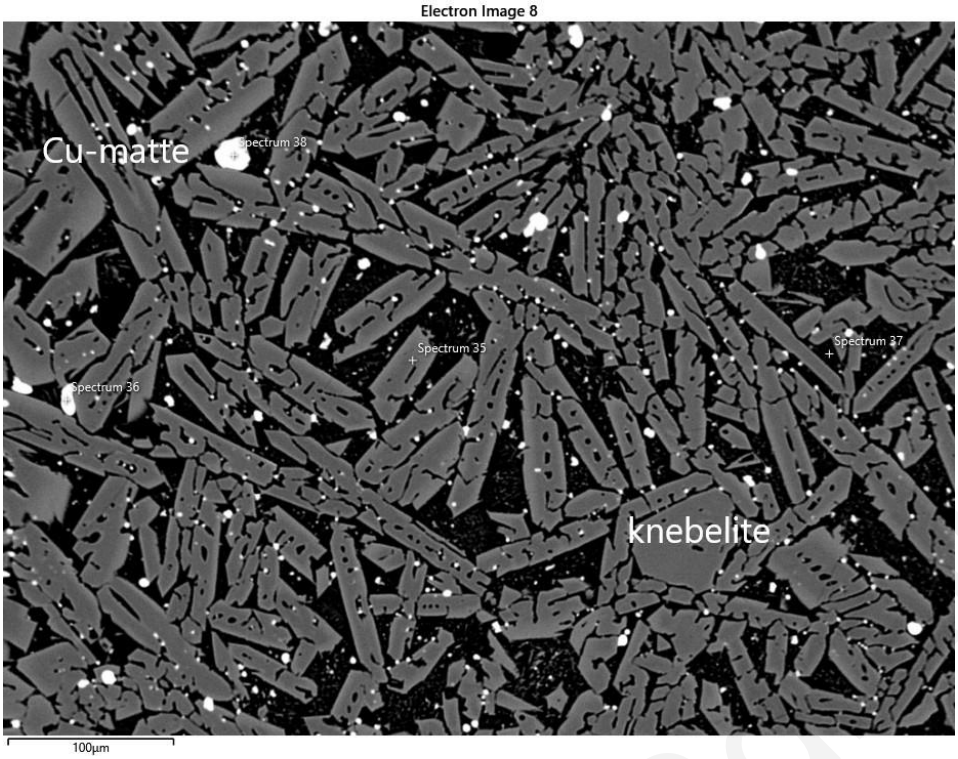

Figure 109. Sample PEL28. Note the copper matte and the elongated skeletal olivine crystals of a knebelite composition.

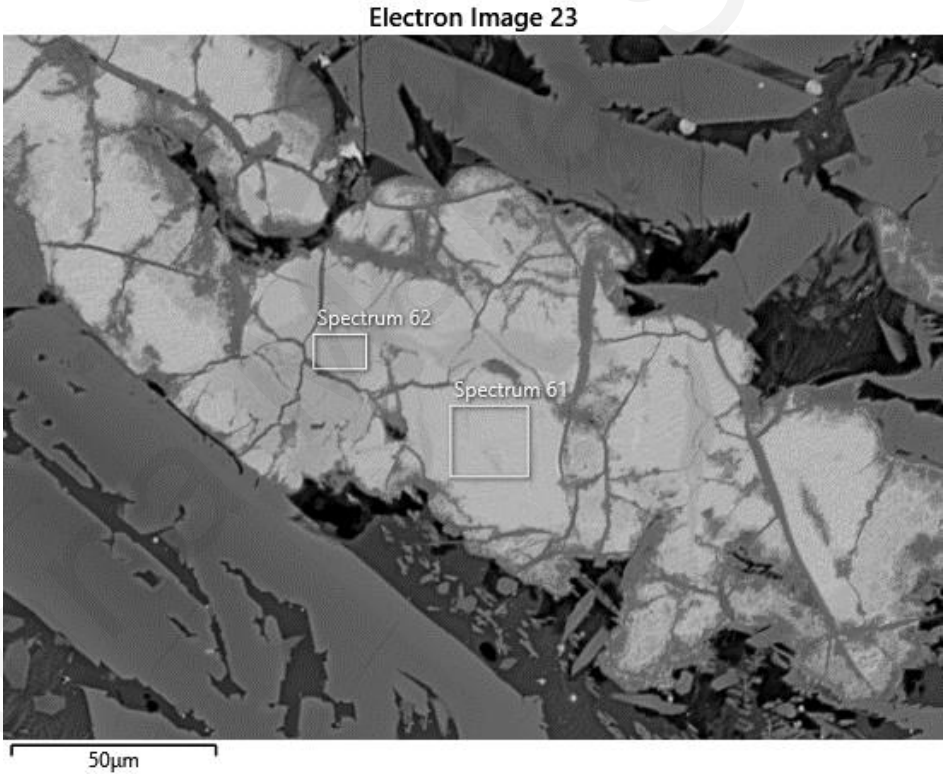

Figure 110. Sample PEL31. Copper matte in the middle and skeletal elongated olivine crystals (of a fayalite composition).

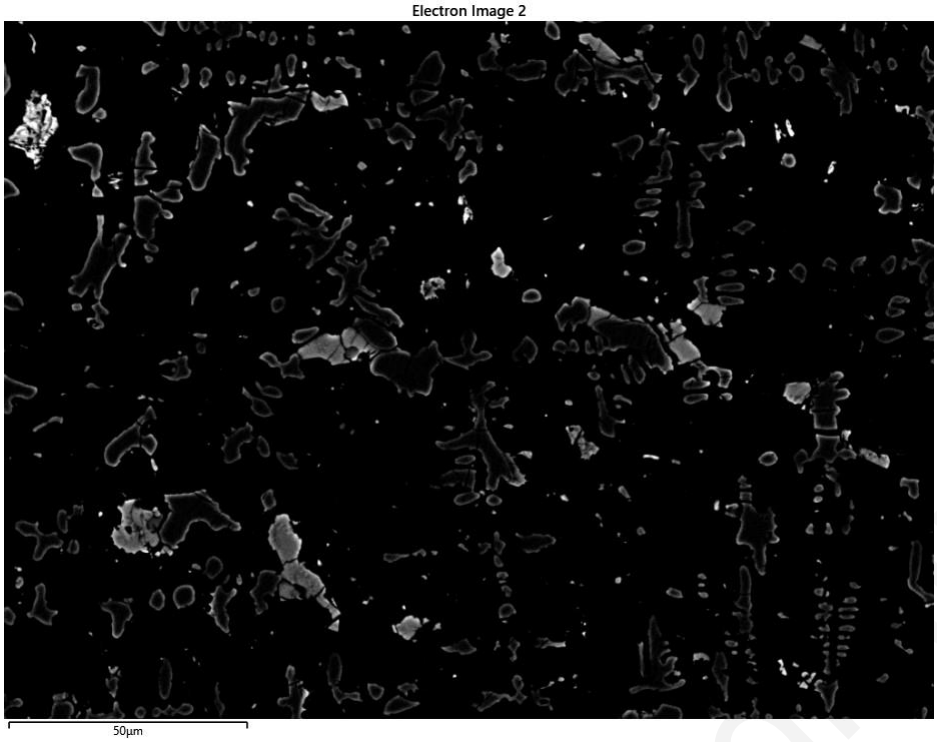

Figure 111. Sample PEL38. When the photo was taken in the SEM-EDS, a high contrast was applied, with little brightness. The formations shown are copper matte (bright grey) which is very closely associated with free iron oxides (only their outline is visible).

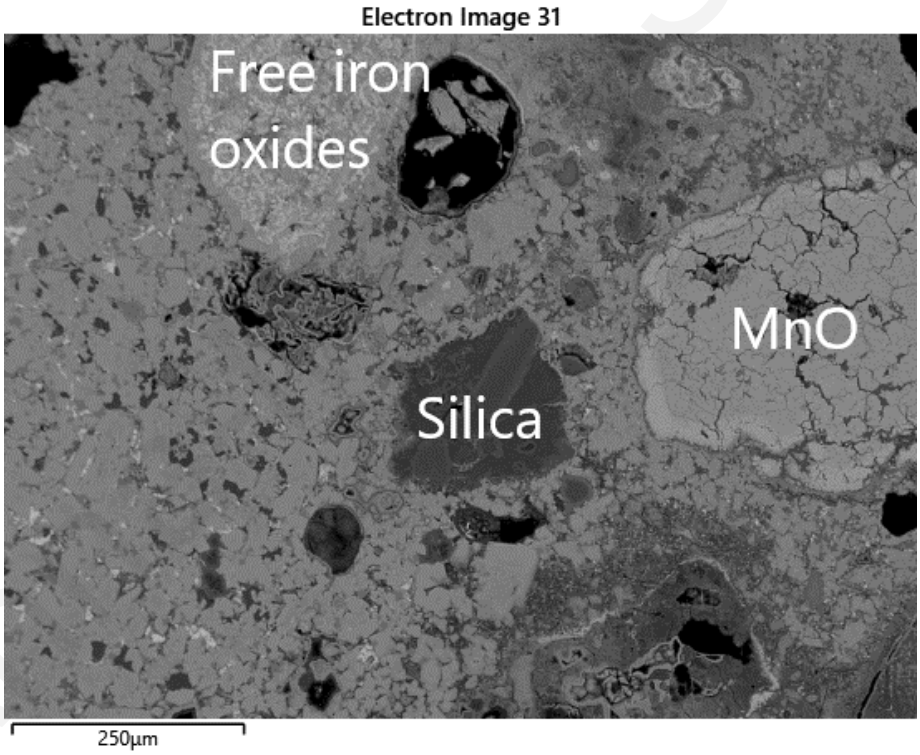

Figure 112. Sample PEL57. Note the heterogeneity of the sample. Preserved are unmolten areas of silica and manganese oxide.

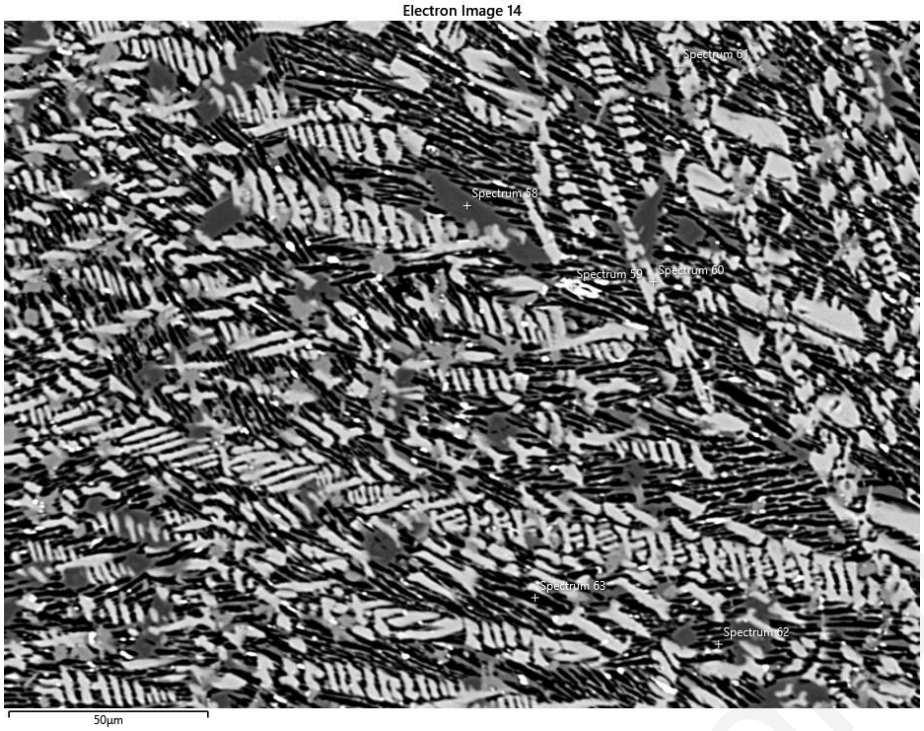

Figure 113. Sample PEL61. Note the microstructure of this sample.

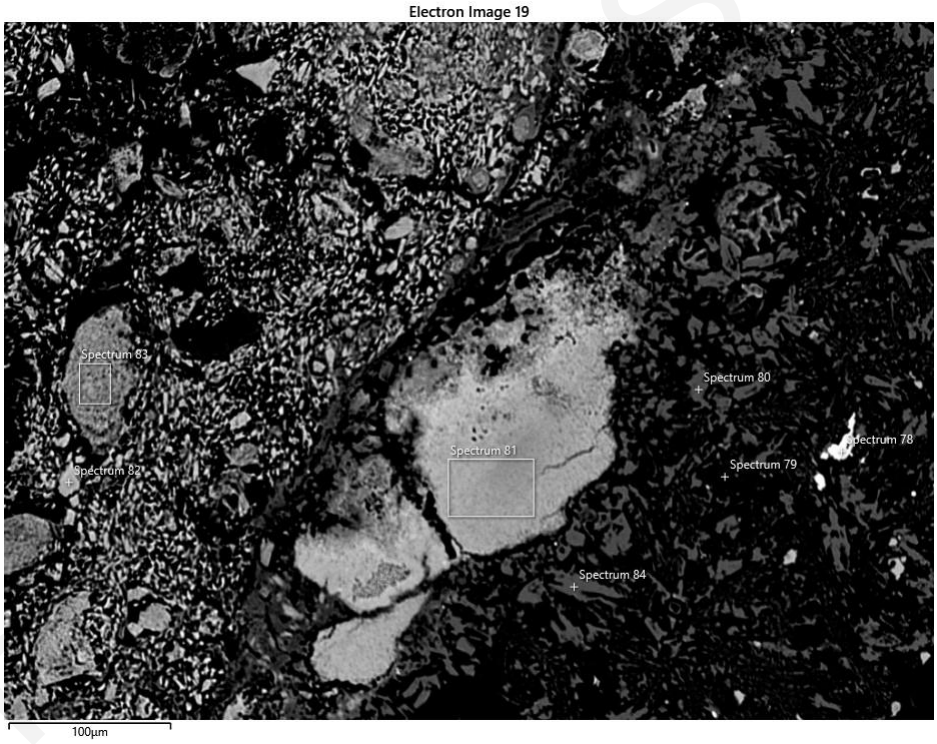

Figure 114. Sample 61. In the center of the picture is an unmolten part of manganese oxides (95.2% Mn, 1.2% Si, 0.9% K in Elements by Stoichiometry in oxides%).